MASTERARBEIT | MASTER'S THESIS

Titel | Title

Evaluating endosomal escape performance of mRNA and oligonucleotide carriers

verfasst von | submitted by

Helene Fasching BSc

angestrebter akademischer Grad | in partial fulfilment of the requirements for the degree of

Master of Science (MSc)

Wien | Vienna, 2024

Studienkennzahl lt. Studienblatt | Degree programme code as it appears on the student record sheet:	UA 066 830
Studienrichtung lt. Studienblatt | Degree programme as it appears on the student record sheet:	Masterstudium Molecular Microbiology, Microbial Ecology and Immunobiology
Betreut von | Supervisor:	Univ.-Prof. Dipl.-Ing. Dr. Manfred Ogris
Mitbetreut von | Co-Supervisor:	Haider Sami Ph.D.

Acknowledgement

Many thanks to Professor Manfred Ogris for giving me the opportunity to work in his group and on cell based projects! Special thanks go to my immediate supervisor Haider Sami, who guided me with great patience and trust, and to Elisa Kulterer and Susanne Wiederkum for their support in preparing the materials.
A big thank you to all MMCT members for teaching me a lot and for their natural friendliness and helpfulness!

I declare that I have written this thesis independently and without using sources or tools other than those cited, including artificial intelligence.

To my knowledge, the use of images in this thesis is in line with the freedom to quote. Should a copyright infringement become apparent nevertheless, please do not hesitate to contact me.

Helene Fasching Vienna, June 2024

Table of Contents

1. Abstract

Therapeutic nucleic acids allow treatment of various diseases by manipulating intracellular molecules inside patients´ cells. Polycationic polymers, including linear polyethyleneimine (LPEI), can be used as carriers to efficiently deliver exogenous nucleic acids to their intracellular site of action. In this thesis, 10 kDa LPEI, 2.5 kDa LPEI and their respective derivatives LPEI 10-PEG-Cys and crosslinked LPEI were evaluated as carriers of mRNA and splice switching oligonucleotides (SSOs) during *in vitro* transfections. A genetically engineered HeLa cell line, which allows the detection of ruptured endosomes via fluorescence microscopy, was used to visualise and quantify the capacity of the polymers to facilitate the release of mRNA into the cytoplasm after endocytosis. The results indicate that 10 kDa LPEI and 2.5 kDa LPEI are less efficient in facilitating the endosomal escape of mRNA than their derivatives, suggesting that PEGylation and crosslinking increase their performance.

In another project, 2.5 kDa LPEI and crosslinked LPEI were used to transfect the cells with Alexa Fluor 750 labelled SSOs in order to detect and semi-quantitatively analyse their endosomal escape and nuclear entry. Furthermore, the effect of SSO transfection – to correct aberrant splicing – was tested using another HeLa cell line. These cells are genetically engineered to stably produce a luciferase which is nonfunctional due to a splice site mutation. According to the results, crosslinked LPEI is more efficient than 2.5 kDa LPEI in promoting endosomal escape and nuclear entry of Alexa Fluor 750 labelled SSOs as well as splice correction.

Zusammenfassung

Therapeutische Nukleinsäuren ermöglichen die Behandlung verschiedener Krankheiten, indem sie intrazelluläre Moleküle in Zellen von Patienten manipulieren. Polykationische Polymere, darunter lineares Polyethylenimin (LPEI), können als Trägermoleküle verwendet werden, um exogene Nukleinsäuren effizient an ihren intrazellulären Wirkungsort zu transportieren. In dieser Arbeit wurden 10-kDa-LPEI, 2,5-kDa-LPEI und deren Derivate LPEI 10-PEG-Cys und quervernetztes LPEI als Träger von Boten-RNA und splice-switching Oligonukleotiden (SSOs) bei *in vitro* Transfektionen untersucht. Dabei wurde eine gentechnisch veränderte HeLa-Zelllinie verwendet, die den Nachweis aufgebrochener Endosomen mittels Fluoreszenzmikroskopie ermöglicht, um die Fähigkeit der Polymere zu analysieren, nach ihrer Aufnahme durch Endozytose die Freisetzung von mRNA ins Zytoplasma zu erleichtern. Die Ergebnisse deuten darauf hin, dass 10-kDa-LPEI und 2,5-kDa-LPEI den endosomalen Austritt von mRNA weniger effizient erleichtern als ihre Derivate. Dies legt den Schluss nahe, dass die PEGylierung beziehungsweise die Quervernetzung deren Leistung erhöhen.

In einem weiteren Projekt wurden 2,5-kDa-LPEI und quervernetztes LPEI verwendet, um die Zellen mit Alexa-Fluor-750-markierten SSOs zu transfizieren und so deren Austritt aus den Endosomen und Eintritt in den Zellkern zu visualisieren und semi-quantitativ zu analysieren. Außerdem wurde die Wirkung der Transfektion mit SSOs – die Korrektur von fehlerhaftem Spleißen – an anderen HeLa-Zellen getestet. Diese Zellen sind gentechnisch so verändert, dass sie eine Luziferase produzieren, die aufgrund von fehlerhaftem Spleißen nicht funktionsfähig ist. Den Ergebnissen zufolge ist quervernetztes LPEI effizienter als 2,5-kDa-LPEI bei der Vermittlung des endosomalen Austritts und des Kerneintritts von Alexa-Fluor-750-markierten SSOs sowie bei der Spleißkorrektur.

2. Introduction

2.1. Delivery of Therapeutic Nucleic Acids

Nucleic acid based therapeutics are aimed to treat infectious diseases and genetic disorders (Kang, et al., 2023). They act by introducing an artificial nucleic acid into patients´ cells. This nucleic acid then utilises the host cells´ gene expression machinery to produce a therapeutic protein or it interferes with the expression of a viral gene or a gene carrying a disease causing mutation (Kulkarni, et al., 2021). Ideally, this approach allows for a highly selective treatment with few harmful effects on healthy cells (Rödl, Taschauer, Schaffert, Wagner, & Ogris, 2019).

Due to the physicochemical properties of nucleic acids there are multiple challenges in their delivery to the respective site of action. They are susceptible to rapid clearance from the bloodstream and degradation by nucleases (Reinhard & Wagner, 2019). Because of their negative charge, naked nucleic acids cannot diffuse through the plasma membrane and typically display a low cellular uptake (Lächelt & Wagner, 2015). Inside the cell, nucleic acids are prone to degradation by cytoplasmic nucleases. Depending on their size, they can diffuse in the cytoplasm and reach their site of action (Lukacs, et al., 2000).

Problems with nucleic acid stability and delivery can be addressed by employing efficient vectors. Various strategies have been explored, involving the use of different viral and non-viral vectors. Introducing nucleic acids into eukaryotic cells through viral vectors is referred to as transduction whereas transfection is the transfer of nucleic acids via non-viral methods (Thermo Fisher Scientific Inc., 2024). Viral vectors are derived from different viruses - including retroviruses, adenoviruses and adeno-associated viruses - and rely on the ability of the viruses to infect cells (Shirley, de Jong, Terhorst, & Herzog, 2020). They are relatively efficient in nucleic acid delivery. Retroviral vectors and, to a small degree, adeno-associated viruses integrate the transgene into the cellular genome, allowing stable

expression (Yin, Kanasty, Eltoukhy, & Vegas, 2014). Non-viral nucleic acid delivery methods include the complexation of the nucleic acid with carrier molecules. Compared to viral vectors, these carriers are less efficient in delivering nucleic acids but also less immunogenic (Pack, Hoffman, Pun, & Stayton, 2005).

Depending on the type of the nucleic acid, different modes of action, at different stages of gene expression and intracellular locations, are possible (Lächelt & Wagner, 2015). This is illustrated in Figure 1. The main focus of this thesis is the intracellular delivery of messenger RNA (mRNA) and splice switching oligonucleotides (SSOs) using polycationic carriers.

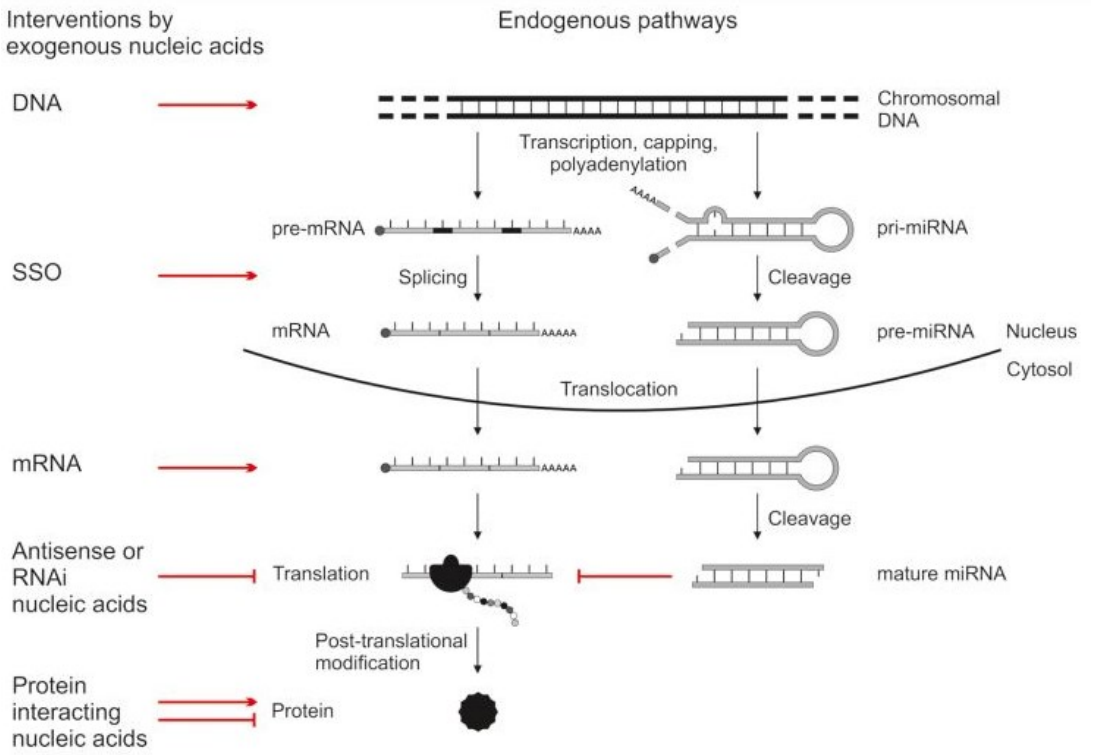

Figure 1: Points of intervention by therapeutic nucleic acids inside the host cell (from Lächelt and Wagner, 2015)

2.1.1. Delivery of mRNAs

DNA and mRNA act as carriers of genetic information. During protein biosynthesis, protein coding genes are transcribed into pre-RNA which undergoes 5′ capping, 3′ polyadenylation and splicing inside the nucleus, as depicted in Figure 1. The resulting mature mRNA is exported from the nucleus and translated in the cytoplasm (Alberts, et al., 2015). Similarly, plasmid DNA (pDNA) and mRNA can be designed to serve as blueprints for the synthesis of a therapeutic protein in transfected cells. Apart from translation, the folding, posttranslational modification and localisation of the protein, which are crucial to its activity, are also accomplished by the host cell. This way, the correct biological function of the protein depends on the cell line but can be achieved relatively easily (Sahin, Karikó, & Türec, 2014).

The mRNA is typically generated through *in vitro* transcription from pDNA which is designed to contain the coding sequence flanked by a 5′ and 3′ untranslated region and a 3′ poly-A tail. Therefore, by varying the plasmid sequence, mRNA production can be readily adapted for different proteins (Weng, et al., 2020). There are advantages to using mRNA as opposed to pDNA, also regarding intracellular delivery. Whilst mRNA is directly translated in the cytoplasm, pDNA needs to enter the nucleus for the production of mRNA which can then be exported. To this end, pDNA must reach the nucleus and be taken up following the transient breakdown of the nuclear envelope during mitosis or by active import through the nuclear pores (Zhou, Geiger, & Dean, 2004). Unlike DNA and viral vectors, mRNA does not integrate into the genome, and hence does not pose the risk of insertional mutagenesis. As a result, only transient protein production is expected, depending on the stability of the mRNA in the cytoplasm (Lächelt & Wagner, 2015).

2.1.2. Delivery of Splice Switching Oligonucleotides

Antisense oligonucleotides (ASOs) are short synthetic oligonucleotides which can bind to RNA in a sequence specific manner. They can be designed to base pair with the transcript of a particular gene, and subsequently alter its expression through knockdown or splice modulation (Lauffer, van Roon-Mom, & Aartsma-Rus, 2024). The latter is mediated by so-called splice switching oligonucleotides (SSOs). These specifically bind to pre-mRNA sequences involved in splicing regulation which sterically blocks the binding of splicing factors and redirects the spliceosome to alternative splice sites, thus yielding a different mRNA splice variant (Havens & Hastings, 2016). Therefore, SSOs can (partially) restore normal protein function in the case of aberrant splicing (Kuijper, Bergsma, Pijnappel, & Aartsma-Rus, 2021). This effect is referred to as splice correction.

Previous research indicates that naked oligonucleotides are internalised by cells through endocytosis (Juliano, Alahari, Yoo, Kole, & Cho, 1999). Since SSOs are aimed to modulate splicing, they must act in the nucleus, as indicated in Figure 1. Accordingly, splice correction occurs in a subpopulation of cells with a high uptake of SSOs, in which SSOs are localised in the nucleus (Ming, Sato, & Juliano, 2011). Also, small oligonucleotides have been shown to rapidly accumulate in the nucleus after microinjection into the cytoplasm, whereby the rate of diffusion in the cytoplasm depends on their molecular weight (Lukacs, et al., 2000). This indicates that the effectiveness of SSOs depends on their ability to pass intracellular barriers and ultimately enter the nucleus. For the nuclear entry of oligonucleotides different mechanisms have been proposed, including passive diffusion (Leonetti, Mechti, Degols, Gagnor, & Lebleu, 1991) or active transport through the nuclear pore complex without the aid of cytoplasmic transport proteins (Hartig, Shoeman, Janetzko, Griib, & Traub, 1998).

Aberrant splicing has been identified as the cause of several genetic disorders, including Duchenne muscular dystrophy and β-thalassemia (Bauman, Jearawiriyapaisarn, & Kole, 2009). Splice correction

by ASOs was demonstrated for the first time on 3 different mutations in the human haemoglobin β-chain gene which lead to incorrect splicing and β-globin deficiency in β-thalassemia (Dominski & Kole, 1993). One of the discussed mutations is a T → G transversion of nucleotide 705 in intron 2, which creates a new 5′ splice site and activates a cryptic 3′ splice site. In the presence of this mutation, intron 2 is only partly excised during splicing, giving rise to a stop codon in the mature mRNA which is then translated into nonfunctional truncated β-globin. Dominski and Kole showed that correct splicing can be restored following treatment with oligonucleotides which are complementary to either the new 5′ splice site or the cryptic 3′ splice site. As part of this thesis, splice correction assays were conducted to analyse the effect of SSOs after *in vitro* transfections using HeLa pLuc 705 cells. For creating this cell line, HeLa cells had been transduced to stably express a firefly luciferase gene interrupted by the β-globin intron 2 with the above mentioned nucleotide 705 mutation (Kang, Cho, & Kole, 1998). Firefly luciferase catalyses the oxidation of D-luciferin. Here, using ATP, the luciferase adenylates D-luciferin and the resulting enzyme bound intermediate reacts with O_2 to produce oxyluciferin in an excited state. The transition of oxyluciferin to the ground state results in the emission of yellow-green light (Fan & Wood, 2007). Therefore, luminescence is measured as an indicator of luciferase activity in the sample. Due to the splice site mutation, HeLa pLuc 705 cells produce truncated inactive luciferase. However, after effective transfection with SSOs which can bind to and mask the 5′ splice site (LucSSOs), functional luciferase is produced and the luminescence is increased. In contrast, SSOs with a non-complementary sequence (NCSSOs) cannot base pair with the reporter gene pre-mRNA and are unable to mediate splice correction. The principle of the HeLa pLuc 705 system and the reaction catalysed by firefly luciferase are depicted in Figure 2.

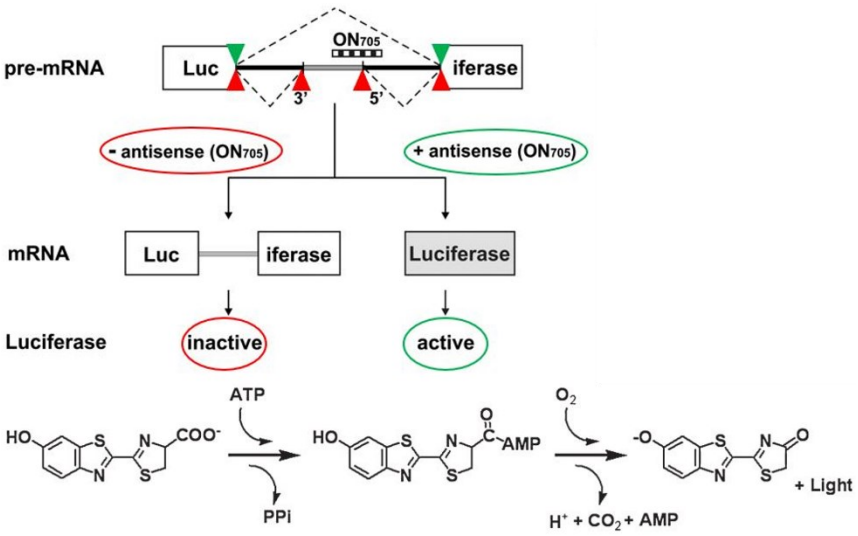

Figure 2: Principle of the splice correction assay with HeLa pLuc 705 and reaction by firefly luciferase
(modified from Boisguérin, 2015 and from Fan and Wood, 2007)

2.2. LPEI Derived Polymers for Delivery of Nucleic Acids

Various cationic molecules, including cationic lipids and polymers, have been employed as nucleic acid carriers for non-viral delivery. Here, the nucleic acid is combined with the carrier molecule and, through electrostatic interactions between its phosphate backbone and positively charged groups of the carrier, it is complexed into particles a few tens to several hundred nanometres in diameter (Pack, Hoffman, Pun, & Stayton, 2005). Nanoparticles of nucleic acids and polymers are termed polyplexes. Polyethyleneimine (PEI), especially branched and linear PEI (BPEI and LPEI, respectively), is frequently used to create polyplexes for transfections *in vitro* and *in vivo* (Eliyahu, Barenholz, & Domb, 2005).

The capacity of PEI for nucleic acid delivery was demonstrated for the first time by Jean-Paul Behr and colleagues in 1995 (Boussif O. , et al., 1995). LPEI can be synthesised from poly(2-ethyl-2-oxazoline) via acidic hydrolysis and subsequent cleavage of side chains (Taschauer, et al., 2019). Like other nucleic acid carriers, PEIs display physicochemical properties that are crucial to nucleic acid complexation and transfection and they are also amenable to chemical modifications for increasing their safety and efficiency (Kircheis, Wightman, & Wagner, 2001). PEIs comprise repeating 43 Da CH_2-CH_2-NH units, and hence display a high content of protonable amines (Rödl, Taschauer, Schaffert, Wagner, & Ogris, 2019). At a physiological pH, approximately 55 % of the amines are protonated (Ziebarth & Wang, 2010). Through these protonated, and hence positively charged, amines PEIs interact with phosphate groups of nucleic acids to form polyplexes. Here, the molar ratio of polymer to nucleic acid, i.e. nitrogen in the polymer to phosphorus in the nucleic acid (N/P ratio), determines the degree of nucleic acid complexation. For efficient transfection, PEI polyplexes are typically created with an N/P ratio of 5 or above, hence with a large amount of free polymer and a positive net charge (Boeckle, et al., 2004). However, the positive surface charge causes them to interact and form aggregates with plasma components, and to be entrapped in the lung shortly after intravenous injection (Rödl, Taschauer, Schaffert, Wagner, & Ogris, 2019). In order to circumvent this problem, LPEI polyplexes have been covalently bound to polyethylene glycol (PEG) which has been shown to reduce their surface charge as well as binding to plasma proteins and erythrocytes *in vitro* and prolonged their circulation in the blood (Ogris, Brunner, Schuller, Kircheis, & Wagner, 1999).

Another factor that affects nucleic acid delivery is the molecular weight of the PEI. Reportedly, high molecular weight PEIs display a greater transfection efficiency but are also more cytotoxic than PEIs of low molecular weight (Hall, Lächelt, Bartek, Wagner, & Moghimi, 2017). In an attempt to counteract the cytotoxicity of high molecular weight LPEIs but maintain their transfection efficiency, lower molecular weight LPEIs have been crosslinked by biodegradable linker molecules, so they can be degraded into less toxic components in the cytoplasm (Bonner, Zhao, Buss, Langer, & Hammond, 2013).

In this thesis, 10 kDa LPEI and 2.5 kDa LPEI (LPEI 10 and LPEI 2.5, respectively) as well as chemically modified polymers derived from both of these LPEIs were used for creating polyplexes. All of the applied polymers are depicted in Figure 3. For the modification of LPEI 10, it had been bound to a 2 kDa PEG linker carrying an N-hydroxysuccinimide group (NHS) and a 3-(2-pyridyldithio) propionamide group (OPSS) at the opposite termini (Kiss, et al., 2011). Here, an amide bond between an amine of LPEI and the NHS group of the linker is formed. By using this heterobifunctional linker, crosslinking of LPEI can be avoided (Rödl, Taschauer, Schaffert, Wagner, & Ogris, 2019). In addition, the conjugate can be bound to synthetic peptide ligands by forming a disulfide bridge between the OPSS group and a cysteine residue. This allows targeting the polyplexes to cell surface receptors (Taschauer, et al., 2019). In the case of LPEI 10-PEG-Cys, which was used in this thesis, LPEI 10 had been coupled to L-cysteine instead of a targeting peptide, using the same methodology (Sperhansl, 2016). LPEI 2.5 had been modified by crosslinking through a homobifunctional N-hydroxysuccinimide ester. The polymer used in this thesis displays a crosslinking ratio of 0.5, i.e. the crosslinking reaction was carried out with a 1:0.5 molar ratio of LPEI 2.5 to the crosslinker (Kaufmann, 2024). The crosslinked LPEI (cLPEI) can be cleaved in endosomes or the cytoplasm by the reduction of the disulfide bridge (Breunig, Lungwitz, Liebl, & Goepferich, 2007).

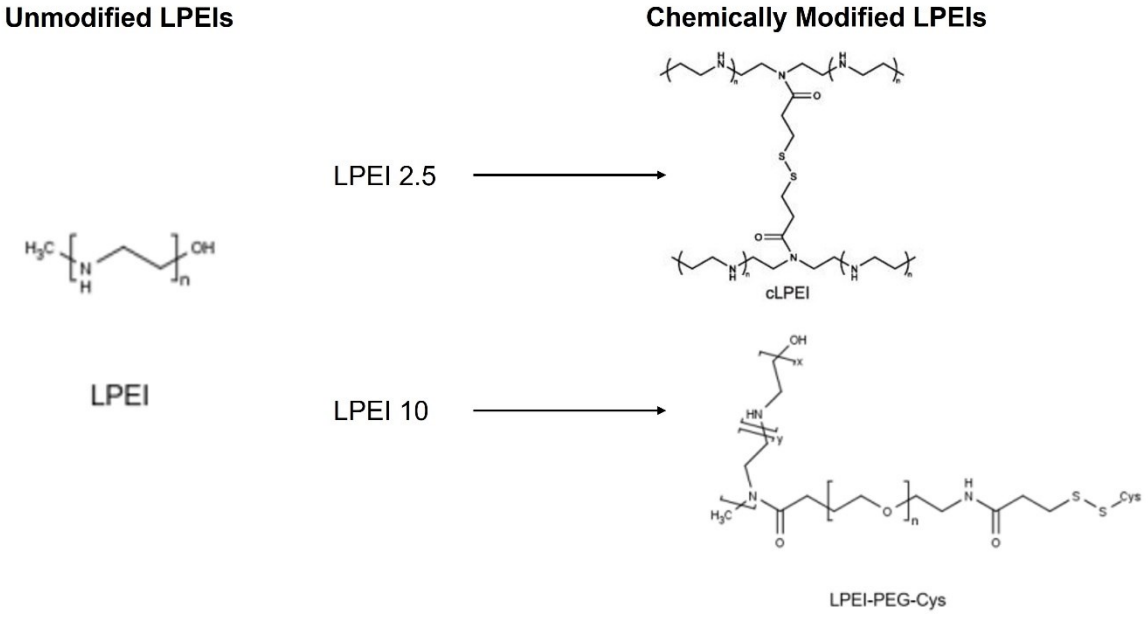

Figure 3: Polymers used in this thesis
(modified from Decker, 2022 and Sperhansl, 2016)

2.2.1. Challenges in Nucleic Acid Delivery by PEI Polyplexes

The positive surface charge allows PEI polyplexes to interact with negatively charged cell surface molecules like proteoglycans, triggering cellular uptake via adsorptive endocytosis (Rödl, Taschauer, Schaffert, Wagner, & Ogris, 2019). Afterwards, the nucleic acid needs to escape from endosomal

vesicles into the cytoplasm prior to their fusion with lysosomes to avoid exocytosis or lysosomal degradation and to reach its point of action (Rejman, Bragonzi, & Conese, 2005). Among other polycationic molecules, PEI has an intrinsic capacity for endosomal escape (Kircheis, Wightman, & Wagner, 2001). After endosomal escape, the nucleic acid has to reach its target site. As mentioned, mRNA acts in the cytoplasm whereas SSOs must also enter the nucleus for mediating splice correction. The intracellular delivery pathways of mRNA and SSO polyplexes are illustrated in Figure 4.

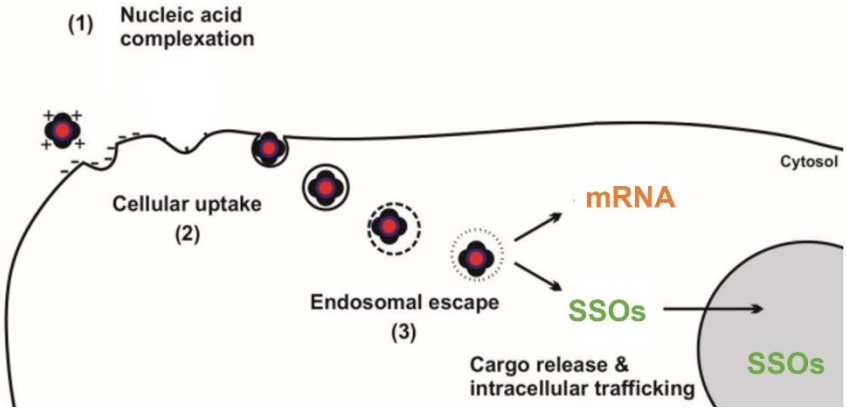

Figure 4: Intracellular delivery of polyplexes with mRNA and SSOs (modified from Lächelt and Wagner, 2015)

2.2.2. Endosomal Escape of PEI Polyplexes

Behr and colleagues have advanced the hypothesis of the proton sponge effect to explain the endosomal escape of nucleic acids during transfection with PEI polyplexes (Boussif O. , et al., 1995). According to this, PEI amines, which have not been protonated at a neutral pH, are protonated inside the endosomes as a result of the acidic pH. This supposedly promotes the active transport of protons by vacuolar ATPases and simultaneous diffusion of chloride counterions into the endosomes. The resulting osmotic effect, i.e. the influx of water, causes the endosomes to swell and eventually rupture, releasing the polyplexes. In line with the proton sponge hypothesis, PEI polyplexes reportedly delay endosome acidification and lead to an increased chloride concentration, swelling and rupture of endosomes - unlike polylysine polyplexes with fixed charges (Sonawane, Szoka, & Verkman, 2003). However, previous research indicates other mechanisms behind the endosomal escape of PEI polyplexes, and it has been suggested that multiple effects are involved (Rehman, Hoekstra, & Zuhorn, 2013). The possible mechanisms described here are summarised in Figure 5. For example, LPEI has been shown to expand with its progressive protonation during endosomal acidification, likely due to the repulsion of positive charges. This has been suggested to contribute to endosomal rupture and the release of polyplexes. Battaglia and colleagues have proposed that the disassembly of PEI polyplexes into free polymers leads to osmotic pressure in endosomes and their subsequent rupture (Massignani, et al., 2010). Moreover, previous research indicates that free PEI and PEI polyplexes interact with endosomal membranes

(Bieber, Meissner, Kostin, Niemann, & Elsasser, 2002), and that PEI causes perforation and increased permeability of vesicles (Clark, et al., 2018). Experiments by Rehman and colleagues suggest that nucleic acids are ejected from a local rift in the endosomal membrane following a buildup of osmotic pressure due to LPEI mediated pH buffering (Rehman, Hoekstra, & Zuhorn, 2013).

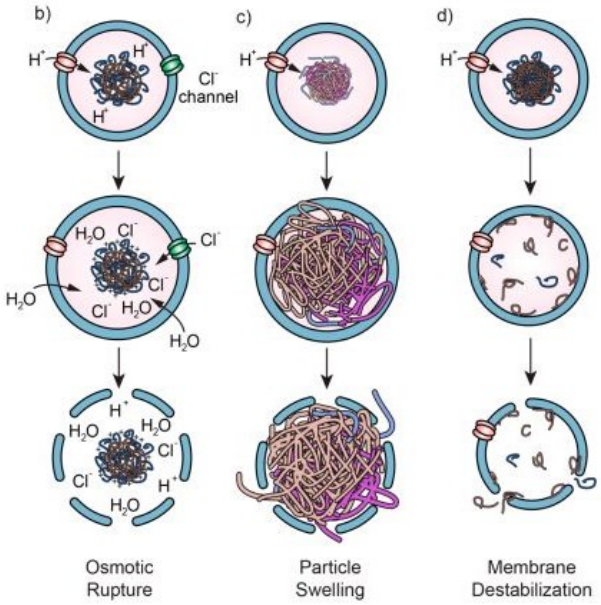

Figure 5: Proposed mechanisms behind the endosomal escape of polyplexes (modified from Smith et al., 2019)

2.2.3. Visualising and Quantifying Endosomal Escape of PEI Polyplexes

Various methods have been applied to analyse the endosomal escape of PEI polyplexes *in vitro*. These include visualising endocytosed material or endosomal damage through fluorescence microscopy and subsequent quantitative analysis using an image analysis software. For example, fluorescent labelling of the nucleic acid or polymer allows tracking their intracellular delivery (Rehman, Hoekstra, & Zuhorn, 2013). When entrapped and concentrated inside endosomal vesicles, the labelled material registers as fluorescent dots. After its endosomal escape and dispersal, it yields diffuse fluorescence in the cytoplasm. However, if endosomal escape is low, the signal in the cytoplasm might be too weak to be detected (Smith, Selby, Johnston, & Such, 2019). Therefore, it cannot be determined if low endosomal escape results from a small degree of endosomal damage or insufficient release from ruptured endosomes (Day & Sletten, 2021).

To indirectly detect the endosomal escape of nanoparticles, cells can additionally be treated with fluorescent dyes or labelled molecules, which are also taken up into endosomes and hence act as reporters. For instance, the membrane impermeable fluorescent dye calcein can be used. Calcein displays self-quenching at high concentrations and low pH. Thus, it produces punctate fluorescence inside endosomes and enhanced diffuse fluorescence upon its release and dispersal in the cytoplasm as illustrated in Figure 6 (Hausig-Punke, Richter, Hoernke, & Brendel, 2022). A main limitation of this

method is that minor leaks in the endosomal membrane may allow the release of calcein, a small molecule, without the endosomal escape of the polyplexes (Smith, Selby, Johnston, & Such, 2019). Alternatively, fluorescently labelled dextrans can be used as reporters of endosomal escape of PEI polyplexes (Ogris, Carlisle, Bettinger, & Seymour, 2001). Dextrans are polysaccharides which are endocytosed and diffuse in the cytoplasm after endosomal escape. Because dextrans exist in different sizes (3-2000 kDa), the extent of the endosomal damage and size of the escaped material can be estimated by using different dextrans (Selby, Cortez-Jugo, Such, & Johnston, 2017).

Furthermore, acidic transport vesicles can be labelled by incubating the cells with acidotropic fluorescent dyes such as LysoTracker dyes, as shown in Figure 6. This way, endosome size and swelling can be monitored. Also, endosomal rupture can be indirectly visualised as the dye disperses in the cytoplasm (Rehman, Hoekstra, & Zuhorn, 2013). There are various LysoTracker dyes with different emission spectra, enabling multiplexing (Day & Sletten, 2021). However, as they accumulate in organelles with an acidic pH, their performance can potentially be affected by PEI mediated pH buffering in the endosomes (Selby, Cortez-Jugo, Such, & Johnston, 2017).

In contrast to the previously mentioned methods, fluorescently labelled proteins of the galectin family can be utilised to detect endosomal damage directly. To this end, cell lines have been genetically engineered for them to produce labelled galectins (Kilchrist, et al., 2019). Galectin 1, 3, 8 and 9 have been shown to be recruited from the cytoplasm to β-galactosides at the inner face of endosomal membranes in response to endosomal damage, forming clusters (Munson, et al., 2021). This is also depicted in Figure 6. Galectin clusters are visible as fluorescent spots whereas cytoplasmic galectins register as diffuse fluorescence. This approach allows to quantify endosomal damage by counting the galectin clusters and normalising by the number of cells, (Day & Sletten, 2021). Importantly, galectin clustering is not influenced by the mechanism of endosomal damage (Aits, et al., 2015).

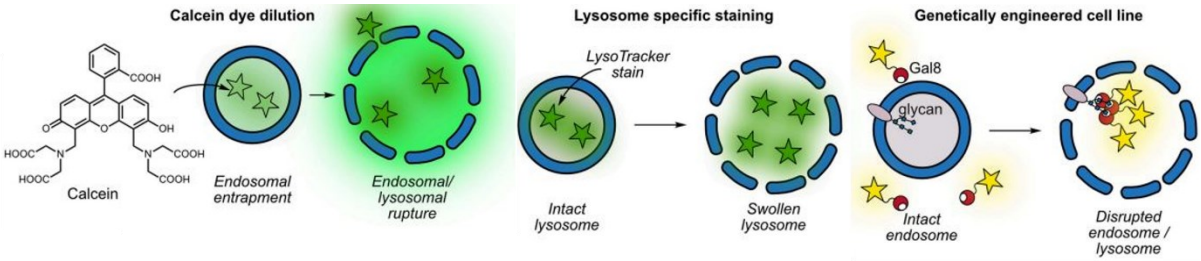

Figure 6: Different methods for visualising endosomal escape of nanoparticles (modified from Day and Sletten, 2021)

3. Aims of the Thesis

This thesis comprises two projects which involve *in vitro* transfections of HeLa cells with Cypridina luciferase encoding mRNA on the one hand and splice switching oligonucleotides (SSOs) on the other hand. In both cases, the main goal was to evaluate LPEIs and LPEI derived polymers as nucleic acid carriers. One subgoal was to analyse how efficiently the polymers facilitate the delivery of mRNA and SSOs to their respective site of action inside the cell. For both mRNA and SSOs, this entailed analysing the endosomal escape of polyplexes. Here, a genetically engineered HeLa cell line, HeLa mRuby-3 galectin 8, was used which stably produces mRuby-3 labelled galectin 8 (Gal8). Gal8 clustering was visualised using fluorescence microscopy and, to quantitatively analyse the endosomal damage, Gal8 clusters were counted and normalised by the number of nuclei in the same field of view using ImageJ via Fiji (Schindelin, et al., 2012). Ahead of the transfection experiments, HeLa mRuby-3 galectin 8 cells were validated as a model system for visualising and quantifying endosomal damage. To this end, the cells were treated with the lysosomotropic agent chloroquine.

In the mRNA transfection experiments, it was analysed how efficiently cLPEI and LPEI 10-PEG-Cys facilitate the endosomal escape of Cypridina mRNA in comparison to the respective unmodified polymers, i.e. LPEI 2.5 and LPEI 10. Beforehand, optimisation experiments were performed with mRNA to select the parameters and experimental design for the final transfections.

In the SSO transfection project, cLPEI and LPEI 2.5 were tested regarding the endosomal escape and nuclear entry of SSOs. To this end, HeLa mRuby-3 galectin 8 cells were transfected with SSOs which were labelled with Alexa Fluor 750 (AF750-SSOs) for visualising and quantification. Before the final experiments, a test transfection of HeLa mRuby-3 galectin 8 cells with AF750-SSOs was performed to determine whether the presence of mRuby-3 and AF750 leads to any cross-over of fluorescence signal between the two fluorophores. In addition, splice correction was analysed in HeLa pLuc 705 via firefly assay after transfection with LucSSOs and NCSSOs in the form of naked SSOs and cLPEI and LPEI 2.5 based polyplexes.

4. Materials and Methods

4.1. Materials

Material	Details
HeLa mRuby-3 galectin 8	provided by Ass.-Prof. Dr. Ulrich Lächelt Division of Pharmaceutical Technology and Biopharmaceutics, University of Vienna
complete medium for HeLa mRuby-3 galectin 8	basal medium: Dulbecco′s Modified Eagle′s Medium - high glucose, Sigma-Aldrich; supplements, all by Sigma-Aldrich: 1 % penicillin-streptomycin, 2 % L-glutamine solution 200 mM, 10 % FCS
T-75 flasks	Cell culture flask, T-75, surface: Standard, Filter cap, Sarstedt
PBS	Dulbecco′s Phosphate Buffered Saline, Sigma-Aldrich
Tryp-LE	Tryp-LE express enzyme 1X phenol red, Gibco
15 ml centrifuge tube	Starlab
centrifuge	Heraeus Megafuge 16 R, Thermo Fisher Scientific
counting chamber	Neubauer-improved, Paul Marienfeld GmbH & Co. KG
transparent 96 well plates	96 Well Microplate, PS, F-Bottom,Greiner Bio-One
microscope	IX73 Inverted Microscope, Olympus
HBG	5 % glucose w/v, 20 mM HEPES pH 7.4, MMCT, University of Vienna
MilliQ (MQ) water	arium® pro, Sartorius
cLPEI 0.5 (2000 µg/ml stock in MQ water)	MMCT, University of Vienna
LPEI 2.5 (2000 µg/ml stock in MQ water)	MMCT, University of Vienna
LPEI 10-PEG-Cys (937.7 µg/ml stock in MQ water)	MMCT, University of Vienna
LPEI 10 (2500 µg/ml stock in MQ water)	MMCT, University of Vienna
AF750-SSOs (1000 µg/ml stock in MQ water)	The oligonucleotides used in this work were supplied by GSK (Glynn Williams, Jonathan Northall) as part of their contribution to the COMPACT project.
white 96 well plates	BRANDplates® microtitration plate, 96-well, cellGrade™, PS, BIO-CERT® CELL CULTURE QUALITY, sterile
HeLa pLuc 705	obtained during the IMI collaborative project COMPACT
complete medium for HeLa pLuc 705	basal medium: Dulbecco′s Modified Eagle′s Medium - high glucose, Sigma-Aldrich; supplements, all by Sigma-Aldrich: 1 % penicillin-streptomycin, 2 % L-glutamine, 10 % FCS, hygromycin B solution
LucSSOs (1000 µg/ml stock in MQ water)	The oligonucleotides used in this work were supplied by GSK (Glynn Williams, Jonathan Northall) as part of their contribution to the COMPACT project.
NCSSOs (1000 µg/ml stock in MQ water)	
LBL	Lar-buffer + 0.474 mM luciferin, 0.2 µl sterile filtered, MMCT, University of Vienna
luminometer	GloMax® Navigator Microplate Luminometer

1 mg/ml DAPI stock solution	DAPI ready made solution, Sigma-Aldrich
chloroquine stock (1 mg/ml)	1:50 dilution in PBS from a stock in MQ water, MMCT, University of Vienna
2 % bovine gelatine	MMCT, University of Vienna

4.2. Endosomal Escape Model Evaluation

4.2.1. Seeding

HeLa mRuby-3 galectin 8 cells were grown in complete medium in T-75 flasks, at 37 °C with 5 % CO_2. For harvesting the cells, the old medium was discarded and the cells were washed with 7 ml PBS. Then, to detach the cells from the culture flask, 1 ml TrypLE was pipetted onto the cells and they were incubated at 37 °C for 4 min. The cells were rinsed off with 7 ml complete medium which inactivates the TrypLE. The suspension was transferred into a 15 ml conical centrifuge tube and centrifuged for 5 min at 200 x g. Afterwards, the supernatant was removed, and the pellet was resuspended in 1 ml complete medium. For counting the cells, the suspension was diluted and cells from the dilution were counted using a counting chamber. These counts were then used to calculate the cell concentration of the original suspension. In the first of 2 model evaluation experiments, the cells were seeded on a transparent 96 well plate. In order to find an adequate cell count to achieve a 60-75% confluency after 24 h, wells with 10,000 and 15,000 cells were prepared. Here, the required amount of cell suspension was added to complete medium to a total volume of 200 µl per well. As a control, the same amounts of HeLa pLuc 705, which do not produce labelled Gal8, were seeded on the same plate.

With the 96 well plates, the cells can be observed under the microscope with only 20 fold magnification. To see if the magnification affects the quantification, a second experiment was conducted which was adapted for seeding on coverslips in 12 well plates to allow imaging with a 60 fold magnification. For preparing the plates, the coverslips were placed into the wells and incubated in 5 ml gelatine for 20 min at room temperature to coat them, so the cells could attach. They were then washed 3 x with 5 ml PBS. Cell suspension with 50,000 cells was pipetted onto each coverslip and the wells were filled with complete medium to a total volume of 2 ml.

4.2.2. Treatment with Chloroquine

On the day after seeding the cells, they were examined under the microscope. Based on the confluency, the wells with 10,000 seeded cells on the 96 well plate (50,000 cells on the 12 well plate) were chosen for the treatment with chloroquine to examine Gal8 clustering. Here, treatments with 60, 40 and 20 µM chloroquine in phenol red free complete medium were prepared using a 1938 µM stock of chloroquine in PBS. Phenol red free medium was used to obtain a lower background fluorescence during live cell imaging. Approximately 24 h after seeding, the medium was removed and the treatments were added in

duplicates - 200 µl per well on the 96 well plate and 2 ml per well on the 12 well plate. Phenol red free complete medium without chloroquine was used as negative control treatment. The cells were incubated at 37 °C with 5 % CO_2.

4.2.3. Live Cell Imaging

During the first experiment, live cell imaging was conducted to monitor the effect of the treatments. Because the cells had been seeded on a 96 well plate, a 20 fold magnification was used. The cells were observed under the microscope, 3, 6, and 24 h after adding the treatments. Phase contrast with an automatically set exposure time was used to examine the cells. To visualise the Gal8, the cells were imaged with the CY3 filter with an exposure time of 1 s.

4.2.4. Cell Fixation and DAPI Staining

To reduce the background fluorescence and enable a time-flexible acquisition of images, the cells were washed and fixed ahead of imaging. Here, the medium was discarded 24 h after adding the treatments. To remove dead cells, the cells were washed twice with 100 µl PBS. The cells were fixed through incubation in 100 µl of 4 % para-formaldehyde in HBS at room temperature for 40 min. They were then washed 3 x with 100 µl PBS. To stain the nuclei, the cells were incubated in 100 µl of 2 µg/ml DAPI in PBS for 20 min at room temperature. After washing 3 x with 100 µl PBS, the cells were covered with 100 µl PBS. The plate was wrapped in aluminium foil for light protection and stored at 4 °C. For fixing and staining the cells on the 12 well plate, 5 times the volumes listed above were used. The coverslips were then mounted onto microscope slides using 7 µl of mounting solution and sealed on with nail polish.

4.2.5. Imaging of Fixed Cells

In the first experiment, the fixed cells were observed under the microscope with a 20 fold magnification. For the quantification of Gal8 clustering, images were taken of 2 fields of view per well. Phase contrast with an automatically set exposure time was used for examining the cells and selecting the fields of view. The nuclei were visualised with the DAPI filter with 400 ms exposure time. To detect the Gal8 clusters, the CY3 filter was used with an exposure time of 1 s. During the second experiment, the fixed cells were imaged with a 20 fold magnification, using the same settings as for the first experiment. With the 60 fold magnification, immersion oil was used. Again, phase contrast was used with an automatically set exposure time. The nuclei were detected with the DAPI filter with a 10 ms exposure time and Gal8 clusters were imaged using the CY3 filter with an exposure time of 200 ms.

4.2.6. Quantitative Analysis

The Gal8 clustering after treatment with 40 and 60 µM chloroquine was quantified. For each field of view, the Gal8 clusters and the nuclei were counted using ImageJ-win64 via Fiji (Schindelin, et al., 2012). To normalise, the number of clusters per cell of each field of view was calculated, whereby the nuclei count was used as the number of cells. For evaluating the effect of the magnification, the clusters per cell were averaged for each treatment at 20 and at 60 fold magnification. The exact steps are described as follows:

To count the clusters, the RGB CY3 image was converted into a 16 bit greyscale image *(Edit – Options – Conversions – check Scale when converting – Image – Type – select 16-bit)*. To reduce the blur, the background was subtracted *(Process – Subtract background – Rolling ball radius: 50 pixels)*. The Gal8 clusters were defined as the region of interest by setting an intensity threshold *(Image – Adjust – Threshold – Set – Lower threshold level: 29 (for 20 fold magnification) / 35 (for 60 fold magnification), Upper threshold level: 65535 – check Dark background – Apply)*. Overlapping clusters were separated *(Process – Binary – Watershed)*. The clusters were counted *(Analyze – Analyze Particles – Size: 0-120 (for 20 fold magnification) / 0-200 (for 60 fold magnification), (check Pixel units) – Circularity: 0.80-1.00 – Show: Bare Outlines – check: Clear Results, Summarize)*. To count the nuclei, the RGB DAPI image of the same field of view was converted into a 16 bit greyscale image as described above. The nuclei were defined by setting an intensity threshold *(Image – Adjust – Threshold – Set – Lower threshold level: 10 (for 20 fold magnification) / 26 (for 60 fold magnification), Upper threshold level: 65535 – check Dark background – Apply)*. Overlapping nuclei were separated as described for the Gal8 clusters. Then, the nuclei were counted *(Analyze – Analyze Particles – Size: 200-Infinity (for 20 fold magnification) / 500-Infinity (for 60 fold magnification), (check Pixel units) – Circularity: 0.00-1.00 – Show: Bare Outlines – check: Clear Results, Summarize)*.

4.3. mRNA Polyplexes

4.3.1. Optimisation of mRNA Transfection

4.3.1.1. Seeding

For this optimisation experiment, 15,000 HeLa mRuby-3 galectin 8 cells per well were seeded on transparent 96 well plates. The cells were incubated for approximately 16 h at 37 °C with 5 % CO_2. Seeding was conducted as previously described for the endosomal escape model evaluation. However, the number of seeded cells was adjusted to the shorter incubation time, to still achieve a 60-75 % confluency at the time of transfection.

4.3.1.2. Transfection

The cells were transfected approximately 16 h after seeding. First, the medium was removed and 90 µl phenol red free basal medium were added per well. Basal medium is generally used for the addition of polyplexes to enhance their cellular uptake. Phenol red free medium was used for this experiment to obtain a lower fluorescence background during live cell imaging. Then, for each of the used polymers – i.e. cLPEI, LPEI 2.5, LPEI 10-PEG-Cys and LPEI 10 - polyplexes with Cypridina mRNA were formed at N/P ratios 9 and 12 and added onto the cells. To this end, equal volumes of mRNA and polymer in HBG were mixed through flash pipetting to obtain a polyplex solution with a final mRNA concentration of 200 µg/ml. The needed amount of polymer was calculated according to the following equation with 43 as the molecular weight (in Da) of one CH2–CH2–NH unit and 330 as the average molecular weight of one nucleotide: µg polymer = µg mRNA * N/P ratio * 43 / 330. The polyplex solution was diluted 1:10 with HBG and 10 µl dilution containing 200 ng of mRNA were added per well. To create a negative control, 10 µl HBG were added instead of polyplex solution. For the positive control, 200 µl of 40 µM chloroquine in phenol red free complete medium were added to the cells after removing the old medium. Each treatment was added in duplicates. The plates were placed into the incubator (37 °C with 5 % CO_2).

4.3.1.3. Live Cell Imaging

The cells were observed under the microscope at different timepoints after the addition of the polyplexes to monitor Gal8 clustering and to estimate the effects of the different polymers over time. Live cell imaging was conducted as described for the endosomal escape model evaluation.

4.3.2. Transfections with mRNA Polyplexes

4.3.2.1. Workflow

For quantifying the endosomal escape of Cypridina mRNA polyplexes, 3 separate experiments with polyplexes of N/P 9 and 2 experiments with N/P 12 polyplexes were performed, all following the workflow depicted in Figure 7.

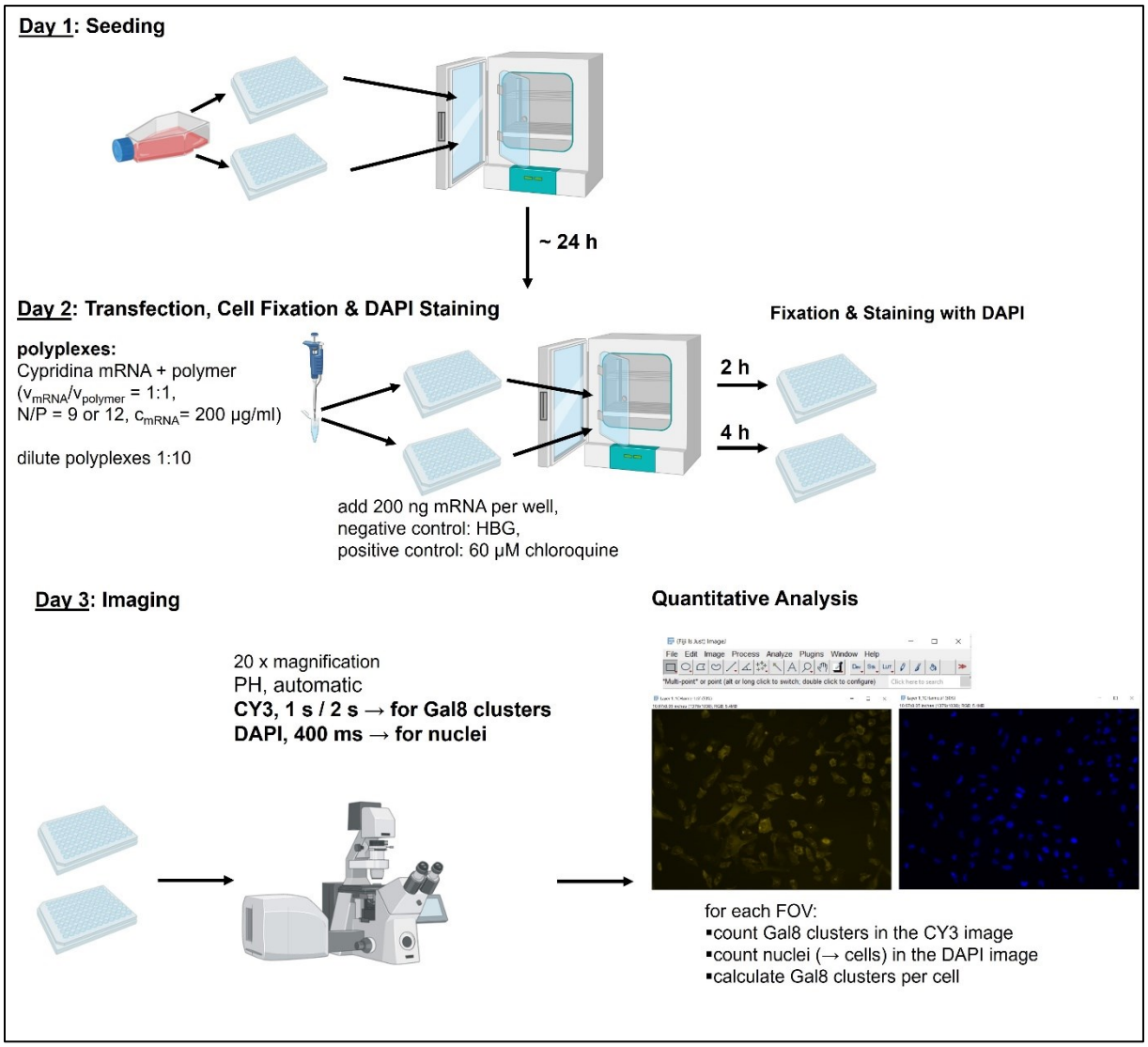

Figure 7: Workflow for analysing the endosomal escape of mRNA polyplexes

4.3.2.2. Seeding

Two transparent 96 well plates were seeded with 10,000 HeLa mRuby-3 galectin 8 cells per well. One plate was prepared for each timepoint (2 h and 4 h after transfection). The plates were placed into the incubator (37 °C, 5 % CO_2).

4.3.2.3. Transfection

After approximately 24 h, the cells were transfected. First, the medium was removed and 90 µl basal medium were added per well. Then, for every polymer - i.e. cLPEI, LPEI 2.5, LPEI 10-PEG-Cys and

LPEI 10 - polyplexes were created at N/P ratios 9 and 12 and 200 ng mRNA were added per well. Polyplex solutions were prepared as described for the optimisation experiment. HBG was used as a negative control. For the positive control, 200 µl of 60 µM chloroquine in complete medium were added onto the cells after removing the old medium. Every treatment was added in duplicates. The plates were incubated at 37 °C with 5 % CO_2 for 2 or 4 h, respectively.

4.3.2.4. Cell Fixation and DAPI Staining

After the respective incubation time, the medium was discarded. Then, cells were fixed and the nuclei were stained with DAPI as described for the endosomal escape model validation.

4.3.2.5. Imaging

The fixed cells were observed under the microscope with a 20 fold magnification. For each well, images were taken of 3 fields of view. Phase contrast with an automatically set exposure time was used for examining the cells and selecting suitable fields of view. The nuclei were visualised with the DAPI filter with 400 ms exposure time. For the Gal8 clusters, the CY3 filter was used and exposure times of 1 s and 2 s were tested.

4.3.2.6. Quantitative Analysis

For each field of view, the Gal8 clusters and nuclei were counted using ImageJ. The protocol for the Gal8 cluster count is similar to that used for the endosomal escape model evaluation, but the settings for the lower intensity threshold, particle size range and circularity were adjusted:

The RGB CY3 image was converted into a 16 bit greyscale image *(Edit – Options – Conversions – check Scale when converting – Image – Type – select 16-bit)*. To reduce the blur, the background was subtracted *(Process – Subtract background – Rolling ball radius: 50 pixels).* The Gal8 clusters were defined as the region of interest by setting an intensity threshold *(Image – Adjust – Threshold – Set – Lower threshold level: 30 (for 1 s exposure time) / 55 (for 2 s exposure time), Upper threshold level: 65535 – check Dark background – Apply).* Overlapping clusters were separated *(Process – Binary – Watershed).* The clusters were counted *(Analyze – Analyze Particles – Size: 4-30 (check Pixel units) – Circularity: 0.90-1.00 – Show: Bare Outlines – check: Clear Results, Summarize).*The RGB DAPI image of the same field of view was converted into a 16 bit greyscale image as described above. The nuclei were defined by setting an intensity threshold *(Image – Adjust – Threshold – Set – Lower threshold level: 10, Upper threshold level: 65535 – check Dark background – Apply)*. Overlapping nuclei were separated as described for the Gal8 clusters. Then, the nuclei were counted *(Analyze – Analyze Particles – Size: 200-Infinity (check Pixel units) – Circularity: 0.00-1.00 – Show: Bare Outlines – check: Clear Results, Summarize)*.

4.3.2.7. Statistical Analysis

To compare the endosomal escape of the different mRNA polyplexes, the mean Gal8 clusters per cell and standard deviation across all experiments were calculated and a two-tailed Welch´s t-test was performed (Two Sample T-Test Calculator (Welch's T-test), 2024).

4.4. SSO Polyplexes

4.4.1. Optimisation of SSO Transfection

A test transfection with AF750-SSOs was conducted using HeLa mRuby-3 galectin 8 and HeLa pLuc 705 cells to see if AF750-SSOs could be tracked without substantial bleed through effects between mRuby-3 and AF750. Here, LPEI 10 was used to create the polyplexes. The workflow of this experiment was kept the same for studying endosomal escape and nuclear entry, which is described below and illustrated in Figure 8.

4.4.2. Transfections with SSO Polyplexes

4.4.2.1. Endosomal Escape and Nuclear Entry

4.4.2.1.1. Workflow

For analysing the endosomal escape and nuclear entry of AF750-SSOs polyplexes, 3 transfection experiments were performed with cLPEI and 2 experiments using LPEI 2.5. All experiments followed the workflow depicted in Figure 8.

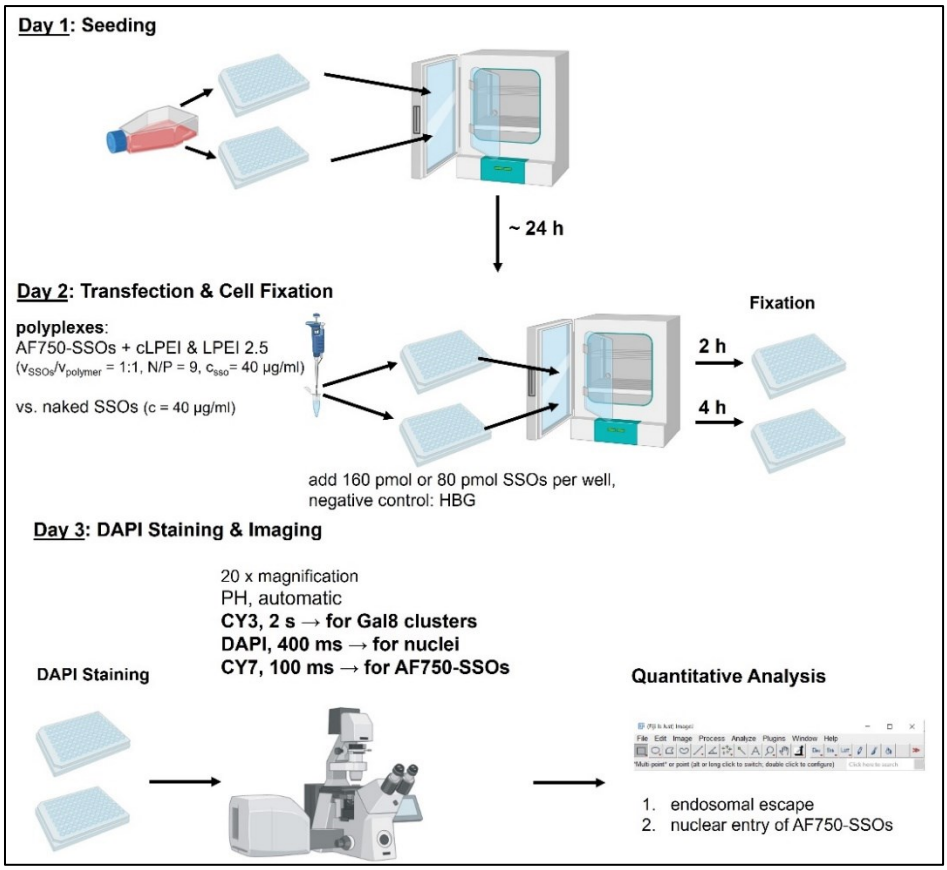

Figure 8: Workflow for analysing the endosomal escape and nuclear entry of AF750-SSO polyplexes

4.4.2.1.2. Seeding

Analogous to the mRNA transfection experiments, for both the 2 h and 4 h timepoint a transparent 96 well plate was seeded with 10,000 HeLa mRuby-3 galectin 8 cells per well. The plates were incubated at 37 °C, with 5 % CO_2.

4.4.2.1.3. Transfection with AF750-SSOs

The cells were transfected with AF750-SSOs approximately 24 h after seeding. Before the transfection, the old medium was removed and 76 µl phenol red free basal medium were added per well. For both cLPEI and LPEI 2.5, fresh polyplexes were created with N/P 9. Here, equal volumes of AF750-SSOs and polymer in HBG were mixed through flash pipetting to obtain a polyplex solution with a final AF750-SSO concentration of 40 µg/ml following the same principle as for the mRNA transfections. Then, 24 µl of polyplex solution were added per well for the 160 pmol treatments. For 80 pmol AF750-SSOs, it was diluted 1:2 beforehand. In addition, the cells were treated with 80 and 160 pmol naked AF750-SSOs in HBG. As a negative control, HBG was used. The plates were placed into the incubator (37 °C, 5 % CO_2).

4.4.2.1.4. Fixation and DAPI Staining

After the respective incubation time, the medium was removed. The cells were then washed and fixed as described for the endosomal escape model validation. After washing the cells twice with 100 µl PBS, they were covered with 100 µl PBS. The plate was wrapped in aluminium foil for light protection and stored overnight at 4 °C. The following day, the nuclei were stained with DAPI as outlined for the model validation.

4.4.2.1.5. Imaging

The fixed cells were observed under the microscope with a 20 fold magnification. For each well, images were taken of 3 fields of view. Phase contrast with an automatically set exposure time was used for examining the cells and selecting the fields of view. The nuclei were visualised with the DAPI filter with 400 ms exposure time. For the Gal8 clusters, the CY3 filter was used with an exposure time of 2 s.

4.4.2.1.6. Quantitative Analysis of Endosomal Escape

The number of Gal8 clusters per cell was determined for each field of view, following the same protocol as for the mRNA transfections.

4.4.2.1.7. Semi-Quantitative Analysis of Nuclear Entry

Three different approaches to semi-quantitatively analysing the nuclear entry of AF750-SSOs were tested.

Percentage of AF750$^+$ Nuclei

For each field of view, the percentage of nuclei exhibiting an AF750 signal above a specified intensity (AF750$^+$ nuclei) was determined. Total nuclei were counted using the DAPI image, as described for the endosomal escape model validation. The number of AF750$^+$ nuclei was determined using the respective CY7 image. To this end, the image was converted to 16 bit *(Edit – Options – Conversions – check Scale when converting – Image – Type – select 16-bit)* and a lower intensity threshold was set for each image individually to select nuclei with a relatively high AF750 signal *(Image – Adjust – Threshold – Set – Lower threshold level: individual value, Upper threshold level: 65535 – check Dark background – Apply)*. With the aim to only include whole nuclei, roughly circular objects were selected *(Analyze – Analyze Particles – Size: 200-Infinity (check Pixel units) – Circularity: 0.40-1.00 – Show: Bare Outlines – check: Clear Results, Summarize)*.

Mean AF750 Intensity in the Nuclei

For measuring the mean AF750 intensity in the nuclei, the DAPI image was converted into a 16 bit image *(Edit – Options – Conversions – check Scale when converting – Image – Type – select 16-bit)*. An intensity threshold was set to define the nuclei (*Image – Adjust – Threshold - Set - Lower threshold level: 10, Upper threshold level: 65535 - check Dark background – Apply*). Then, the selected nuclei were defined as the region of interest (*Edit – Selection - Create Selection*). The corresponding 16 bit CY7 image was overlaid with the outlines of the nuclei (*Edit – Selection - Restore Selection*). Finally, the mean intensity across this area was measured (*Analyze – Set Measurements (select: area, mean grey value, SD) - Redirect to: CY7 16-bit image) Ctrl + M).*

Ratio of Mean AF750 Intensity in the Nuclei to Mean AF750 Intensity Outside

In addition, the ratio of the mean intensity in the nuclei to the mean intensity on the outside was calculated. For determining the mean intensity outside the nuclei, the same steps as for the mean intensity inside were carried out, yet a white background was set (*Image – Adjust – Threshold - Set - Lower threshold level: 10, Upper threshold level: 65535 - uncheck Dark background – Apply*).

4.4.2.1.8. Statistical Analysis

To evaluate the endosomal escape and nuclear entry of the different polyplexes, the values were averaged across all experiments, and the calculated mean values were compared by conducting Welch´s t-test as described for the mRNA transfection.

4.4.2.2. Splice Correction

4.4.2.2.1. Workflow

For determining the transfection efficiency of cLPEI and LPEI 2.5 based SSO polyplexes, 3 splice correction assays using the HeLa pLuc 705 model were performed according to the workflow depicted in Figure 9.

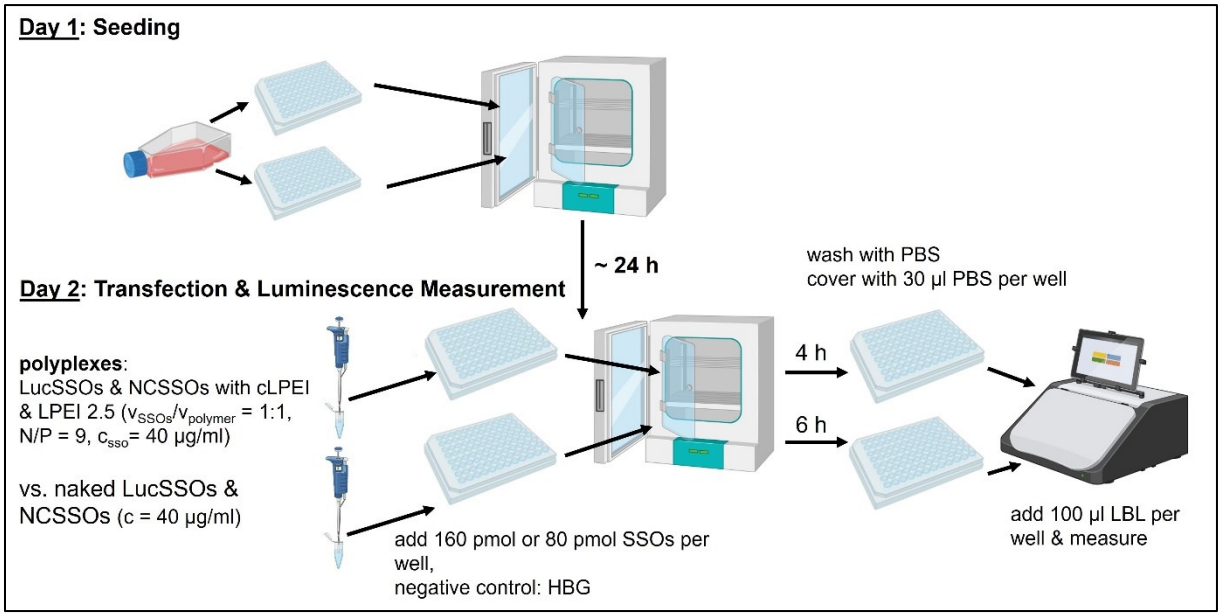

Figure 9: Workflow for analysing splice correction by SSO polyplexes

4.4.2.2.2. Seeding

For the luminescence measurement, 2 white 96 well plates were seeded with 10,000 HeLa pLuc 705 cells per well – one plate for the 4 h and another for the 6 h readout. The plates were placed into the incubator (37 °C, 5 % CO_2).

4.4.2.2.3. Transfection with LucSSOs and NCSSOs

The cells were transfected approximately 24 h after seeding. Before the transfection, the old medium was removed and 76 µl basal medium were added per well. For both cLPEI and LPEI 2.5 fresh polyplexes with N/P 9 were created. In this instance, separate polyplex solutions were prepared for the 2 plates and the 2 SSO dosages. Equal volumes of SSOs and polymer in HBG were mixed through flash pipetting to obtain a polyplex solution with a final SSO concentration of 40 µg/ml following the same principle as for the mRNA transfections. Then, 24 µl of polyplex solution were added per well. In addition, the cells were treated with 80 and 160 pmol of both naked LucSSOs and naked NCSSOs in

HBG. As a negative control, HBG was used. The treatments were added in triplicates. The plates were placed into the incubator (37 °C, 5 % CO_2).

4.4.2.2.4. Luminescence Measurement

After 4 and 6 h, the cells on the respective plate were washed with PBS and covered with 30 µl PBS. The luminescence was then measured with a luminometer which was set to inject 100 µl LBL per well. To account for the background signal, empty wells were included in the measurement. Regarding the incubation times until the luminescence measurement, it was decided to add 2 h to the selected timepoints for the endosomal escape and nuclear entry experiments (2 and 4 h after transfection) to allow more time for splice correction.

4.4.2.2.5. Statistical Analysis

The luminescence values were averaged across 3 experiments, and the mean background value was subtracted from the mean values. In addition, the splice factors were calculated for the carriers and naked SSOs. Here, the mean luminescence value after transfection with LucSSOs was divided by the mean value after transfection with NCSSOs. To determine the statistical significance of the differences between the treatments, Welch´s t-test was carried out as for the mRNA and AF750-SSO transfections.

5. Results

5.1. Endosomal Escape Model Evaluation

HeLa mRuby-3 galectin 8 was first studied for background fluorescence levels and validating the endosomal disruption behaviour by employing chloroquine, which is a reported lysosomotropic agent. As depicted in Figure 10, untreated (UT) HeLa pLuc 705 show no signal in the CY3 channel. In contrast, HeLa mRuby-3 galectin 8 cells exhibit diffuse fluorescence in the cytoplasm, indicating dispersed Gal8. With the 60 µM chloroquine treatment, occasional clusters appear after 3 h, mainly visible in rounded cells. After 6 h, a few Gal8 clusters can be detected in living cells. Some of the clusters are indicated by blue arrows. This suggests an onset of Gal8 clustering between 3 and 6 h after adding 60 µM chloroquine.

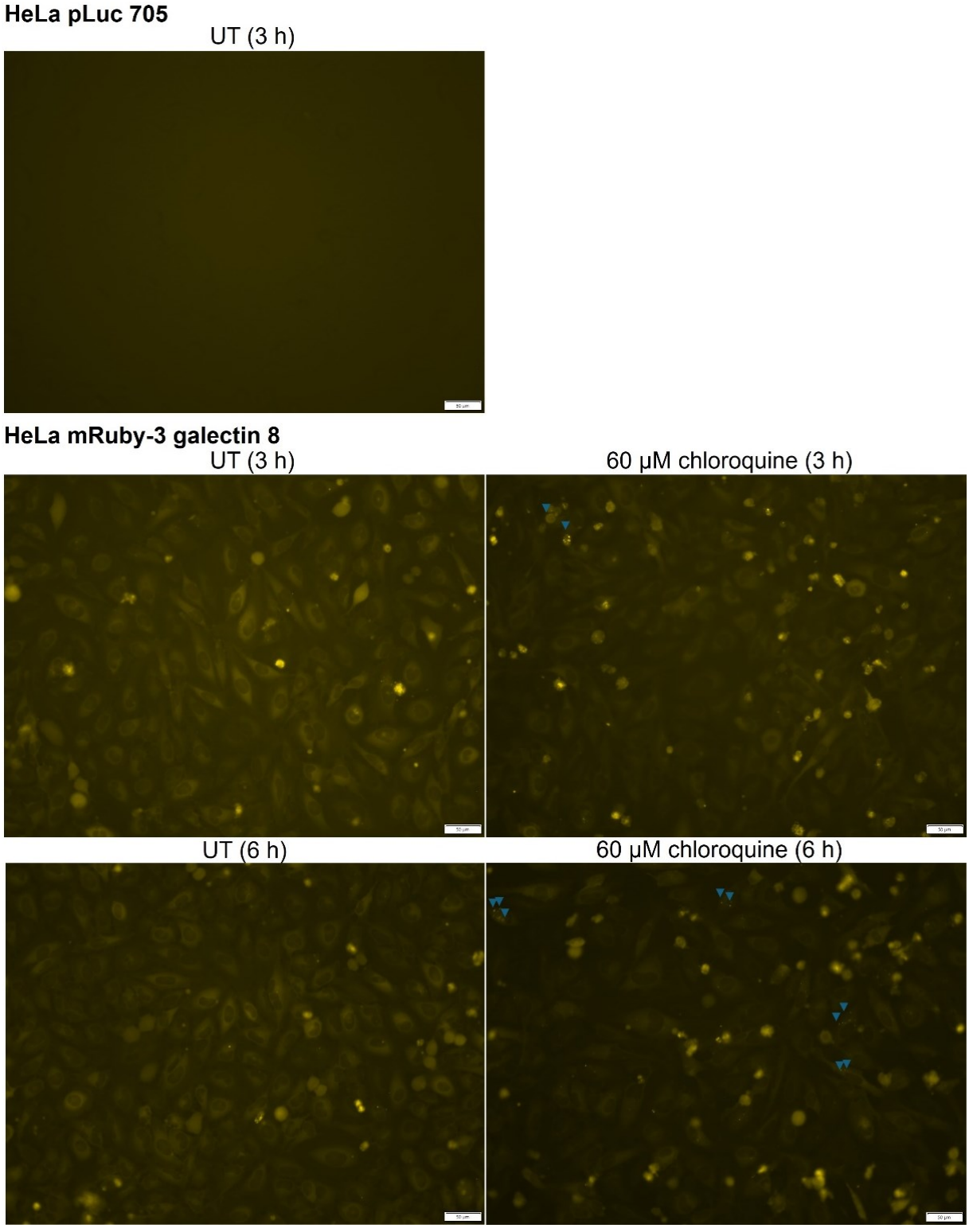

Figure 10: Live cell imaging of HeLa pLuc 705 (control) and HeLa mRuby-3 galectin 8 cells, 3 and 6 h after the chloroquine treatment; magnification: 20 x (scale bar: 50 µm), channel: CY3, exposure time: 1 s

Shown in Figure 11 are images of living and fixed HeLa mRuby-3 galectin 8 cells, 24 h after adding the chloroquine treatments. Here, 60 and 40 µM chloroquine led to clear Gal8 clusters whereas the 20 µM treatment did not cause comparable clustering. Also, a high number of dead cells can be observed in live cell imaging after adding 60 and 40 µM chloroquine, demonstrating the cytotoxic effect of chloroquine.

The images of fixed cells display a lower background fluorescence and fewer rounded cells. The cell morphology resembles that of untreated living cells, indicating that the fixation does not damage the cells. Therefore, the same cell fixation protocol was followed in subsequent experiments for quantifying Gal8 clustering.

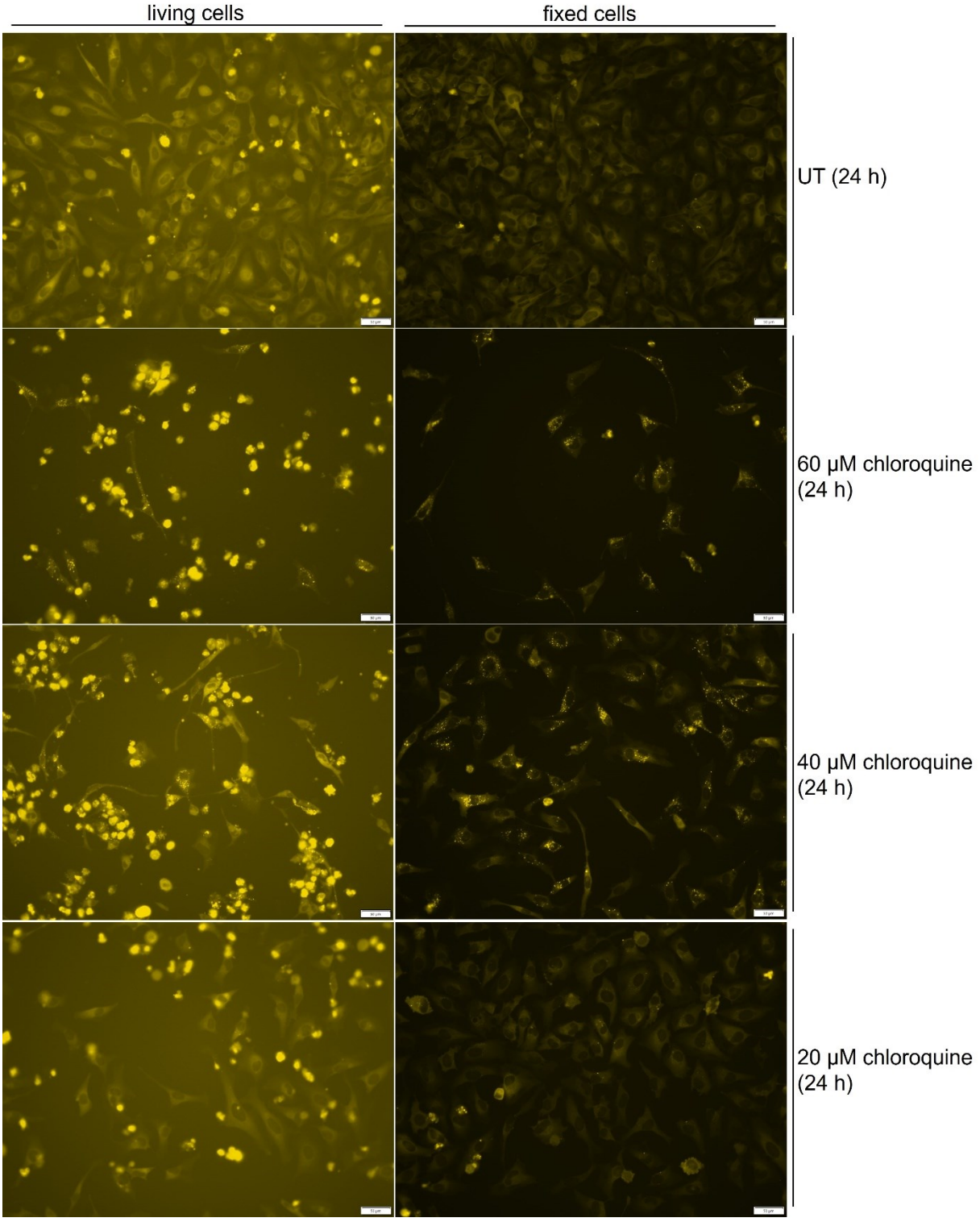

Figure 11: Living and fixed HeLa mRuby-3 galectin 8 cells, 24 h after the chloroquine treatment; magnification: 20 x (scale bar: 50 µm), channel: CY3, exposure time: 1 s

Figure 12 depicts 20 and 60 fold magnified images of HeLa mRuby-3 galectin 8 cells, fixed 24 h after the chloroquine treatment. In Figure 13, the results of the 2 chloroquine assays are compiled. For each experiment, 2 wells per treatment and images of 2 fields of view per well were included. Hence, the columns are means of 8 values for Gal8 clusters per cell. The error bars represent the standard deviations. Expectedly, because a smaller section of the sample is shown in greater detail with a 60 fold magnification, the number of Gal8 clusters per cell is larger than with 20 fold magnification. With the 60 fold magnification, more images per sample would have to be taken for a realistic representation of Gal8 clustering. When the cells were imaged with 60 fold magnification, the values for both chloroquine concentrations are twice as high as with the 20 fold magnification. This suggests that the difference between the treatments is comparable, and that the results are reproducible. To save material, it was decided to use 96 well plates and image with a 20 fold magnification in the final experiments.

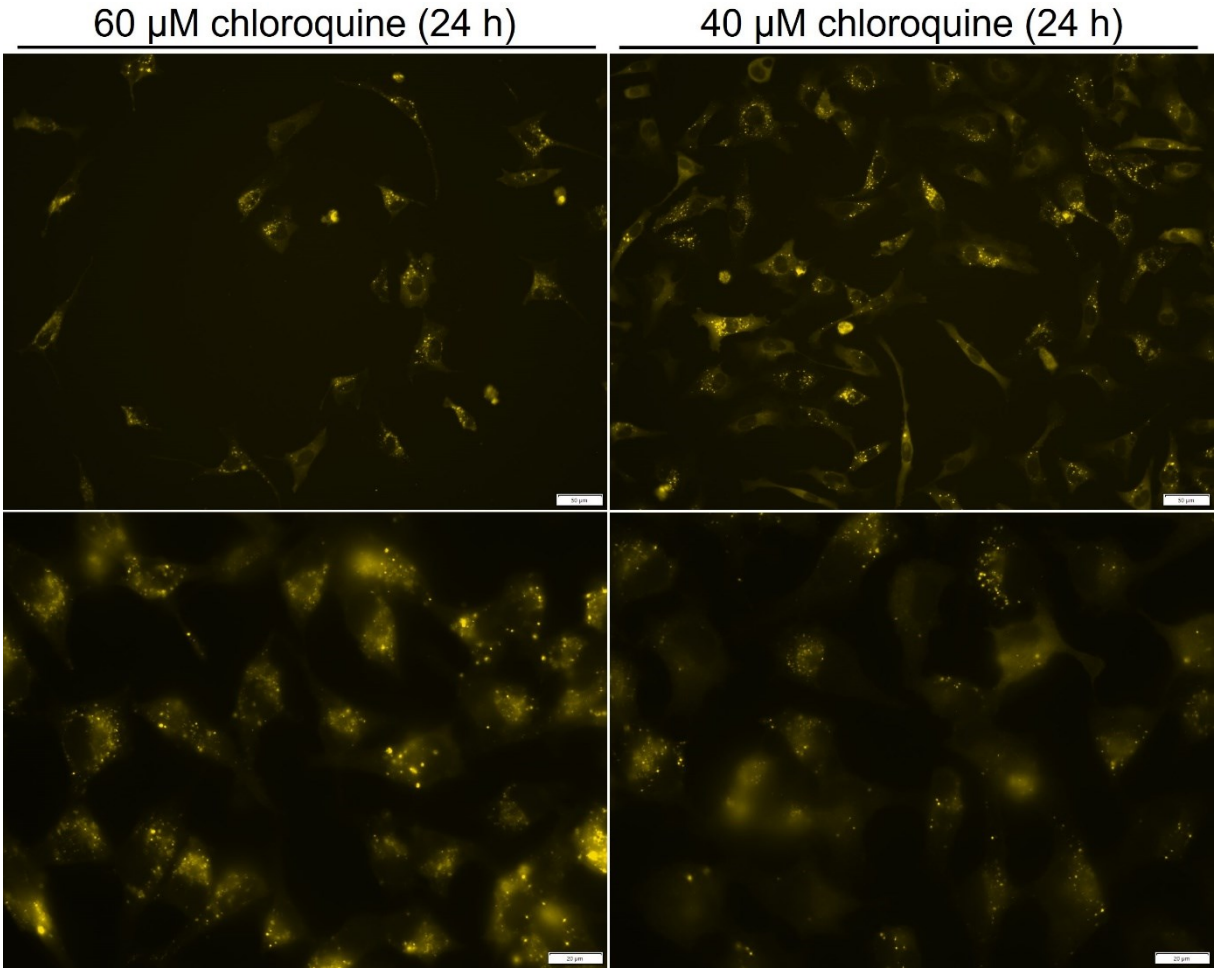

Figure 12: 20 and 60 fold magnified images of fixed HeLa mRuby-3 galectin 8 cells, 24 h after the chloroquine treatment; top: magnification: 20 x (scale bar: 50 µm), channel: CY3, exposure time: 1 s; bottom: magnification: 60 x (scale bar: 20 µm), channel: CY3, exposure time: 200 ms

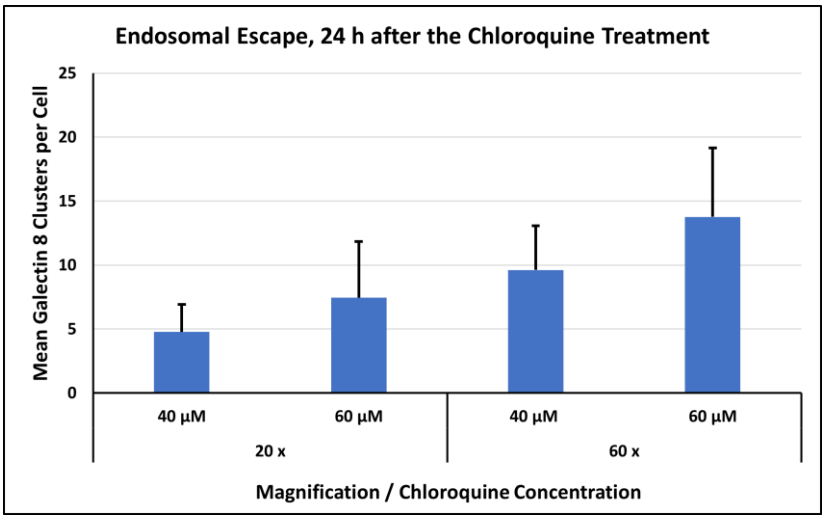

Figure 13: Mean Galectin 8 clusters per cell, 24 h after the chloroquine treatment; means and standard deviations from 8 values (2 experiments with 2 wells per treatment and 2 fields of view per well)

5.2. mRNA Polyplexes

5.2.1. Optimisation of mRNA Transfection

Depicted in Figure 14 are images of HeLa mRuby-3 galectin 8 cells from live cell imaging at 2 timepoints (i.e. at 1.5 h or 2 h and at 4 h) after transfection with cLPEI and LPEI 2.5 based mRNA polyplexes. At the earlier timepoints, there is a higher level of Gal8 clustering with cLPEI than with LPEI 2.5. Four h after adding the polyplexes, considerably more dead cells are visible with cLPEI, suggesting that it is more cytotoxic than LPEI 2.5. Moreover, transfection with cLPEI polyplexes displays less Gal8 clustering after 4 h than after 1.5 h. This suggests that endosomal damage by cLPEI and escape of polyplexes largely occurs within this timeframe. In contrast, with LPEI 2.5 new Gal8 clusters emerged between 2 and 4 h after transfection. These results indicate that cLPEI causes endosomal damage faster than LPEI 2.5. Similar effects were observed for LPEI 10-PEG-Cys and LPEI 10. Results from live cell imaging of HeLa mRuby-3 galectin 8 cells after adding LPEI 10-PEG-Cys and LPEI 10 based mRNA polyplexes and after adding HBG buffer and 40 µM chloroquine in phenol red free complete medium as a negative and positive control are depicted in Figure I and Figure II in the appendix.

To reflect the kinetics of endosomal escape, it was decided to fix the cells 2 and 4 h after transfection. This required preparing separate plates for the timepoints. Also, because these incubation times are relatively short, all treatments had to be added within a short period of time. For this reason, the final mRNA transfections were carried out as partner experiments whereby the polyplex solutions to be added where prepared by Elisa Kulterer. In addition, it was decided to use 60 µM chloroquine as a positive control to obtain a higher level of Gal8 clustering.

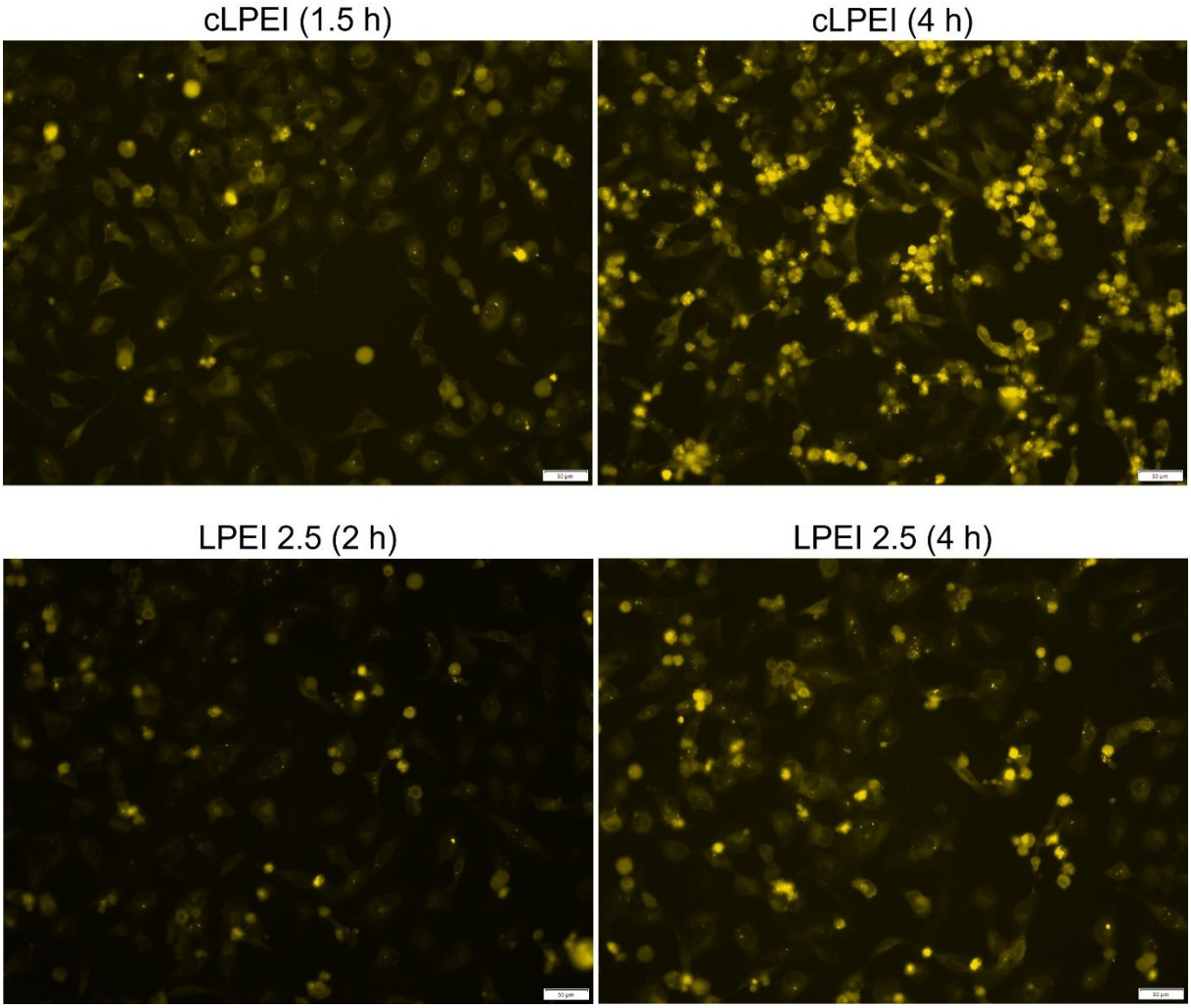

Figure 14: Live cell imaging of HeLa mRuby-3 galectin 8 cells at an earlier timepoint (1.5 or 2 h) and 4 h after adding Cypridina mRNA polyplexes with cLPEI and LPEI 2.5; polyplexes formed with N/P = 12 and c_{mRNA} = 200 µg/ml; 200 ng of mRNA added per well; magnification: 20 x (scale bar: 50 µm), channel: CY3, exposure time: 1 s

5.2.1. Transfections with mRNA Polyplexes

Shown in Figure 15 are images of HeLa mRuby-3 galectin 8 cells after receiving HBG buffer and 60 µM chloroquine as a negative and positive control for Gal8 clustering, respectively. HBG treated cells do not exhibit Gal8 clustering whereas clusters can be seen 4 h after the 60 µM chloroquine treatment.

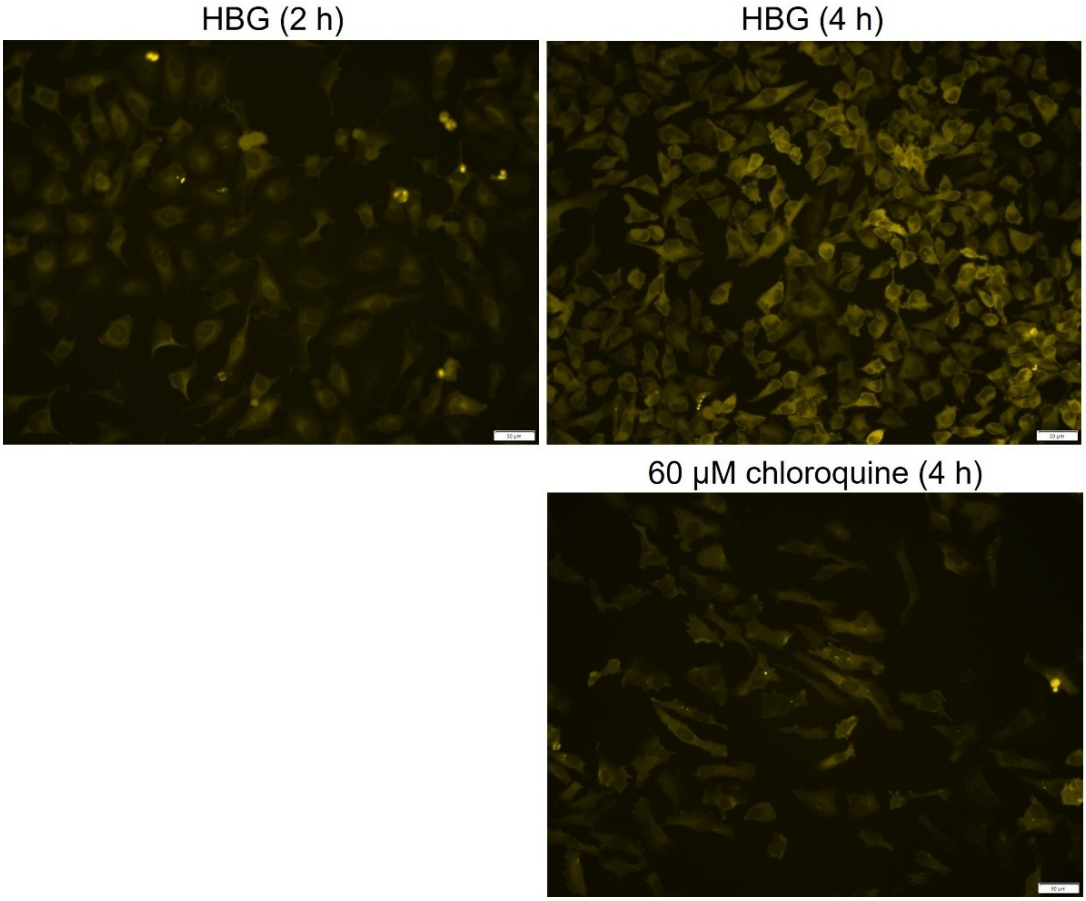

Figure 15: HeLa mRuby-3 galectin 8 cells 2 and 4 h after treatment with HBG (negative control) and 4 h after adding 60 µM chloroquine (positive control); magnification: 20 x (scale bar: 50 µm), channel: CY3, exposure time: 1 s

Figure 16 shows representative images of cells 2 h and 4 h after transfection with Cypridina mRNA polyplexes based on cLPEI, LPEI 2.5, LPEI 10-PEG-Cys and LPEI 10 and prepared with N/P 9. At the 2 h timepoint, cells treated with cLPEI and LPEI 10-PEG-Cys based polyplexes exhibit more Gal8 clustering compared to when the respective unmodified polymers, LPEI 2.5 and LPEI 10, were used. After 4 h, they display less clustering compared to 2 h after the transfection, whereas no definite time difference can be seen for LPEI 2.5 and LPEI 10 polyplexes.

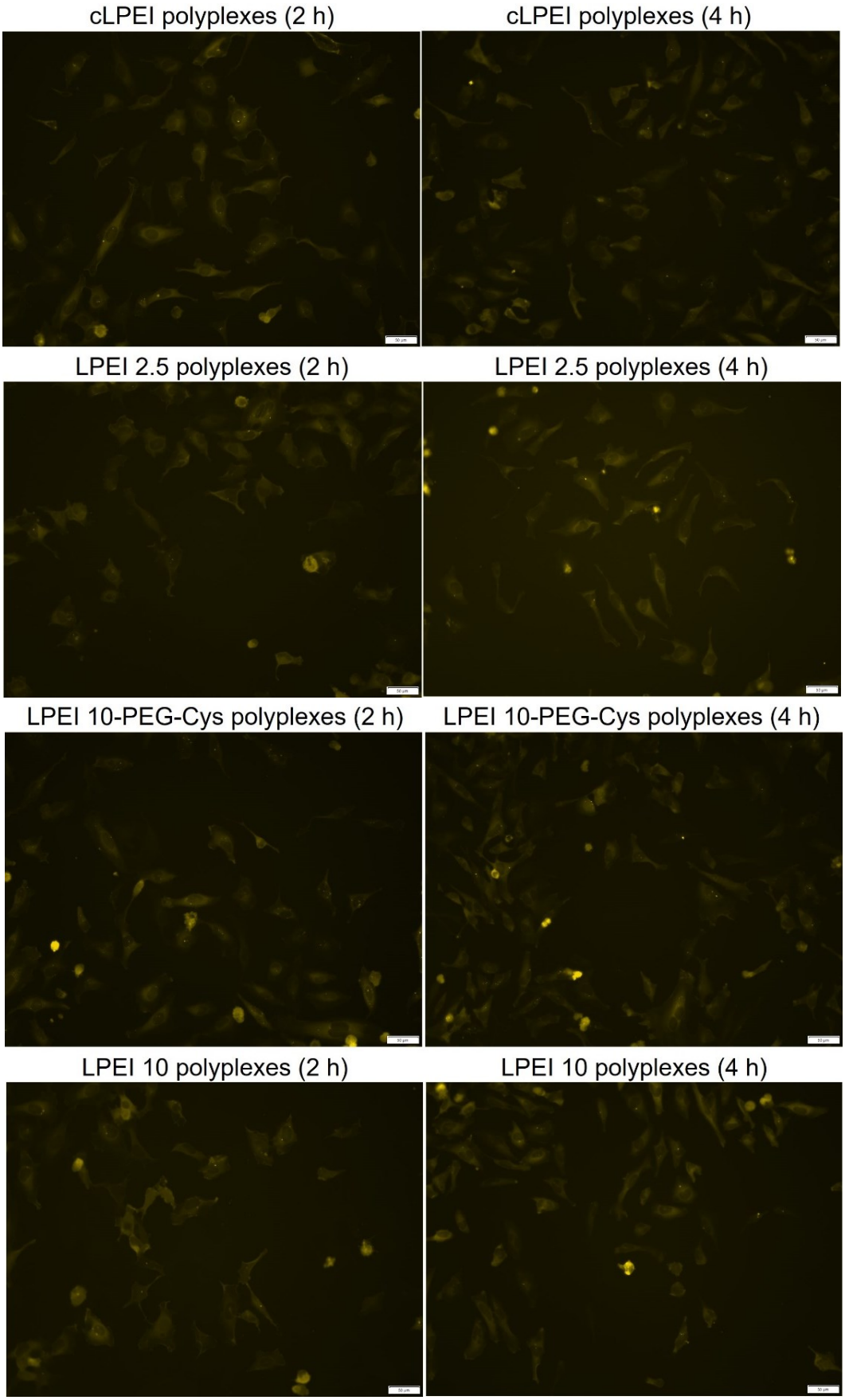

Figure 16: HeLa mRuby-3 galectin 8 cells 2 and 4 h after adding Cypridina mRNA polyplexes with cLPEI, LPEI 2.5, LPEI 10-PEG-Cys and LPEI 10; polyplexes formed with N/P = 9 and c_{mRNA} = 200 µg/ml; 200 ng of mRNA added per well; magnification: 20 x (scale bar: 50 µm), channel: CY3, exposure time: 1 s

To illustrate the performance of the ImageJ count, a representative DAPI and CY3 image of cells treated with LPEI 10-PEG-Cys based mRNA polyplexes at the 2 h timepoint are compared to the outlines of the counted nuclei and Gal8 clusters in Figure 17. The same protocol was used for the other treatments and timepoints, for which similar figures are included in the appendix (Figures IV-X).

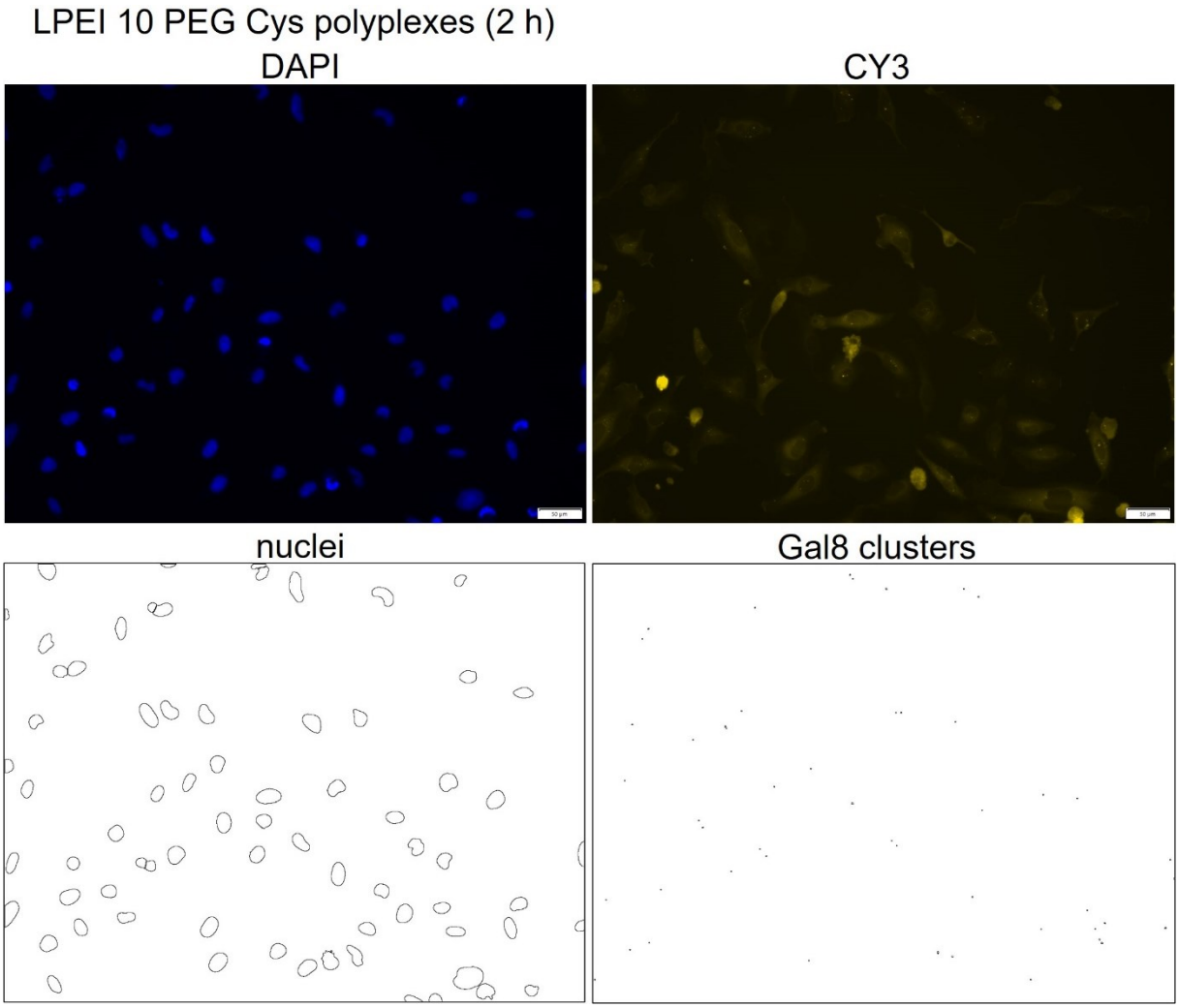

Figure 17: Visualisation and counting of nuclei and Gal8 clusters 2 h after adding Cypridina mRNA polyplexes with LPEI 10-PEG-Cys; polyplexes formed with N/P = 9 and c_{mRNA} = 200 µg/ml; 200 ng of mRNA added per well; magnification: 20 x (scale bar: 50 µm), DAPI: 400 ms exposure time; CY3: 1 s exposure time

The mean Gal8 clusters per cell across all transfections with mRNA are compiled in Figure 18 for cLPEI and LPEI 2.5 and in Figure 19 for LPEI 10-PEG-Cys and LPEI 10. Here, the clusters were visualised in CY3, with 1 s exposure time. With an exposure time of 2 s and an adjusted intensity threshold for the ImageJ count, as specified in the methods part, similar values were obtained as depicted in Figure III in the appendix. At the 2 h timepoint, cLPEI and LPEI 10-PEG-Cys polyplexes display significantly more Gal8 clustering than LPEI 2.5 and LPEI 10 polyplexes, respectively. Moreover, they show significantly fewer clusters per cell at 4 h compared to 2 h after the transfection, whereas there is no significant time dependent difference with LPEI 2.5 and LPEI 10. For all polymers except LPEI 10-PEG-Cys, Gal8 clustering is increased with the higher N/P ratio. Apart from LPEI 2.5 polyplexes, which led to significantly more clusters per cell with N/P 12, no significant differences with N/P ratio can be seen.

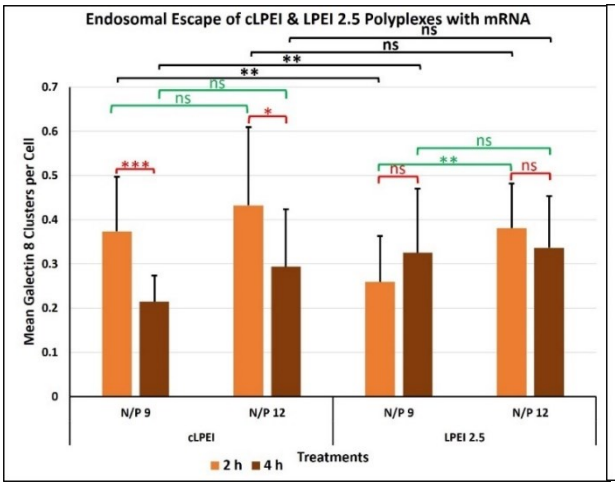

Figure 18: Mean Gal8 clusters per cell 2 and 4 h after adding Cypridina mRNA polyplexes with cLPEI and LPEI 2.5; means and standard deviations from 17-18 values for N/P 9 polyplexes (3 experiments, duplicates, 3 fields of view) and 11-12 values for N/P 12 polyplexes (2 experiments, duplicates, 3 fields of view); polyplexes formed with c_{mRNA} = 200 µg/ml; 200 ng of mRNA added per well; magnification: 20 x, channel: CY3, exposure time: 1 s; Welch´s t-test: * $p < 0.05$, ** $p < 0.01$, *** $p < 0.001$, ns non-significant; black: differences between polymers; green: differences between N/P ratios; red: differences between timepoints

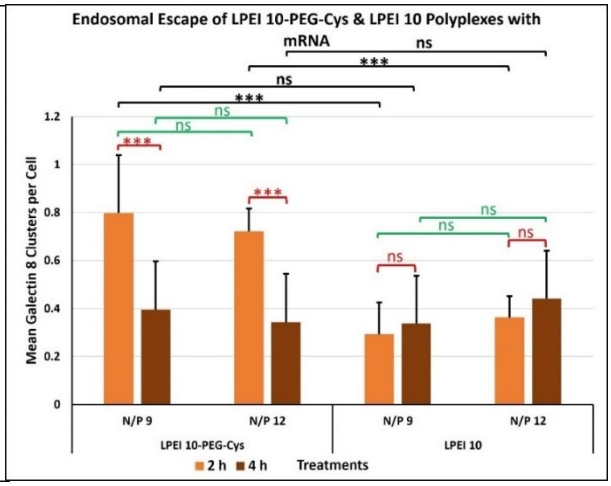

Figure 19: Mean Gal8 clusters per cell 2 and 4 h after adding Cypridina mRNA polyplexes with LPEI 10-PEG-Cys and LPEI 10; means and standard deviations from 15-18 values for N/P 9 polyplexes (3 experiments, duplicates, 3 fields of view) and 11-12 values for N/P 12 polyplexes (2 experiments, duplicates, 3 fields of view); polyplexes formed with c_{mRNA} = 200 µg/ml; 200 ng of mRNA added per well; magnification: 20 x, channel: CY3, exposure time: 1 s; Welch´s t-test: * $p < 0.05$, ** $p < 0.01$, *** $p < 0.001$, ns non-significant; black: differences between polymers; green: differences between N/P ratios; red: differences between timepoints

5.3. SSO Polyplexes

5.3.1. Optimisation of SSO Transfections

Depicted in Figure 20 are images of HeLa mRuby-3 galectin 8 cells treated with HBG or LPEI 10 based AF750-SSO polyplexes (160 pmol SSOs per well, N/P 9) as well as transfected HeLa pLuc 705 cells, 2 h after treatment. The transfected HeLa mRuby-3 galectin 8 cells show a few mRuby-3 labelled Gal8 clusters in the CY3 channel and AF750 signal in the nucleus from accumulated AF750-SSOs in CY7. In contrast, the HBG treated cells display a diffuse mRuby-3 signal in the cytoplasm, however no signal is present when using the CY7 filter. This indicates that no bleed through from CY3 occurs. The transfected HeLa pLuc 705 cells also show nuclear entry of AF750-SSOs when using the CY7 filter. In addition, there is a faint signal in the CY3 channel. As HeLa pLuc 705 cells do not produce mRuby-3 labelled Gal8, this suggests bleed through from CY7. As the bleed through was slight, HeLa mRuby-3 galectin 8 were used to study endosomal escape and nuclear entry of AF750-SSOs.

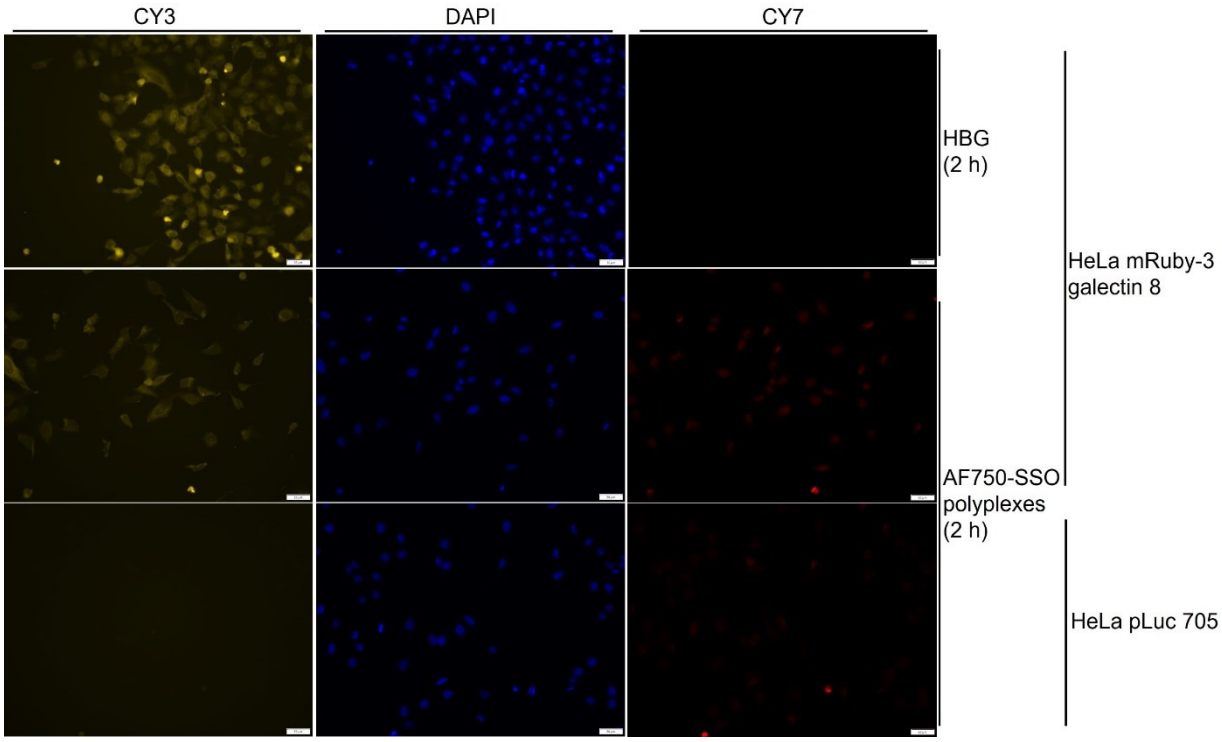

Figure 20: HeLa mRuby-3 galectin 8 cells 2 h after adding HBG buffer and HeLa mRuby-3 galectin 8 and HeLa pLuc 705 cells 2 h after transfection with LPEI 10 based AF750-SSO polyplexes; polyplexes formed with N/P = 9 and c_{SSOs} = 40 µg/ml; 160 pmol of SSOs added per well; magnification: 20 x (scale bar: 50 µm), DAPI: 400 ms exposure time; CY3: 1 s exposure time; CY7: 80 ms exposure time

5.3.2. Endosomal Escape of SSOs

Figure 21 shows representative images of HeLa mRuby-3 galectin 8 cells 2 and 4 h after treatment with HBG, naked AF750-SSOs and cLPEI and LPEI 2.5 based polyplexes. Neither HBG nor naked AF750-SSOs led to Gal8 clustering. The highest degree of clustering is observed 2 h after adding cLPEI based polyplexes with 160 pmol SSOs per well.

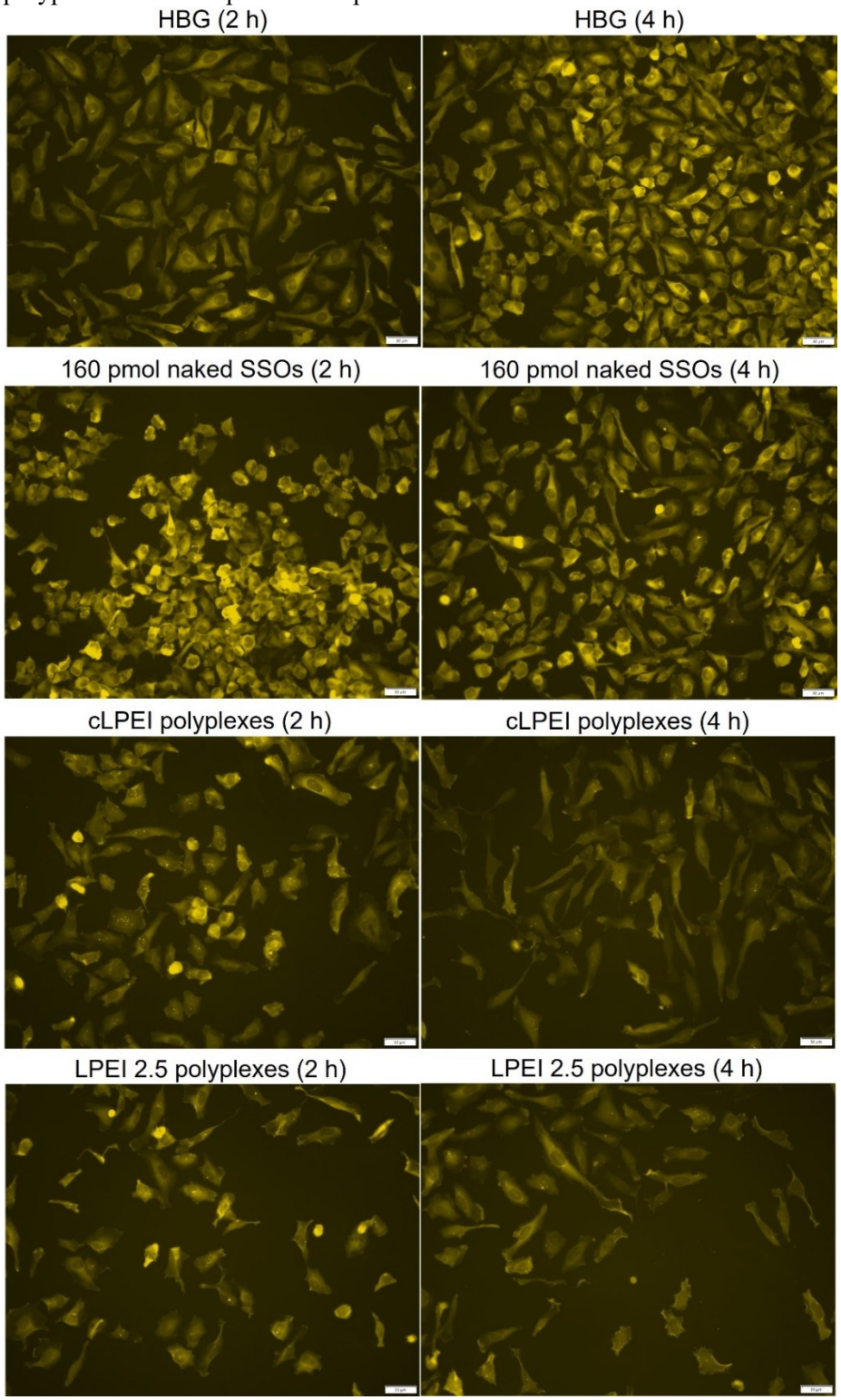

Figure 21: HeLa mRuby-3 galectin 8 cells 2 and 4 h after adding HBG, naked AF750-SSOs and AF750-SSO polyplexes with cLPEI and LPEI 2.5; polyplexes formed with N/P = 9 and c_{SSOs} = 40 µg/ml; 160 pmol of SSOs added per well; magnification: 20 x (scale bar: 50 µm); channel: CY3; exposure time: 2 s

To illustrate the performance of the ImageJ count, a DAPI and CY3 image of HeLa mRuby-3 galectin 8 cells 2 h after adding cLPEI based AF750-SSO polyplexes are compared to the outlines of the counted nuclei and Gal8 clusters in Figure 22. The same protocol was used across all samples, and similar figures for the other treatments and timepoints are included in the appendix (Figures X-XIII).

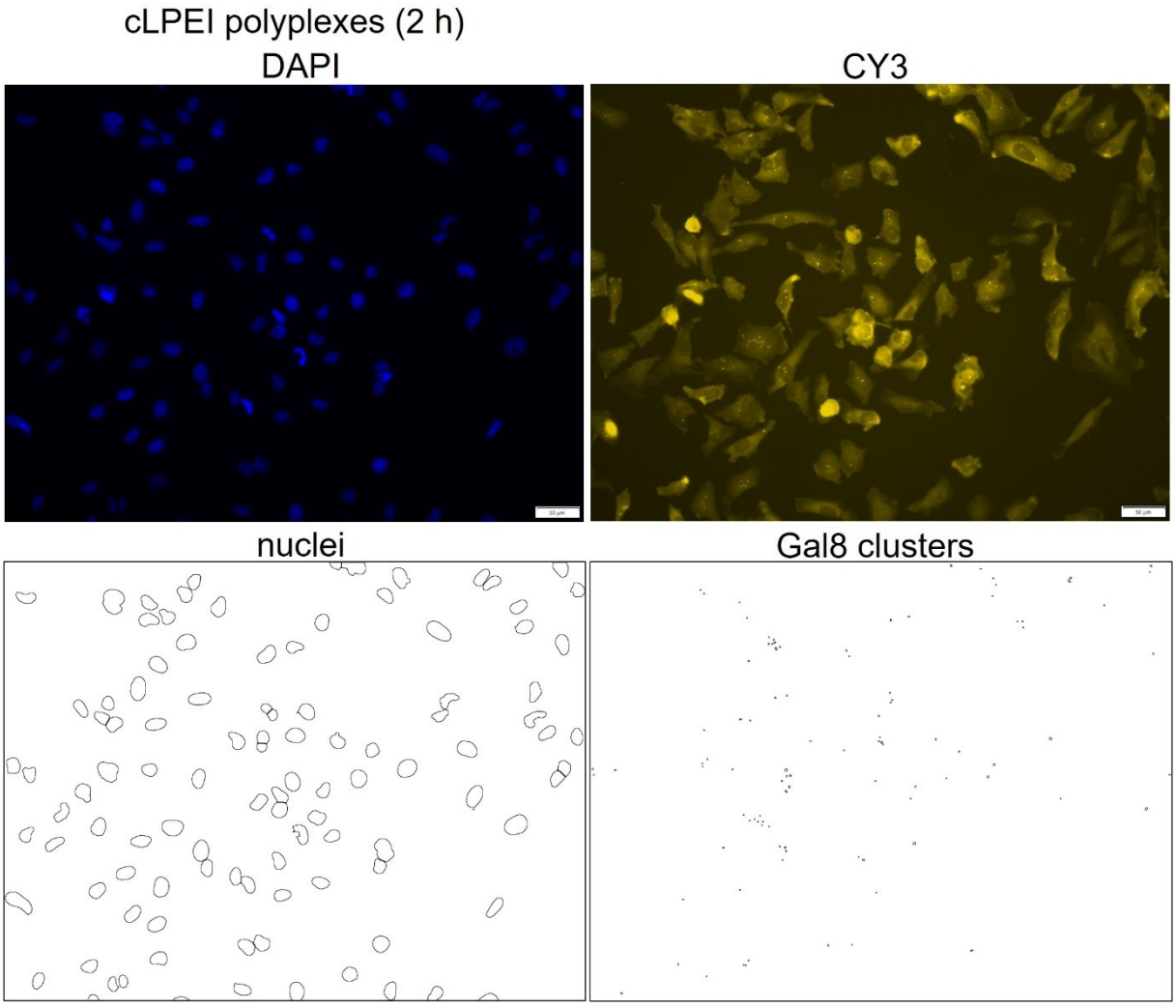

Figure 22: Visualisation and counting of nuclei and Gal8 clusters 2 h after adding AF750-SSO polyplexes with cLPEI; polyplexes formed with c_{SSOs} = 40 µg/ml; 160 pmol AF750-SSOs added per well; magnification: 20 x (scale bar: 50 µm), DAPI: 400 ms exposure time; CY3: 2 s exposure time

In the case of cLPEI based AF750-SSO polyplexes with 160 pmol SSOs added per well, there are significantly less Gal8 clusters per cell after 4 h compared to 2 h after transfection, as displayed in Figure 23. This indicates that the polyplexes cause endosomal damage and escape into the cytoplasm within 4 h after the transfection for the most part. In contrast, for the other polyplexes, there is no significant difference in Gal8 clustering between the timepoints. Moreover, with cLPEI as the carrier, the 160 pmol SSO treatment produced significantly more clusters per cell after 2 h than the 80 pmol treatment, whereas LPEI 2.5 based polyplexes do not display a significant change with SSO dosage. These results suggest that cLPEI is more efficient in mediating endosomal escape of polyplexes with AF750-SSOs.

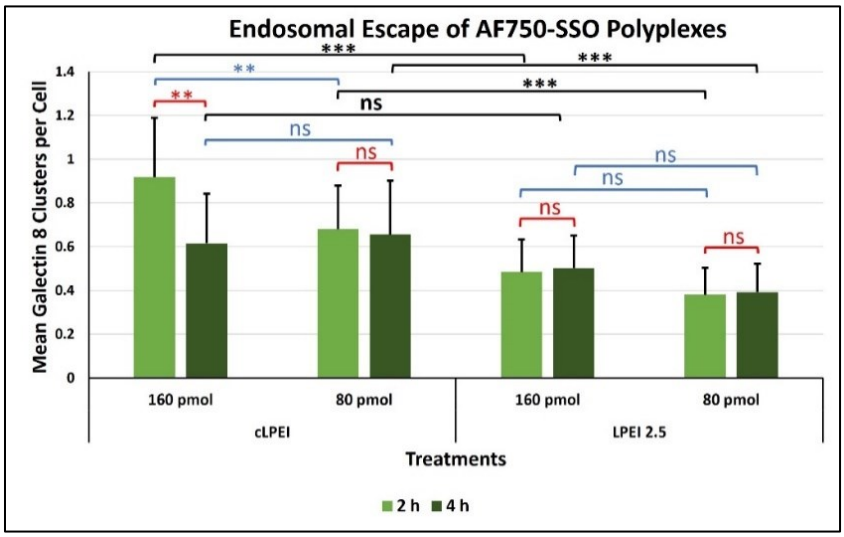

Figure 23: Mean Gal8 clusters per cell 2 and 4 h after adding AF750-SSO polyplexes with cLPEI and LPEI 2.5; means and standard deviations from 17-18 values for cLPEI (3 experiments, duplicates, 3 fields of view) and 12 values for LPEI 2.5 (2 experiments, duplicates, 3 fields of view); polyplexes formed with N/P = 9 and c_{SSOs} = 40 µg/ml; 160 and 80 pmol of SSOs added per well; magnification: 20 x; channel: CY3; exposure time: 2 s; Welch´s t-test (two-tailed): * $p < 0.05$, ** $p < 0.01$, *** $p < 0.001$, ns non-significant; black: differences between polymers; blue: differences between AF750-SSO dosages; red: differences between timepoints

5.3.3. Nuclear Entry of SSOs

As shown in Figure 24, cells treated with naked SSOs display a low AF750 signal after 2 and 4 h. Still, as could be visualised with a longer exposure time, AF750-SSOs were internalised. In contrast, no signal can be detected when adding HBG. Compared to naked SSOs, cLPEI and LPEI 2.5 polyplexes yielded a higher AF750 signal. Here, AF750-SSOs are largely accumulated in the nuclei, indicating efficient nuclear entry. The overall AF750 signal is higher at 4 h compared to the 2 h timepoint, suggesting a progressive cellular uptake of AF750-SSOs. When comparing the different polyplexes, with cLPEI polyplexes the AF750 signal is more concentrated inside the nuclei than with LPEI 2.5 polyplexes.

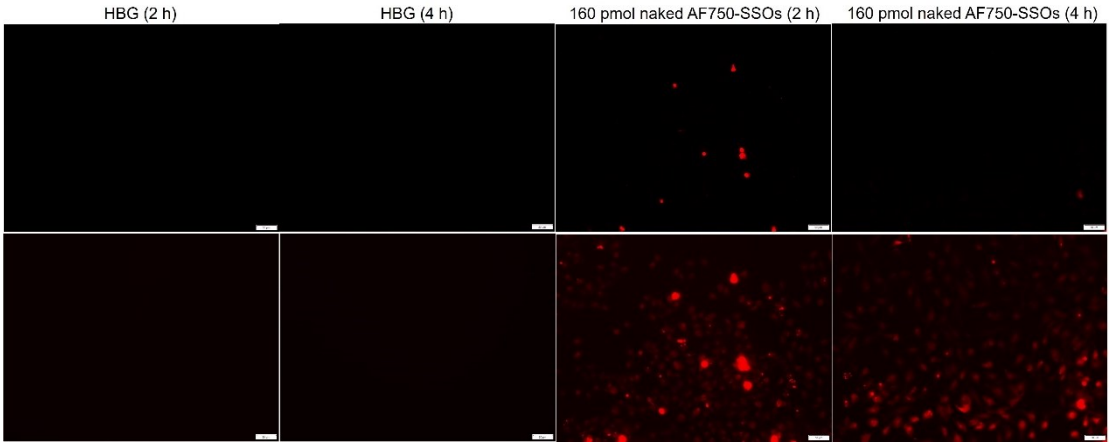

Figure 24: Detection of AF750-SSOs 2 and 4 h after treatment with 160 pmol naked AF750-SSOs or HBG (negative control); magnification: 20 x (scale bar: 50 µm), channel: CY7; exposure times: 100 ms (top row) and 5 s (bottom row)

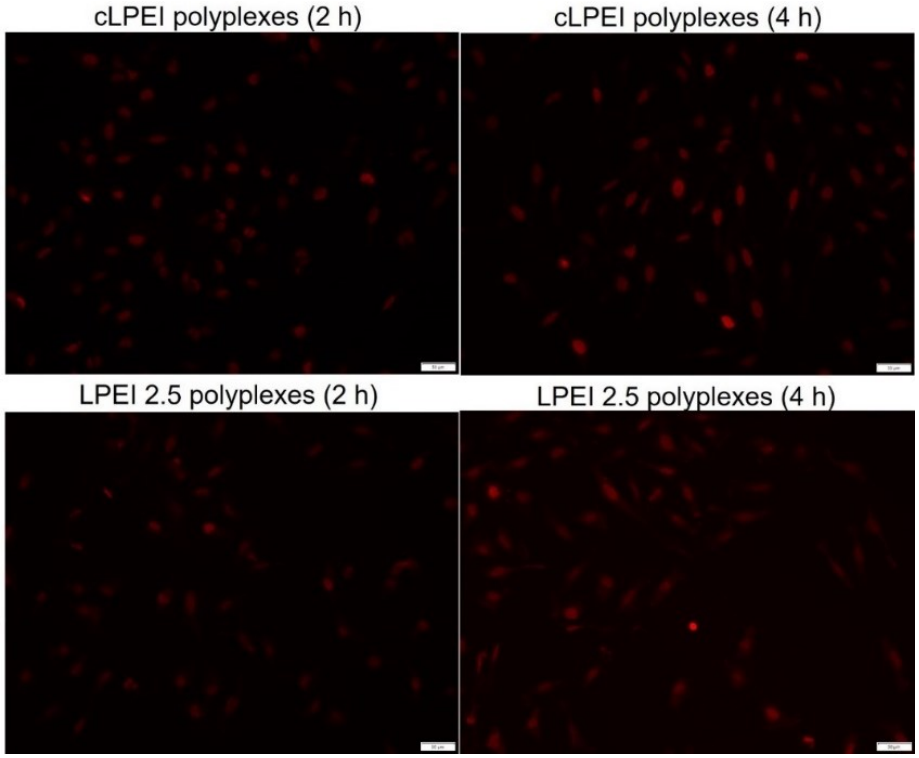

Figure 25: Detection of AF750-SSOs 2 and 4 h after adding AF750-SSO polyplexes with cLPEI and LPEI 2.5; polyplexes formed with N/P = 9 and c_{SSOs} = 40 µg/ml; 160 pmol of SSOs added per well; magnification: 20 x (scale bar: 50 µm), channel: CY7; exposure time: 100 ms

Figure 26 depicts representative images of HeLa mRuby-3 galectin 8 cells treated with cLPEI and LPEI 2.5 based AF750-SSO polyplexes, whereby the DAPI, CY3 and CY7 channels were merged. As is shown by the magnified image sections, cells with a large extent of Gal8 clustering display a comparatively high AF750 signal in the nucleus, indicating effective endosomal escape and nuclear entry of AF750-SSOs.

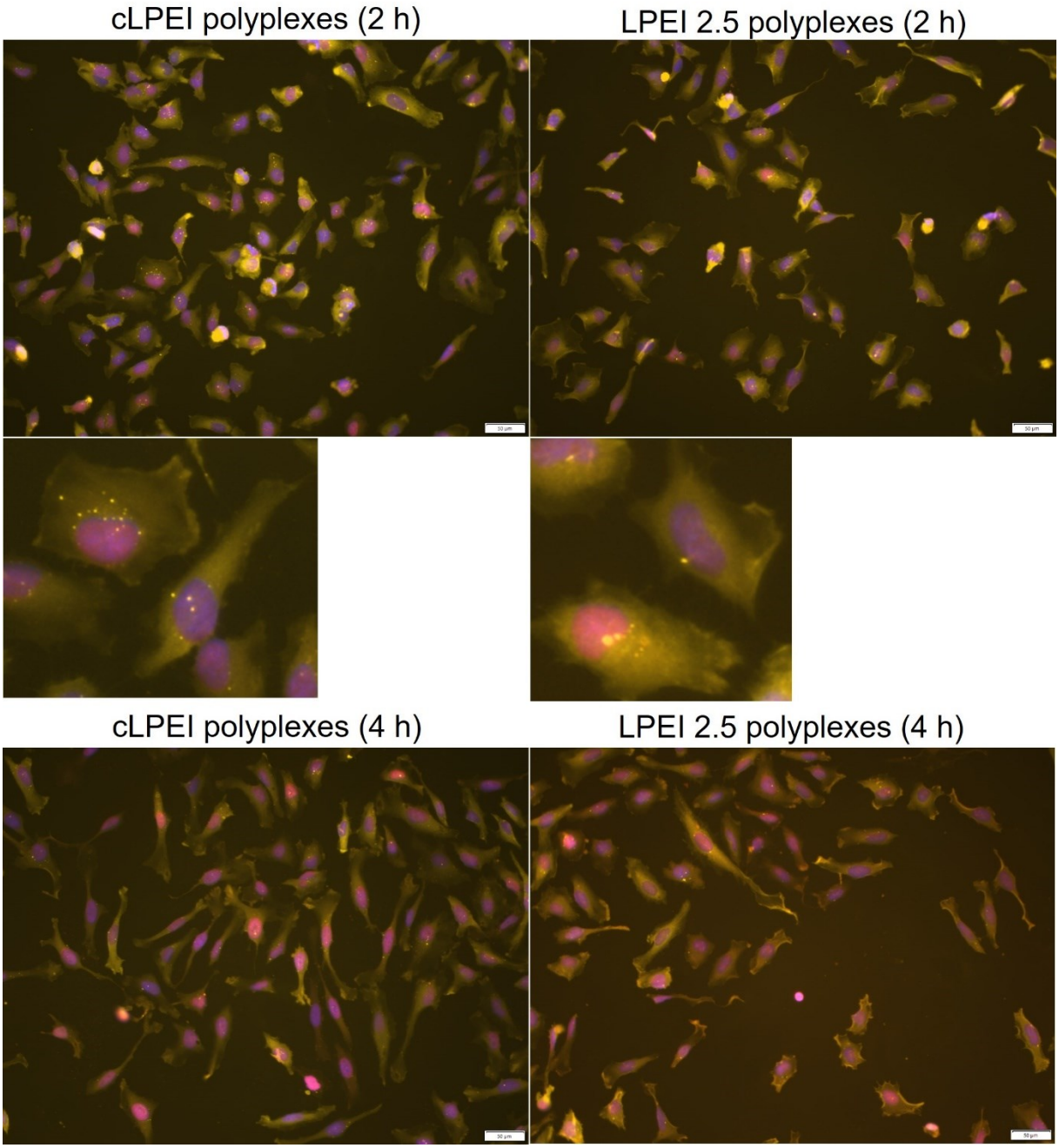

Figure 26: Merged DAPI, CY3 and CY7 channels of images from 2 and 4 h after adding AF750-SSO polyplexes with cLPEI and LPEI 2.5; polyplexes formed with N/P = 9 and c_{SSOs} = 40 µg/ml; 160 pmol of SSOs added per well; magnification: 20 x (scale bar: 50 µm); DAPI: 400 ms; CY3: 2 s; CY7: 100 ms

For analysing the nuclear entry of AF750-SSOs, CY7 images with an exposure time of 100 ms were used. Therefore, naked SSOs were excluded and only the different polyplexes were compared. No significant difference in the percentage of $AF750^+$ nuclei can be observed between cLPEI and LPEI 2.5 polyplexes, as depicted in Figure 27, A. The proportion of $AF750^+$ nuclei is significantly higher after adding 160 pmol SSOs per well compared to 80 pmol, both when using cLPEI and LPEI 2.5. This dosage dependent difference is higher 2 h after transfection than after 4 h. Plotting the mean AF750 intensity inside the nuclei reveals a similar pattern as shown in Figure 27, B. Notably, with cLPEI polyplexes the AF750 signal was mainly concentrated inside the nuclei whilst there was more signal in the cytoplasm after transfection with LPEI 2.5 polyplexes. Accordingly, the mean AF750 intensity inside the nucleus relative to the mean intensity outside is significantly higher for cLPEI than LPEI 2.5, as depicted in Figure 27, C. This indicates that cLPEI is more efficient than LPEI 2.5 in facilitating the nuclear entry of SSOs.

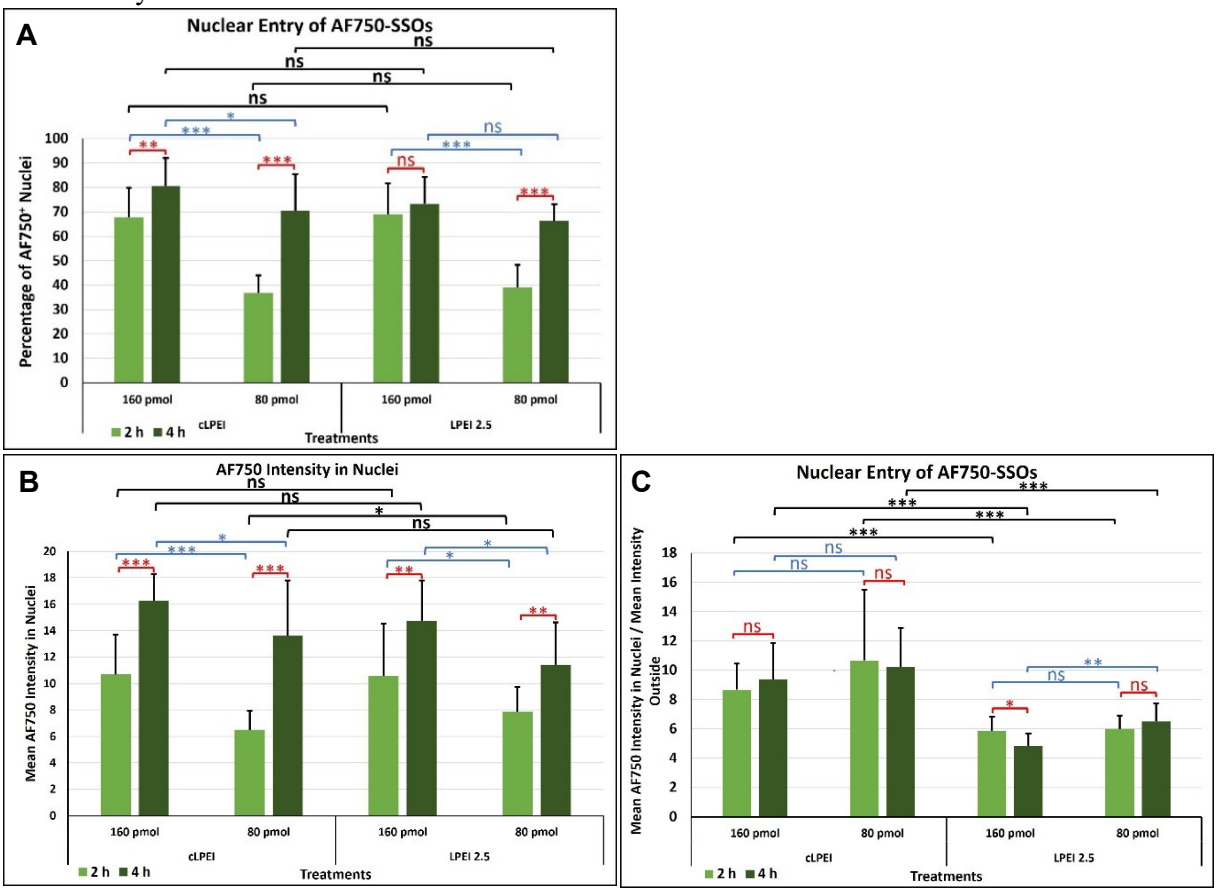

Figure 27: Nuclear entry of AF750-SSOs after transfection with cLPEI and LPEI 2.5 polyplexes **A**: Percentage of AF750+ nuclei; **B**: Mean AF750 intensity in nuclei; **C**: Ratio of the mean AF750 intensity in nuclei to the mean AF750 intensity outside of nuclei means and standard deviations from 17-18 values for cLPEI (3 experiments, duplicates, 3 fields of view) and 12 values for LPEI 2.5 (2 experiments, duplicates, 3 fields of view); polyplexes formed with N/P = 9 and c_{SSOs} = 40 µg/ml; 160 and 80 pmol of SSOs added per well; Welch´s t-test (two-tailed): * $p < 0.05$, ** $p < 0.01$, *** $p < 0.001$, ns non-significant; black: differences between polymers; blue: differences between AF750-SSO dosages; red: differences between timepoints

5.3.4. Splice Correction

Depicted in Figure 28 are the mean luminescence values across all 3 splice correction assays. The luminescence from HeLa pLuc 705 cells transfected with NCSSOs and naked LucSSOs is in the same range as the value from HBG treated cells. However, after adding polyplexes with LucSSOs, the values are higher by 1 or 2 orders of magnitude, indicating upregulated luciferase activity. Here, the luminescence is significantly higher when using cLPEI as opposed to LPEI 2.5. For normalisation, to compare the carriers with regard to splice correction, the splice factors were calculated, i.e. the ratios of luminescence signal when using LucSSOs to the signal with NCSSOs. As displayed in Figure 29, the splice factors of cLPEI are significantly higher than the splice factors of LPEI 2.5. With LPEI 2.5, the splice factor is only slightly increased with the dosage. These results suggest that splice correction by LucSSOs in HeLa pLuc 705 is more efficient with cLPEI as opposed to LPEI 2.5.

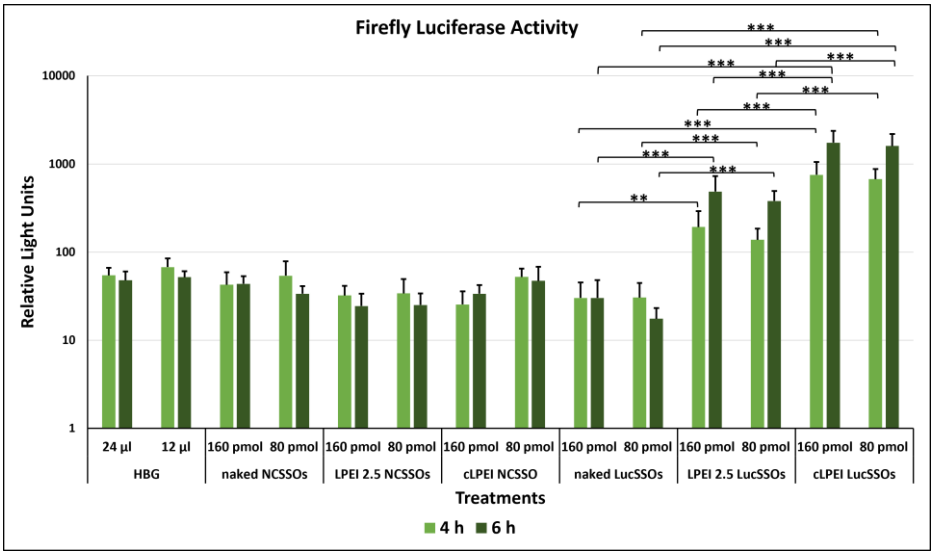

Figure 28: Luminescence 4 and 6 h after transfection with LucSSOs and NCSSOs; N/P =9; means and standard deviations from 9 values (3 experiments, triplicates); polyplexes formed with N/P = 9 and c_{SSOs} = 40 µg/ml; Welch´s t-test (two-tailed): * p < 0.05, ** p < 0.01, *** p < 0.001, ns non-significant

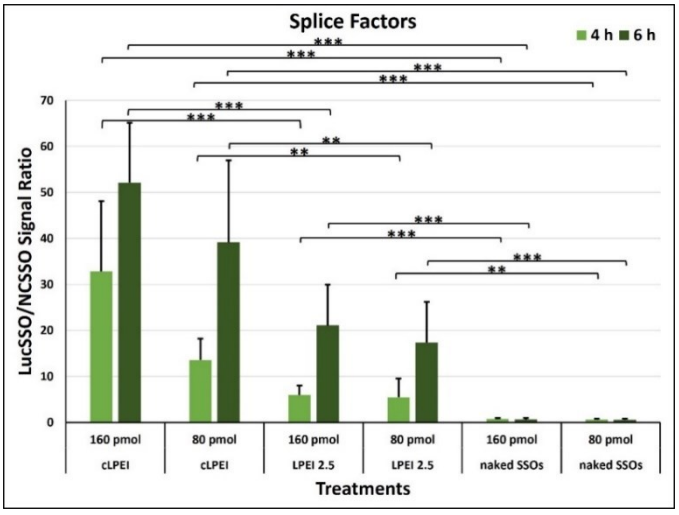

Figure 29: Splice factors of cLPEI, LPEI 2.5 and naked SSOs; means and standard deviations from 9 values (3 experiments, triplicates); polyplexes formed with N/P = 9 and c_{SSOs} = 40 µg/ml; Welch´s t-test (two-tailed): * p < 0.05, ** p < 0.01, *** p < 0.001, ns non-significant

6. Discussion

6.1. mRNA Polyplexes

The experiments in this thesis indicate that cLPEI and LPEI 10-PEG-Cys are more efficient at facilitating endosomal escape of mRNA than their unmodified counterparts, LPEI 2.5 and LPEI 10. This suggests that the chemical modifications, i.e. disulfide crosslinking and NHS-PEG-OPSS coupling, increase the ability of the LPEIs to cause endosomal damage.

Of all used carriers, LPEI 10-PEG-Cys produced the highest degree of endosomal damage, suggesting a superior efficiency at mediating endosomal escape of mRNA. This is surprising as PEGylation, whilst reportedly being beneficial during systemic application (Ogris, Brunner, Schuller, Kircheis, & Wagner, 1999), has been shown to negatively correlate with the performance of PEI polyplexes inside cells – a problem referred to as the PEG dilemma (Kiss, et al., 2011). For instance, incorporating PEGylated PEI has been shown to reduce the *in vitro* transfection efficiency of pDNA polyplexes, as determined via luciferase assay (Kursa, Walker, Roessler, Ogris, & Roedl, 2003). Reportedly, whilst the *in vitro* transfection is less efficient, PEGylation of BPEI polyplexes does not inhibit their cellular uptake. Therefore, it has been suggested that PEGylation reduces the endosomal escape of PEI polyplexes (Mishraa, Webster, & Davis, 2004). In this regard, various possible explanations have been put forward. For example, it has been proposed that shielding the positive charges of PEI through PEG impedes it in interacting with and damaging the endosomal membrane (Walker, et al., 2005). Moreover, PEGylation prevents the aggregation of BPEI polyplexes both outside the cells and inside endosomes as shown through dynamic light scattering and transmission electron microscopy. Here, large aggregates of unmodified BPEI polyplexes appear to expand and distort the endosomes (Mishraa, Webster, & Davis, 2004). The widely reported decreased *in vitro* transfection efficiency of PEI due to PEGylation has been addressed by the development of different PEG-PEI conjugates. For example, coupling PEI to a ligand via an acid labile PEG linker has increased receptor targeted transfection *in vitro* and *in vivo* compared to using a stable PEG linker (Walker, et al., 2005). Schaffert and colleagues have shown that the length of the PEG molecule impacts the effect of LPEI-NHS-PEG-OPSS conjugates with 2 kDa and 5 kDa PEG merely reducing polyplex activity, whereas 10 kDa PEG renders them completely ineffective. Also, incorporating EGF as a targeting ligand has increased the *in vitro* efficacy of LPEI conjugates with 2 kDA PEG and, to a lesser extent, of 5 kDa PEG-LPEI conjugates, yet it did not restore the activity of 10 kDa PEG-LPEI conjugates (Kiss, et al., 2011). Such a 2 kDa NHS-PEG-OPSS linker was used for synthesising LPEI 10-PEG-Cys. To summarise, the relatively high endosomal escape efficiency of LPEI 10-PEG-Cys observed in this work cannot be confirmed by previous research and further experiments would be necessary to analyse the effects of the polymer.

Concerning the second pair of polymers, the results suggest that cLPEI is more efficient at facilitating endosomal escape than LPEI 2.5. Similarly, as previously shown by Bonner et al. in a high throughput calcein assay, disulfide cLPEI and nondegradable cLPEI based polyplexes display a higher endosomal escape efficiency than LPEI polyplexes (Bonner, Zhao, Buss, Langer, & Hammond, 2013). Moreover, both of these cLPEIs reach a slightly higher transfection efficiency and a considerably higher cell viability than BPEI and LPEI. Because the cLPEIs require a relatively high N/P ratio for maximum transfection efficiency compared to BPEI and LPEI, the impact of free cLPEI has been tested. Here, adding free cLPEI 4 h after transfection with BPEI polyplexes, i.e. after cellular uptake, leads to a higher transfection efficiency compared to adding free BPEI. In contrast, simultaneous addition of free polymer reduces cellular uptake of polyplexes, but there are no differences between adding disulfide cLPEI, nondegradable cLPEI or BPEI. Therefore, the relatively high transfection efficiency of cLPEI based polyplexes has been attributed to enhanced endosomal escape by free cLPEI rather than to the cleavage of the disulfide bond (Bonner, Zhao, Buss, Langer, & Hammond, 2013). In line with these results, Boeckl and colleagues have shown that purification of PEI polyplexes increases their cellular uptake, suggesting that free PEI competes with polyplexes for the association with the plasma membrane. Moreover, adding free PEI 4 h after transfection with purified PEI polyplexes reportedly elevates reporter gene expression, and endosomal vesicles containing both polyplexes and free polymer have been observed. It has thus been proposed that free PEI is also internalised into vesicles and that, after fusion with polyplex containing vesicles, it facilitates the endosomal escape of polyplexes (Boeckle, et al., 2004). In order to further analyse the effects of the polymers on the cellular uptake and endosomal escape of the polyplexes, perhaps similar experiments involving the addition of free polymer at different timepoints after transfection could be performed.

6.2. SSO Polyplexes

6.2.1. Endosomal Escape of SSOs

The *in vitro* transfections with AF750-SSO polyplexes indicate clear endosomal escape within 4 h only for cLPEI based polyplexes at the higher concentration of 160 pmol SSOs. Judging by these results, cLPEI is more efficient than LPEI 2.5 at facilitating the endosomal escape of polyplexes. This is consistent with the results from the transfection experiments with Cypridina mRNA polyplexes.

6.2.2. Nuclear Entry of SSOs

The ImageJ AF750 intensity measurements indicate that cLPEI polyplexes lead to a smaller proportion of AF750-SSOs outside the nuclei compared to LPEI 2.5 polyplexes. As the same SSO amounts, i.e. 80 or 160 pmol per well, were used for cLPEI and LPEI 2.5, this suggests that more AF750-SSOs enter the nuclei with cLPEI as opposed to LPEI 2.5 as a carrier. This would be consistent with previous *in vitro* transfections of HeLa pLuc 705 with 160 pmol AF647-SSOs in which cLPEI polyplexes of N/P 9 lead

to a visibly higher AF647 signal in the nuclei compared to BPEI or LPEI 10 based polyplexes. Because BPEI, LPEI 10 and cLPEI polyplexes display a similar cellular uptake of AF647-SSOs, it has been suggested that cLPEI is more efficient in mediating the intracellular delivery of SSOs (Decker, 2022).

With the imaging parameters applied in this thesis, no definite polymer specific differences in the percentage of $AF750^+$ nuclei and mean AF750 intensity in nuclei can be seen. To detect a difference in nuclear AF750 intensity, a shorter exposure time would probably be necessary. Further experiments could be conducted to quantify and compare the uptake of cLPEI and LPEI 2.5 based polyplexes with labelled SSOs into HeLa cells using flow cytometry. This way, it might be possible to rule out that the observed difference in endosomal escape of cLPEI and LPEI 2.5 polyplexes results from different amounts of polyplexes in the cell.

6.2.3. Splice Correction

Judging by the luminescence measurements of HeLa pLuc 705 4 h and 6 h after transfection, splice correction by LucSSOs occurs with both cLPEI and LPEI 2.5 as a carrier, whereby cLPEI is more efficient. This is in line with the higher degree of endosomal damage with cLPEI which was observed within 4 h after transfection.

Similarly, previous splice correction assays with HeLa pLuc 705 have shown that cLPEI exhibits a higher splice correction efficiency than LPEIs (Decker, 2022); (Kaufmann, 2024). For instance, cLPEI polyplexes reportedly lead to a luminescence increase with 20, 30 and 40 pmol LucSSOs, as measured in cell lysate 24 h after transfection. In contrast, adding LPEI 10 shows a comparable increase from 30 pmol LucSSOs. Moreover, cLPEI based polyplexes, prepared with an N/P ratio of 9, display a higher splice ratio than naked SSOs, however this difference is non-significant with 40 pmol and relatively small with 80 pmol SSOs. When adding 160 pmol SSOs, luminescence is approximately 50 times higher with LucSSOs compared to NCSSOs. The splice ratio of naked SSOs is significantly lower (Decker, 2022). In line with these results, using polyplexes based on cLPEIs with a crosslinking ratio of 0.5 produces splice ratios between 50 and 100, 24 h after transfection with 160 pmol SSOs, however with 80 pmol SSOs, only a 1-5 fold increase in splice correction is achieved with LucSSOs. For 3 kDa LPEI both 80 and 16 pmol SSOs lead to splice ratios between 1 and 5 (Kaufmann, 2024). Therefore, in line with the results of this thesis, cLPEI shows a dosage dependent increase in splice correction whereas lower molecular weight LPEI is less efficient.

7. References

Aits, S., Kricker, J., Liu, B., Ellegaard, A.-M., Hämälistö, S., Tvingsholm, S., . . . Jäättelä, M. (2015). Sensitive detection of lysosomal membrane permeabilization by lysosomal galectin puncta assay. *Autophagy*, 1408-1424.

Alberts, B., Johnson, A., Lewis, J., Morgan, D., Raff, M., Roberts, K., & Walter, P. (2015). *Molecular Biology of the Cell.* New York: Garland Science.

Bauman, J., Jearawiriyapaisarn, N., & Kole, R. (2009). Therapeutic Potential of Splice-Switching Oligonucleotides. *Oligonucleotides*, 1–13.

Bieber, T., Meissner, W., Kostin, S., Niemann, A., & Elsasser, H.-P. (2002). Intracellular route and transcriptional competence of polyethylenimine–DNA complexes. *Journal of Controlled Release*, 441–454.

Boeckle, S., von Gersdorff, K., van der Piepen, S., Culmsee, C., Wagner, E., & Ogris, M. (2004). Purification of polyethylenimine polyplexes highlights the role of free polycations in gene transfer. *J Gene Med*, 1102–1111.

Bonner, D. K., Zhao, X., Buss, H., Langer, R., & Hammond, P. T. (2013). Crosslinked Linear Polyethyleneimine Enhances Delivery of DNA to the Cytoplasm. *J Control Release*, 101–107.

Boussif, O., Lezoualc'h, F., Zanta, M. A., Mergny, M. D., Scherman, D., Demeneix, B., & Behr, J.-P. (1995). A versatile vector for gene and oligonucleotide transfer into cells in culture and in vivo: polyethylenimine. *Proc. Natl. Acad. Sci. USA*, 7297-7301.

Boussif, O., Lezoualc'h, F., Zanta, M., Mergny, M., Scherman, D., Demeneix, B., & Behr, J. (1995). A versatile vector for gene and oligonucleotide transfer into cells in culture and in vivo: polyethylenimine. *PNAS*, 92 (16) 7297-7301.

Breunig, M., Lungwitz, U., Liebl, R., & Goepferich, A. (2007). Breaking up the correlation between efficacy and toxicity for nonviral gene delivery. *PNAS*, 14454–14459.

Clark, S. R., Lee, K. Y., Lee, H., Khetan, J., Kim, H. C., Choi, Y. H., . . . Won, Y.-Y. (2018). Determining the effects of PEI adsorption on the permeability of 1,2-

dipalmitoylphosphatidylcholine/bis(monoacylglycero)phosphate membranes under osmotic stress. *Acta Biomaterialia*, 317–326.

Day, R. A., & Sletten, E. M. (2021). Experimental Perspectives on Direct Visualization of Endosomal Rupture. *Chemistry and Biochemistry*, 22, 3277-3282.

Decker, S. (2022). Peptide targeted gene therapy using functionalized polyethylenimine and dendrimer based nucleic acid carriers. Vienna.

Dominski, Z., & Kole, R. (1993). Restoration of correct splicing in thalassemic pre-mRNA by antisense oligonucleotides. *Proc Natl Acad Sci USA*, 8673-8677.

Eliyahu, H., Barenholz, Y., & Domb, A. (2005). Polymers for DNA Delivery . *Molecules*, 34-64.

Fan, F., & Wood, K. V. (2007). Bioluminescent Assays for High-Throughput Screening. *ASSAY and Drug Development Technologies*, 127-136.

Hall, A., Lächelt, U., Bartek, J., Wagner, E., & Moghimi, S. M. (2017). Polyplex Evolution: Understanding Biology, Optimizing Performance. *Molecular Therapy*, 1476-1490.

Hartig, R., Shoeman, R. L., Janetzko, A., Griib, S., & Traub, P. (1998). Active nuclear import of single-stranded oligonucleotides and their complexes with non-karyophilic macromolecules . *Biology of the Cell*, 407-426.

Hausig-Punke, F., Richter, F., Hoernke, M., & Brendel, J. C. (2022). Tracking the Endosomal Escape: A Closer Look at Calcein and Related Reporters. *Macromol. Biosci.*, 1-26.

Havens, M. A., & Hastings, M. L. (2016). Splice-switching antisense oligonucleotides as therapeutic drugs. *Nucleic Acids Research*, 6549–6563.

Juliano, R. L., Alahari, S., Yoo, H., Kole, R., & Cho, M. (1999). Antisense Pharmacodynamics: Critical Issues in the Transport and Delivery of Antisense Oligonucleotides. *Pharmaceutical Research*, 494-502.

Kang, H., Ga, Y. J., Kim, S. H., Cho, Y. H., Kim, J. W., Kim, C., & Yeh, J.-Y. (2023). Small interfering RNA (siRNA)-based therapeutic applications against viruses: principles, potential, and challenges. *Journal of Biomedical Science*, 1-18.

Kang, S.-H., Cho, M.-J., & Kole, R. (1998). Up-Regulation of Luciferase Gene Expression with Antisense Oligonucleotides: Implications and Applications in Functional Assay Development. *Biochemistry*, 6235-6239.

Kaufmann, S. (2024). Optimization of multiplexed assays for in vitro splice correction and cytotoxicity. Vienna.

Kilchrist, K. V., Dimobi, S. C., Jackson, M. A., Evans, B. C., Dailing, E. A., Bedingfield, S. K., . . . Duvall, C. L. (2019). Gal8 Visualization of Endosome Disruption Predicts CarrierMediated Biologic Drug Intracellular Bioavailability. *ACS Nano*, 1136–1152.

Kircheis, R., Wightman, L., & Wagner, E. (2001). Design and gene delivery activity of modified polyethylenimines. *Advanced Drug Delivery Reviews*, 341–358.

Kiss, M., &, D. S., Rödl, W., Shir, A., Levitzki, A., Ogris, M., & Wagner, E. (2011). Poly(I:C)-Mediated Tumor Growth Suppression in EGF-Receptor Overexpressing Tumors Using EGF-Polyethylene Glycol-Linear Polyethylenimine as Carrier. *Pharm Res*, 731–741.

Kuijper, E. C., Bergsma, A. J., Pijnappel, W. P., & Aartsma-Rus, A. (2021). Opportunities and challenges for antisense oligonucleotide therapies. *J Inherit Metab Dis.*, 72–87.

Kulkarni, K. A., Witzigmann, D., Thomson, S. B., Chen, S., Leavitt, B. R., Cullis, P. R., & van der Meel, R. (2021). The current landscape of nucleic acid therapeutics. *nature nanotechnology*, 630–643.

Kursa, M., Walker, G. F., Roessler, V., Ogris, M., & Roedl, W. (2003). Novel Shielded Transferrin-Polyethylene Glycol-Polyethylenimine/DNA Complexes for Systemic Tumor-Targeted Gene Transfer. *Bioconjugate Chem.*, 222−231.

Lächelt, U., & Wagner, E. (2015). Nucleic Acid Therapeutics Using Polyplexes: A Journey of 50 Years. *Chemical Reviews*, 11043−11078.

Lauffer, M. C., van Roon-Mom, W., & Aartsma-Rus, A. (2024). Possibilities and limitations of antisense oligonucleotide therapies for the treatment of monogenic disorders. *Communications Medicine*, 1-11.

Leonetti, J. P., Mechti, N., Degols, G., Gagnor, C., & Lebleu, B. (1991). Intracellular distribution of microinjected antisense oligonucleotides. *Proc. Natl. Acad. Sci. USA*, 2702-2706.

Lukacs, G. L., Haggie, P., Seksek, O., Lechardeur, D., Freedman, N., & Verkman, A. S. (2000). Size-dependent DNA Mobility in Cytoplasm and Nucleus. *The Journal of Biological Chemistry*, 1625–1629.

Massignani, M., Canton, I., Sun, T., Hearnden, V., MacNeil, S., Blanazs, A., . . . Battaglia, G. (2010). Enhanced Fluorescence Imaging of Live Cells by Effective Cytosolic Delivery of Probes. *PLoS ONE*, 1-11.

Ming, X., Sato, K., & Juliano, R. L. (2011). Unconventional internalization mechanisms underlying functional delivery of antisense oligonucleotides via cationic lipoplexes and polyplexes. *Journal of Controlled Release*, 83–92.

Mishraa, S., Webster, P., & Davis, M. E. (2004). PEGylation significantly affects cellular uptake and intracellular trafficking of non-viral gene delivery particles. *Eur. J. Cell Biol.*, 97-111.

Munson, M. J., O'Driscoll, G., Silva, A. M., Lázaro-Ibáñez, E., Gallud, A., Wilson, J. T., . . . Sabirsh, A. (2021). A high-throughput Galectin-9 imaging assay for quantifying nanoparticle uptake, endosomal escape and functional RNA delivery. *communications biology*, 1-14.

Ogris, M., Brunner, S., Schuller, S., Kircheis, R., & Wagner, E. (1999). PEGylated DNA/transferrin–PEI complexes: reduced interaction with blood components, extended circulation in blood and potential for systemic gene delivery. *Gene Therapy*, 595-605.

Ogris, M., Carlisle, R. C., Bettinger, T., & Seymour, L. W. (2001). Melittin Enables Efficient Vesicular Escape and Enhanced Nuclear Access of Nonviral Gene Delivery Vectors. *The Journal of Biological Chemistry*, 47550–47555.

Pack, D. W., Hoffman, A. S., Pun, S., & Stayton, P. S. (2005). Design and development of polymers for gene delivery. *Nature Reviews*, 581-593.

Rehman, Z. u., Hoekstra, D., & Zuhorn, I. S. (2013). Mechanism of Polyplex- and Lipoplex-Mediated Delivery of Nucleic Acids: Real-Time Visualization of Transient Membrane Destabilization without Endosomal Lysis. *acsnano*, 3767–3777.

Reinhard, S., & Wagner, E. (2019). Sequence-Defined Cationic Lipo-Oligomers Containing Unsaturated Fatty Acids for Transfection. In M. Ogris, & H. Sami, *Nanotechnology for Nucleic Acid Delivery* (p. 1). New York: Humana Press.

Rejman, J., Bragonzi, A., & Conese, M. (2005). Role of Clathrin- and Caveolae-Mediated Endocytosis in Gene Transfer Mediated by Lipo- and Polyplexes. *MOLECULAR THERAPY*, 468-474.

Rödl, W., Taschauer, A., Schaffert, D., Wagner, E., & Ogris, M. (2019). Synthesis of Polyethylenimine-Based Nanocarriers for Systemic Tumor Targeting of Nucleic Acids. In M. Ogris, & H. Sami, *Nanotechnology for Nucleic Acid Delivery - Methods and Protocols* (pp. 83-99). New York: Springer Nature.

Sahin, U., Karikó, K., & Türec, Ö. (2014). mRNA-based therapeutics - developing a new class of drugs. *Nature Reviews Drug Discovery*, 759–780.

Schindelin, J., Arganda-Carreras, I., Frise, E., Kaynig, V., Longair, M., Pietzsch, T., . . . Cardona, A. (2012). Fiji: an open-source platform for biological-image analysis. *Nature Methods*, 676–682.

Selby, L. I., Cortez-Jugo, C. M., Such, G. K., & Johnston, A. P. (2017). Nanoescapology: progress toward understanding the endosomal escape of polymeric nanoparticles. *WIREs Nanomed Nanobiotechnol*, 1-23.

Shirley, J. L., de Jong, Y. P., Terhorst, C., & Herzog, R. W. (2020). Immune Responses to Viral Gene Therapy Vectors. *Molecular Therapy*, 709–722.

Smith, S. A., Selby, L. I., Johnston, A. P., & Such, G. K. (2019). The Endosomal Escape of Nanoparticles: Toward More Efficient Cellular Delivery. *Bioconjugate Chem.*, 263-272.

Sonawane, N., Szoka, F. C., & Verkman, A. S. (2003). Chloride Accumulation and Swelling in Endosomes Enhances DNA Transfer by Polyamine-DNA Polyplexes. *The Journal of Biological Chemistry*, 44826–44831.

Sperhansl, J. (2016). Synthesis of polycationic gene carrier systems and their biophysical evaluation. Vienna.

Taschauer, A., Polzer, W., Alioglu, F., Billerhart, M., Decker, S., Kittelmann, T., . . . Ogris, M. (2019). Peptide-Targeted Polyplexes for Aerosol-Mediated Gene Delivery to CD49f-Overexpressing Tumor Lesions in Lung. *Molecular Therapy: Nucleic Acids*, 774-786.

Thermo Fisher Scientific Inc. (2024, March 10). *Validation of Gene Transfection / Transduction*. Retrieved from Thermo Fisher Scientific: https://www.thermofisher.com/at/en/home/life-

science/pcr/real-time-pcr/real-time-pcr-applications/real-time-pcr-protein-analysis/protein-expression-taqman-assays/validation-transfection-transduction.html

Two Sample T-Test Calculator (Welch's T-test). (2024, April 29). Retrieved from Statistics Kingdom: https://www.statskingdom.com/150MeanT2uneq.html

Walker, G. F., Fella, C., Pelisek, J., Fahrmeir, J., Boeckle, S., Ogris, M., & Wagner, E. (2005). Toward Synthetic Viruses: Endosomal pH-Triggered Deshielding of Targeted Polyplexes Greatly Enhances Gene Transfer in Vitro and in Vivo. *Molecular Therapy*, 418-425.

Weng, Y., Li, C., Yang, T., Hu, B., Zhang, M., Guo, S., . . . Huang, Y. (2020). The challenge and prospect of mRNA therapeutics landscape. *Biotechnology Advances*, 1-23.

Yin, H., Kanasty, R. L., Eltoukhy, A. A., & Vegas, A. J. (2014). Non-viral vectors for gene-based therapy. *Nature Reviews*, 541-555.

Zhou, R., Geiger, R. C., & Dean, D. A. (2004). Intracellular trafficking of nucleic acids. *Expert Opin Drug Deliv*, 127–140.

Ziebarth, J. D., & Wang, Y. (2010). Understanding the protonation behavior of linear polyethylenimine in solutions through Monte Carlo simulations. *Biomacromolecules*, 1-29.

8. Table of Figures

9. Appendix

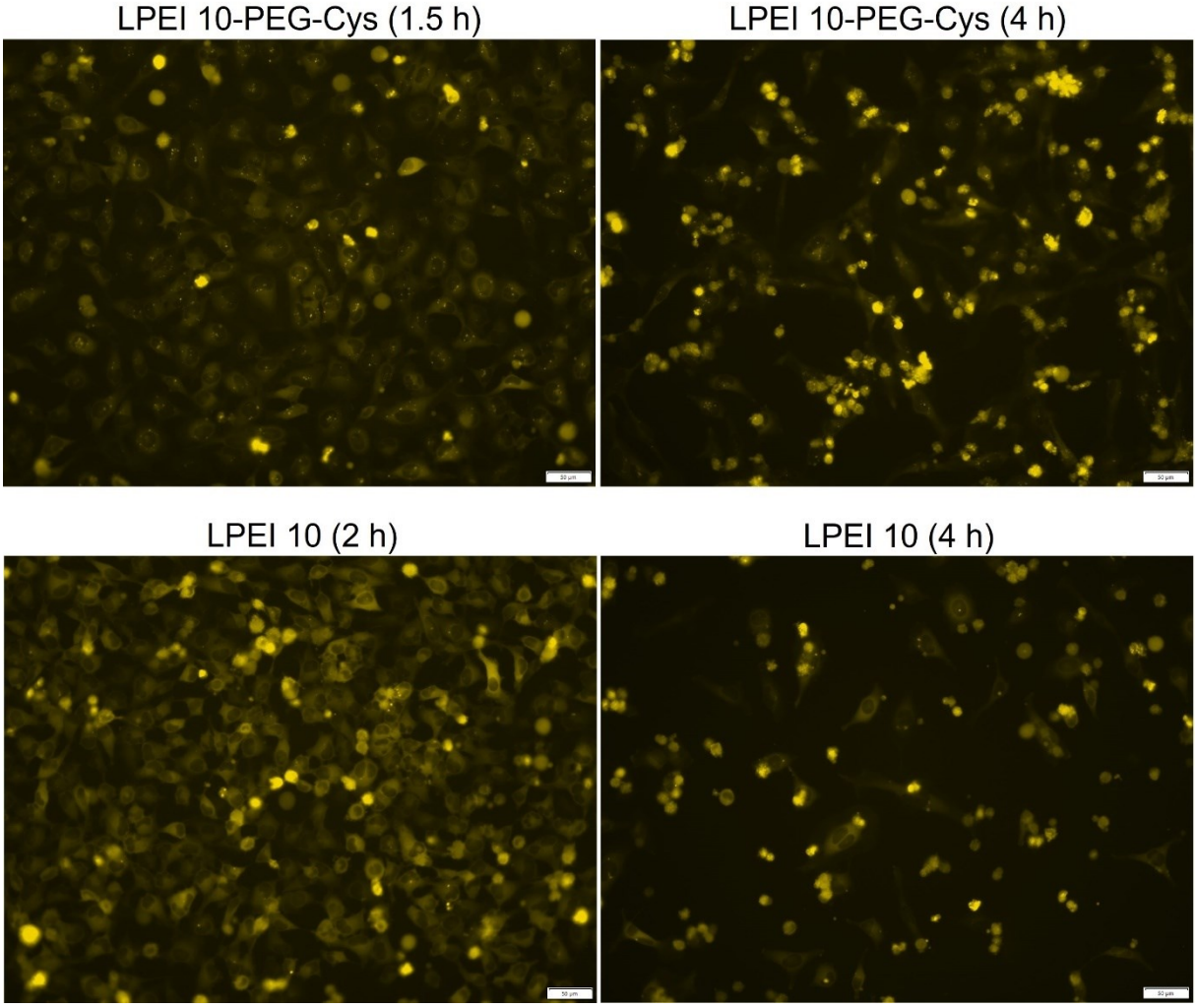

Figure I: Live cell imaging of HeLa mRuby-3 galectin 8 cells at an earlier timepoint (1.5 or 2 h) and 4 h after transfection with LPEI 10-PEG-Cys and LPEI 10 based mRNA polyplexes; polyplexes formed with N/P = 12 and c_{mRNA} = 200 µg/ml; 200 ng of mRNA added per well; magnification: 20 x, channel: CY3, exposure time: 1 s

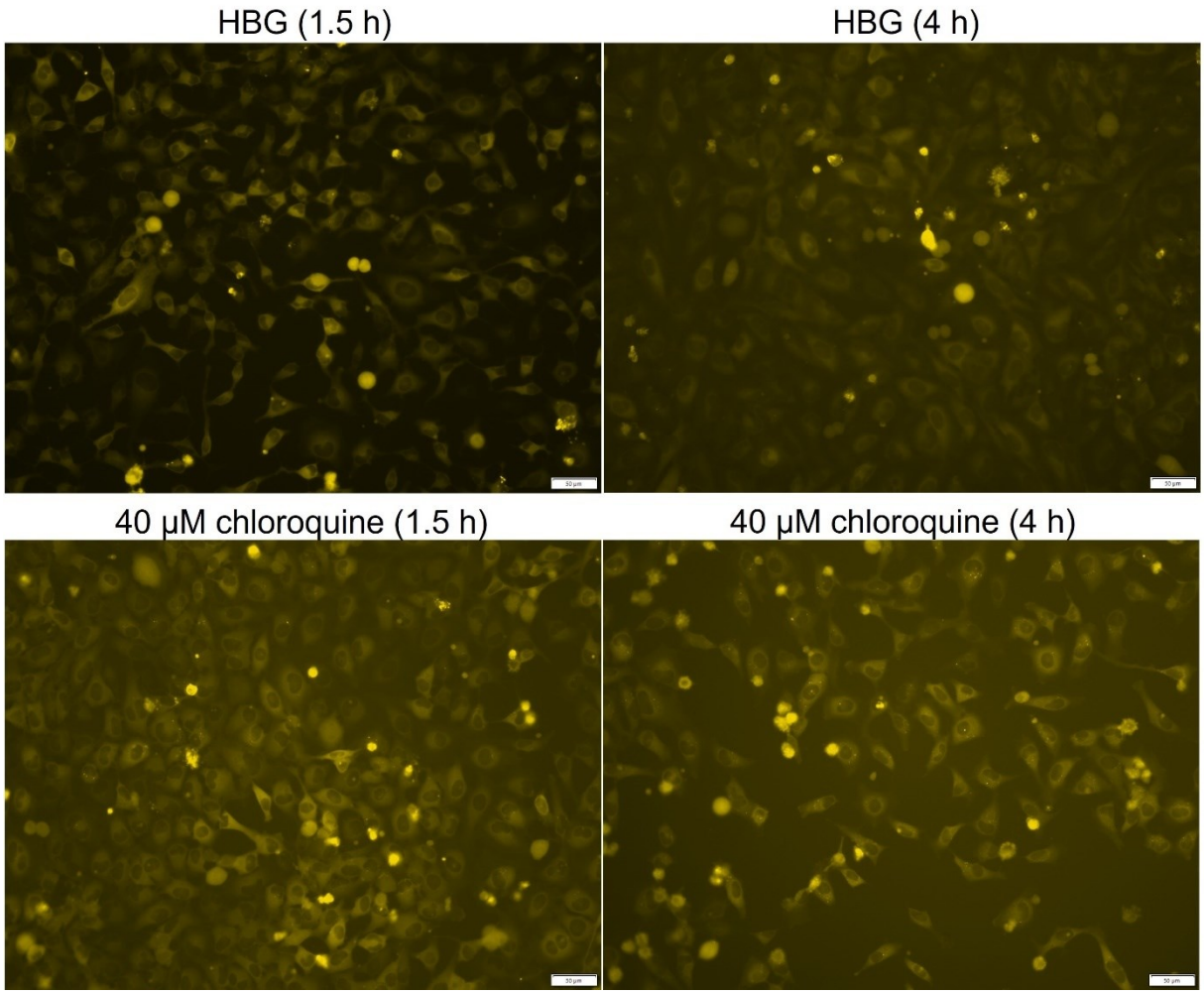

Figure II: Live cell imaging of HeLa mRuby-3 galectin 8 cells 1.5 and 4 h after adding HBG buffer and 40 µM chloroquine; magnification: 20 x, channel: CY3, exposure time: 1 s

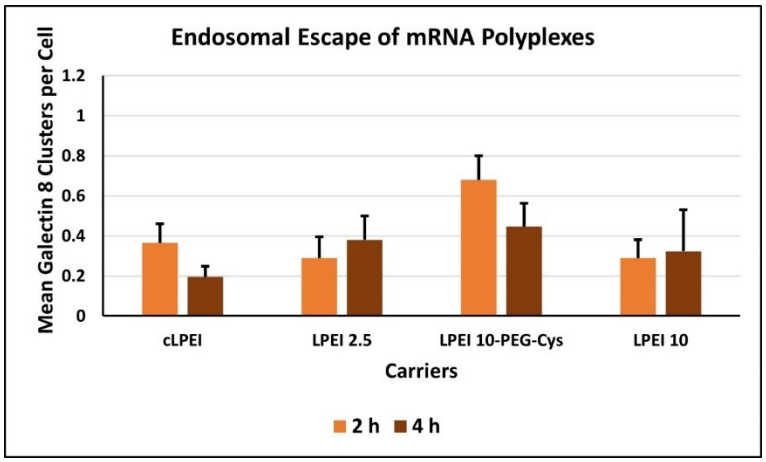

Figure III: Mean Gal8 clusters per cell 2 and 4 h after adding mRNA polyplexes with cLPEI, LPEI 2.5, LPEI 10-PEG-Cys and LPEI 10; means and standard deviations from 11-12 values for N/P 9 polyplexes (2 experiments with 2 wells per treatment and 3 fields of view per well); polyplexes formed with N/P 9 and c_{mRNA} = 200 µg/ml; 200 ng of mRNA added per well; magnification: 20 x, channel: CY3, exposure time: 2 s

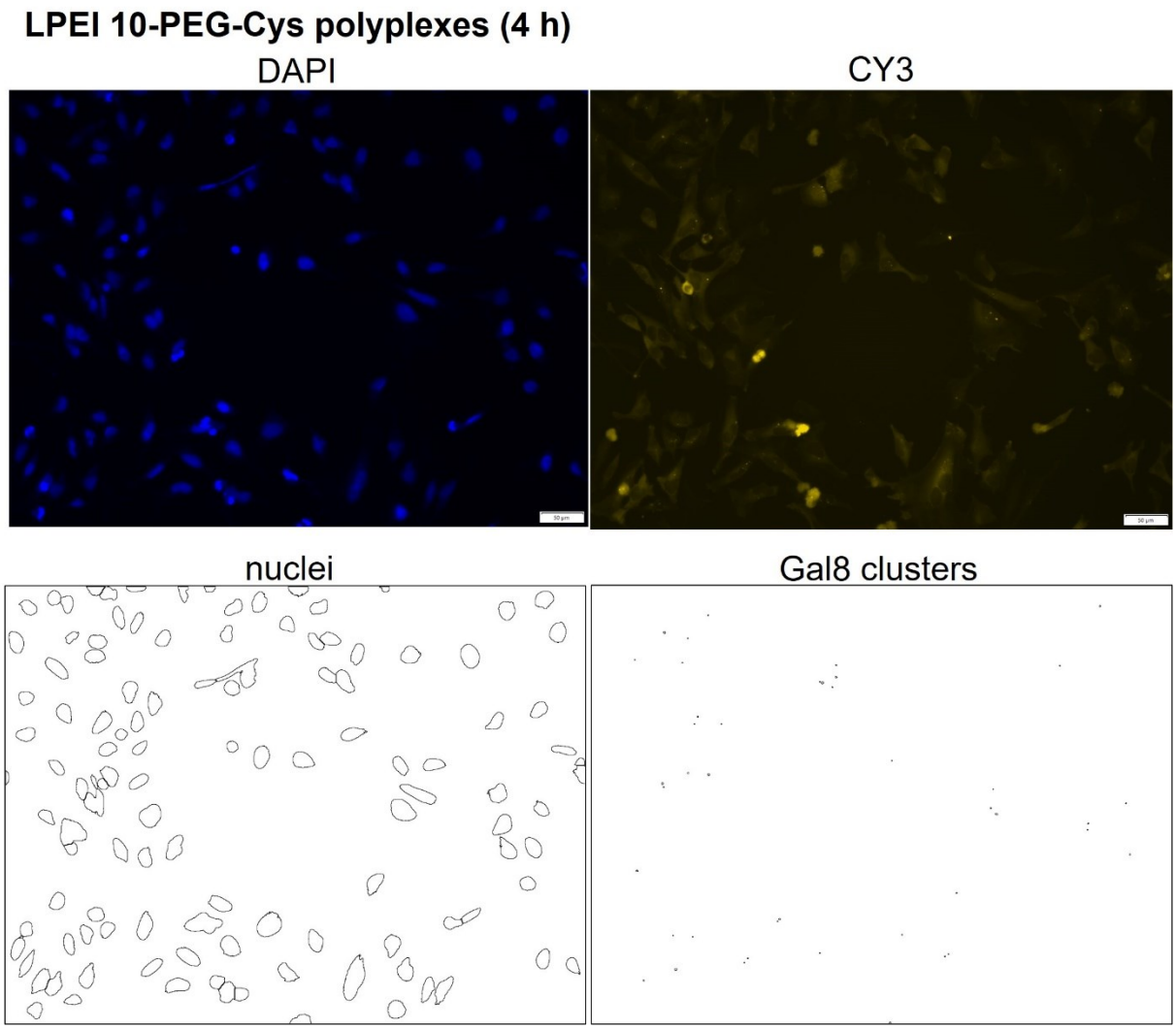

Figure IV: Visualisation and counting of nuclei and Gal8 clusters 4 h after adding Cypridina mRNA polyplexes with LPEI 10-PEG-Cys; polyplexes formed with N/P = 9 and c_{mRNA} = 200 µg/ml; 200 ng of mRNA added per well; magnification: 20 x, DAPI: 400 ms exposure time; CY3: 1 s exposure time

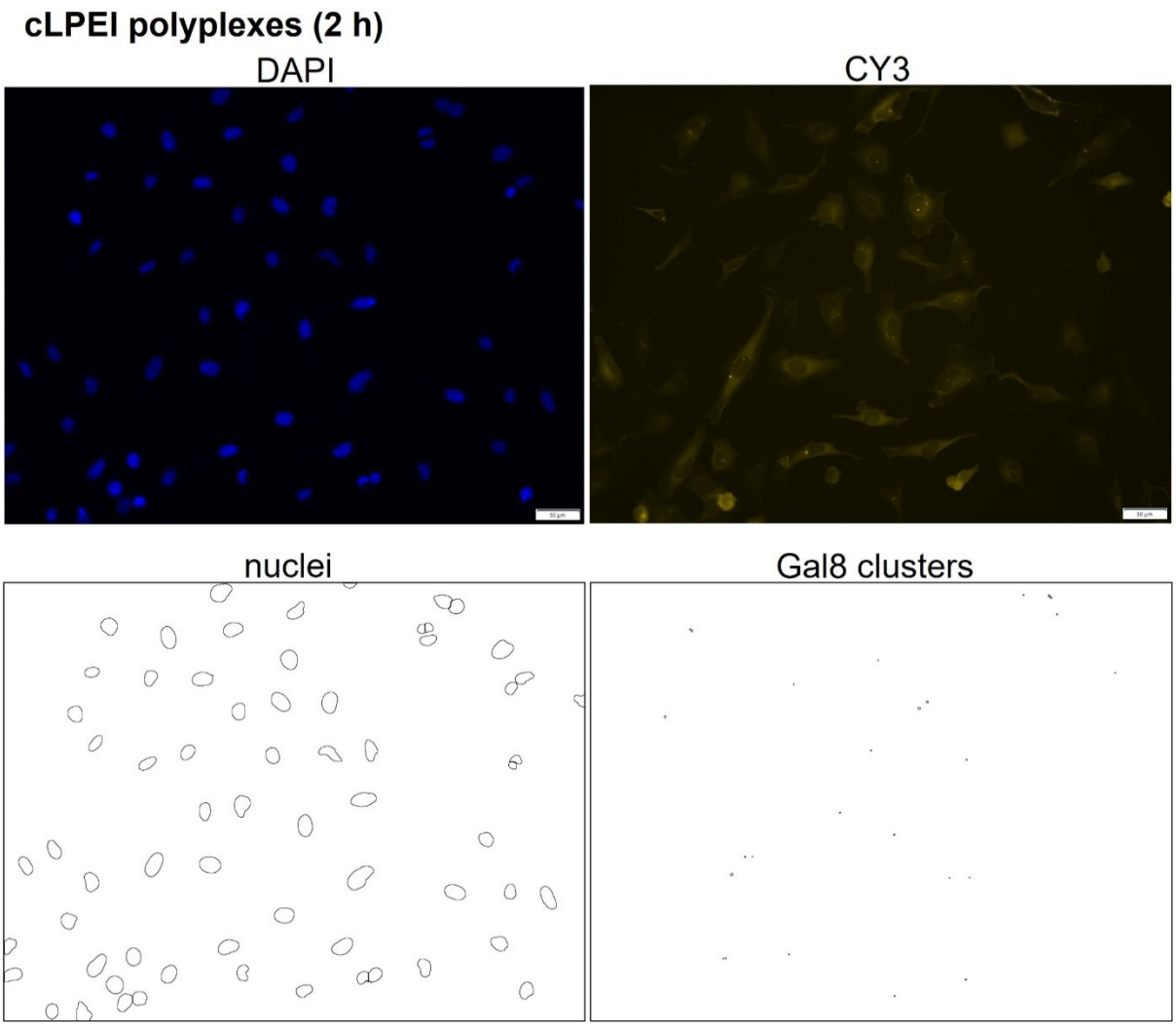

Figure V: Visualisation and counting of nuclei and Gal8 clusters 2 h after adding Cypridina mRNA polyplexes with cLPEI; polyplexes formed with N/P = 9 and c_{mRNA} = 200 µg/ml; 200 ng of mRNA added per well; magnification: 20 x, DAPI: 400 ms exposure time; CY3: 1 s exposure time

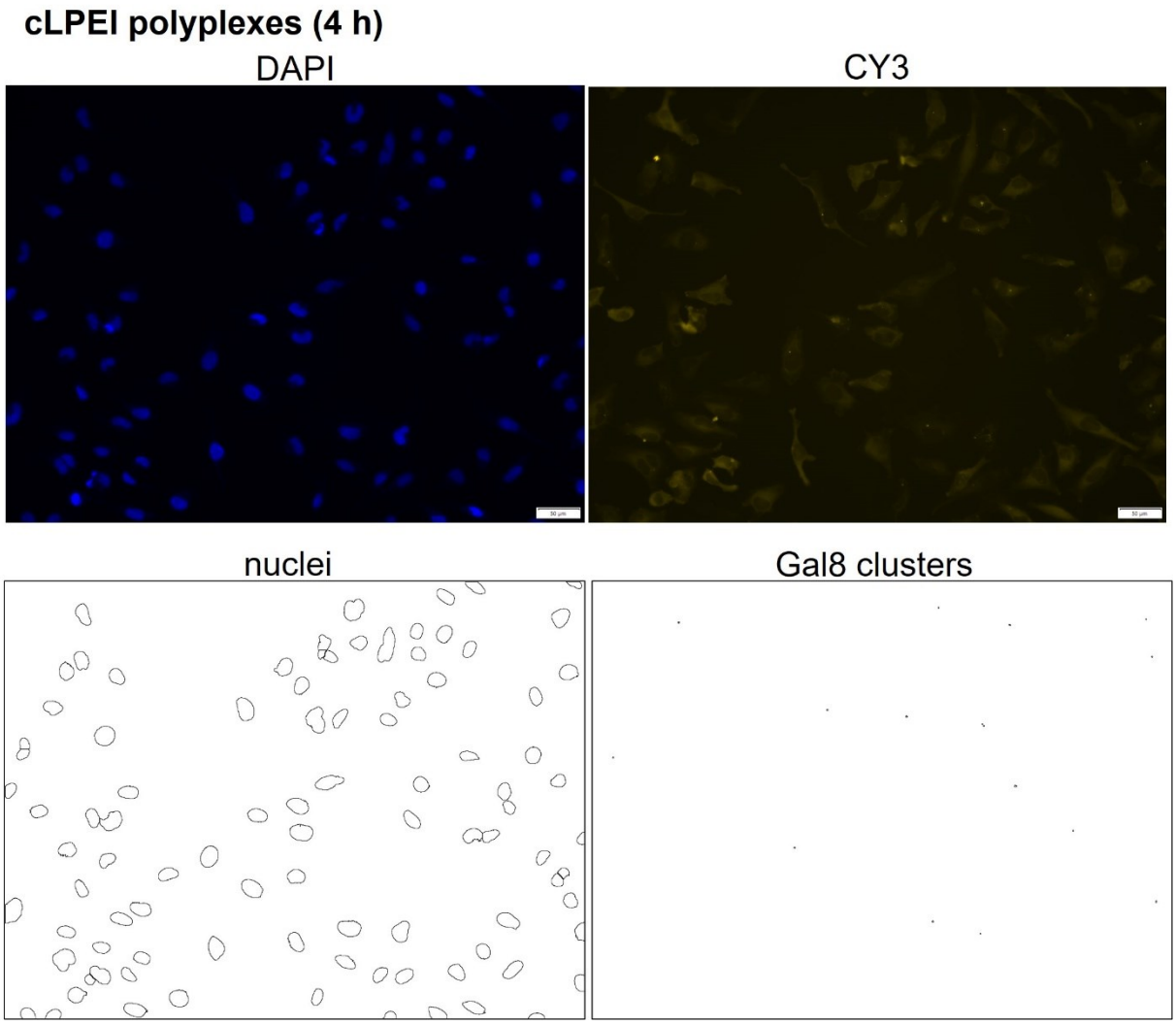

Figure VI: Visualisation and counting of nuclei and Gal8 clusters 4 h after adding Cypridina mRNA polyplexes with cLPEI; polyplexes formed with N/P = 9 and c_{mRNA} = 200 µg/ml; 200 ng of mRNA added per well; magnification: 20 x, DAPI: 400 ms exposure time; CY3: 1 s exposure time

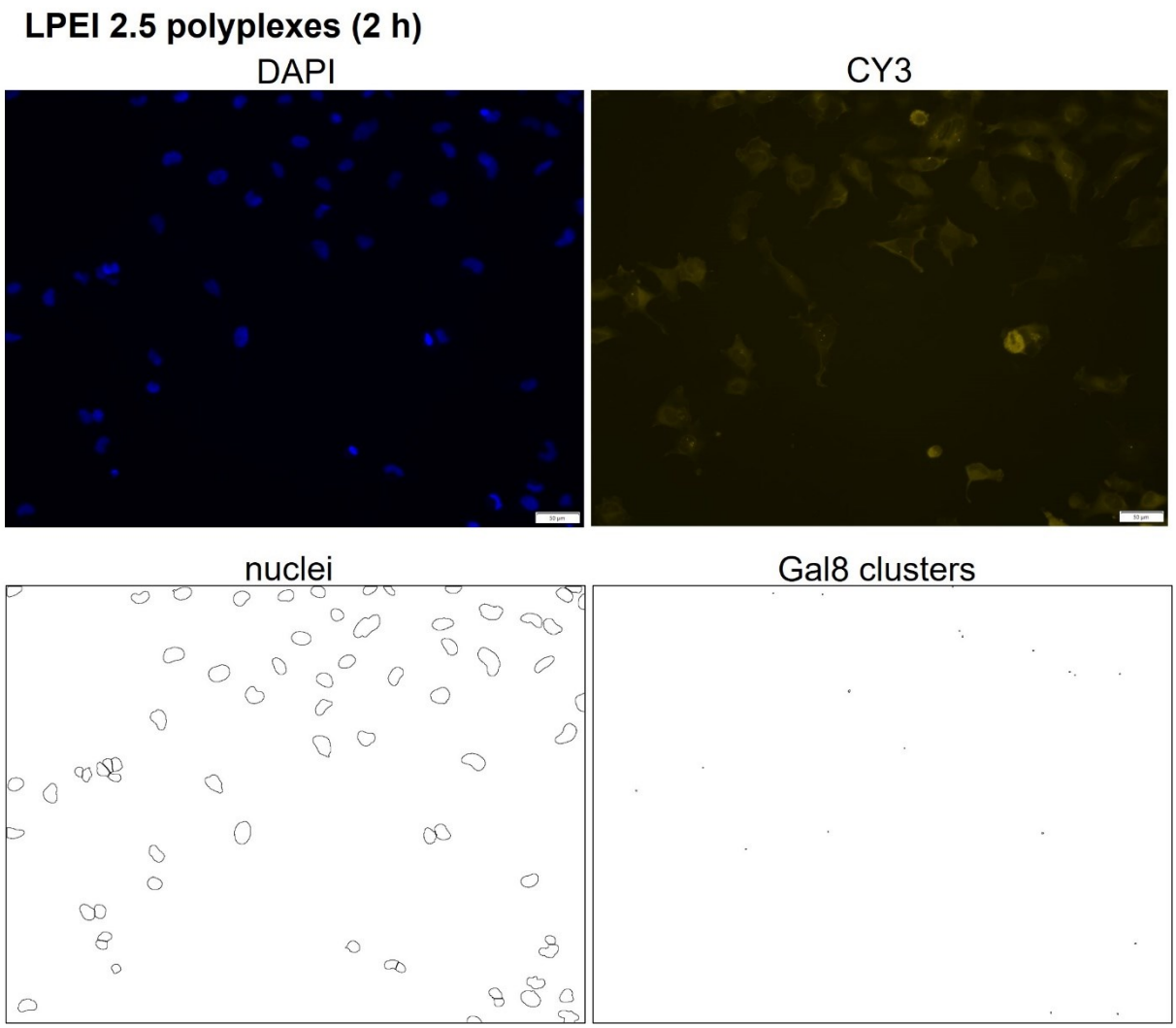

Figure VII: Visualisation and counting of nuclei and Gal8 clusters 2 h after adding Cypridina mRNA polyplexes with LPEI 2.5; polyplexes formed with N/P = 9 and c_{mRNA} = 200 µg/ml; 200 ng of mRNA added per well; magnification: 20 x, DAPI: 400 ms exposure time; CY3: 1 s exposure time

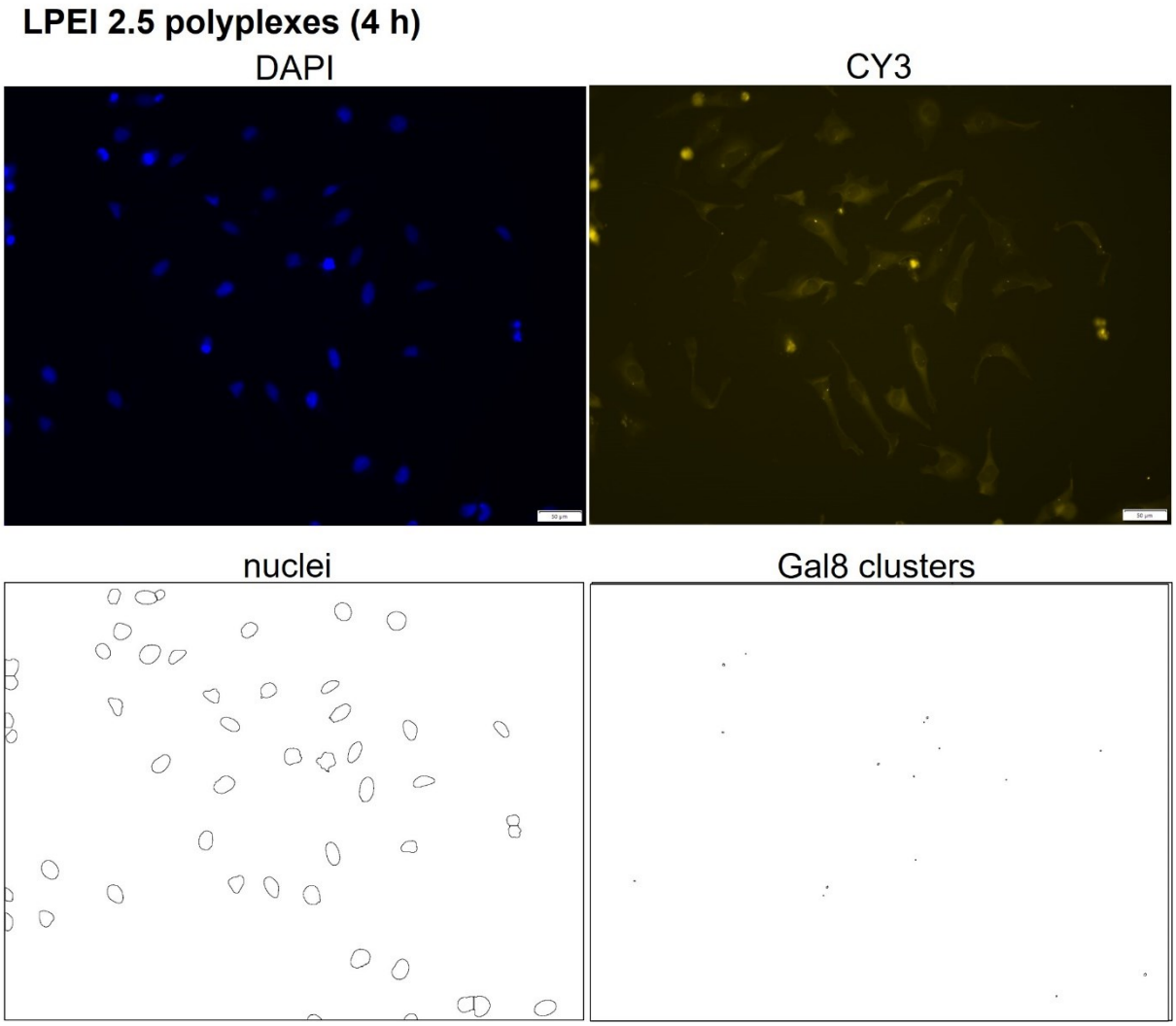

Figure VIII: Visualisation and counting of nuclei and Gal8 clusters 4 h after adding Cypridina mRNA polyplexes with LPEI 2.5; polyplexes formed with N/P = 9 and c_{mRNA} = 200 µg/ml; 200 ng of mRNA added per well; magnification: 20 x, DAPI: 400 ms exposure time; CY3: 1 s exposure time

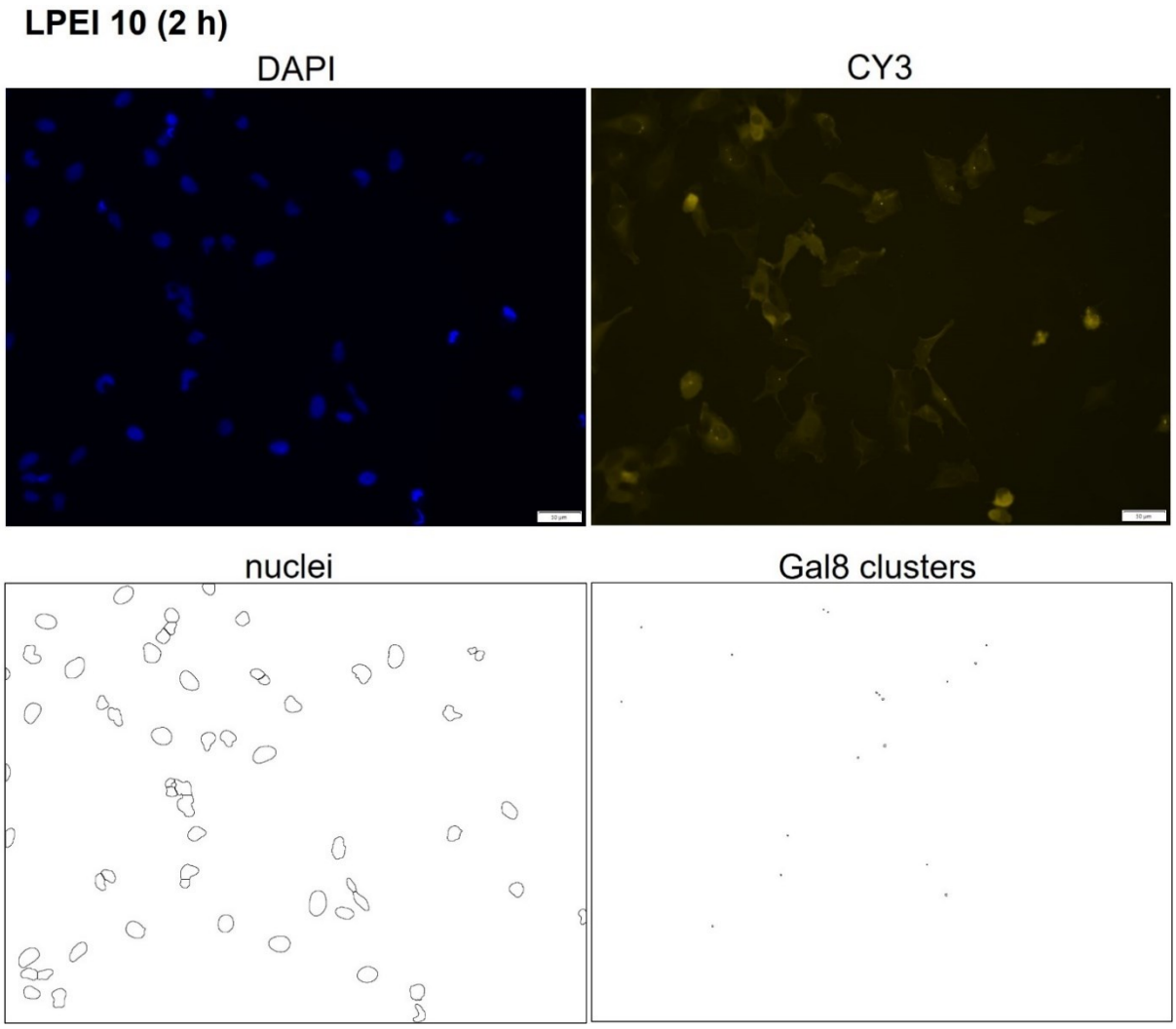

Figure IX: Visualisation and counting of nuclei and Gal8 clusters 2 h after adding Cypridina mRNA polyplexes with LPEI 10; polyplexes formed with N/P = 9 and c_{mRNA} = 200 µg/ml; 200 ng of mRNA added per well; magnification: 20 x, DAPI: 400 ms exposure time; CY3: 1 s exposure time

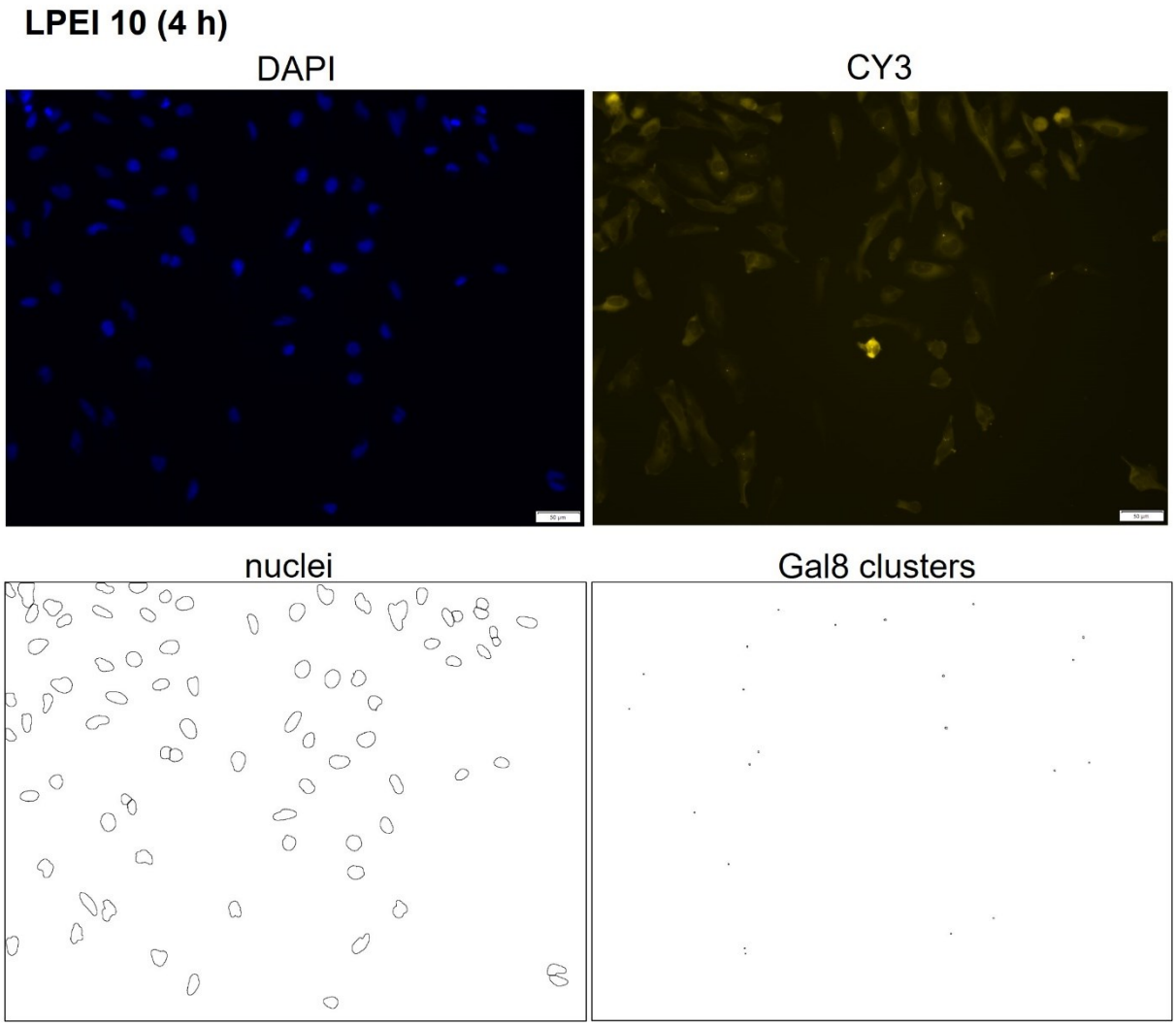

Figure X: Visualisation and counting of nuclei and Gal8 clusters 4 h after adding Cypridina mRNA polyplexes with LPEI 10; polyplexes formed with N/P = 9 and c_{mRNA} = 200 µg/ml; 200 ng of mRNA added per well; magnification: 20 x, DAPI: 400 ms exposure time; CY3: 1 s exposure time

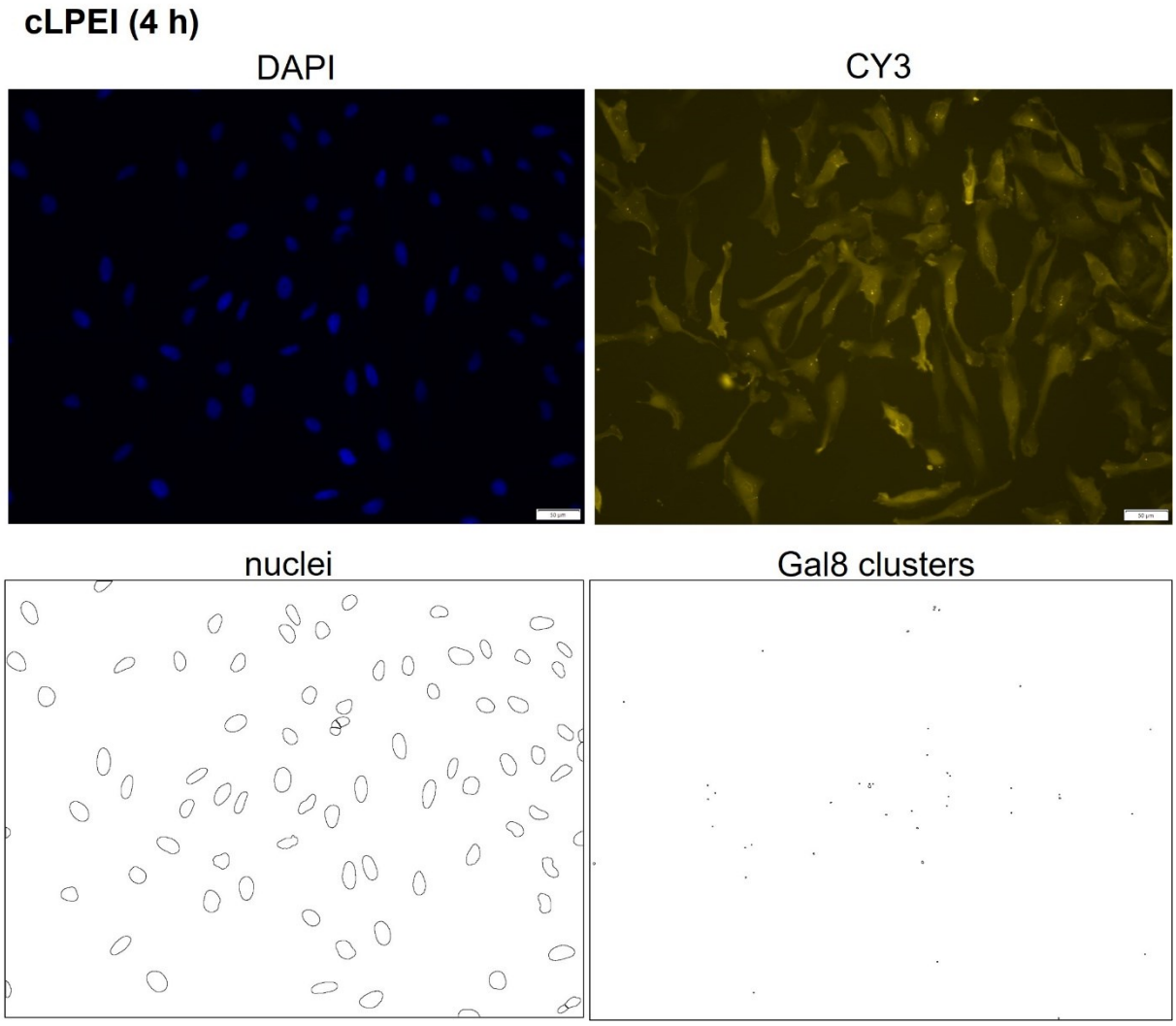

Figure XI: Visualisation and counting of nuclei and Gal8 clusters 4 h after adding AF750-SSO polyplexes with cLPEI; polyplexes formed with c_{SSOs} = 40 µg/ml; 160 pmol AF750-SSOs added per well; magnification: 20 x, DAPI: 400 ms exposure time; CY3: 2 s exposure time

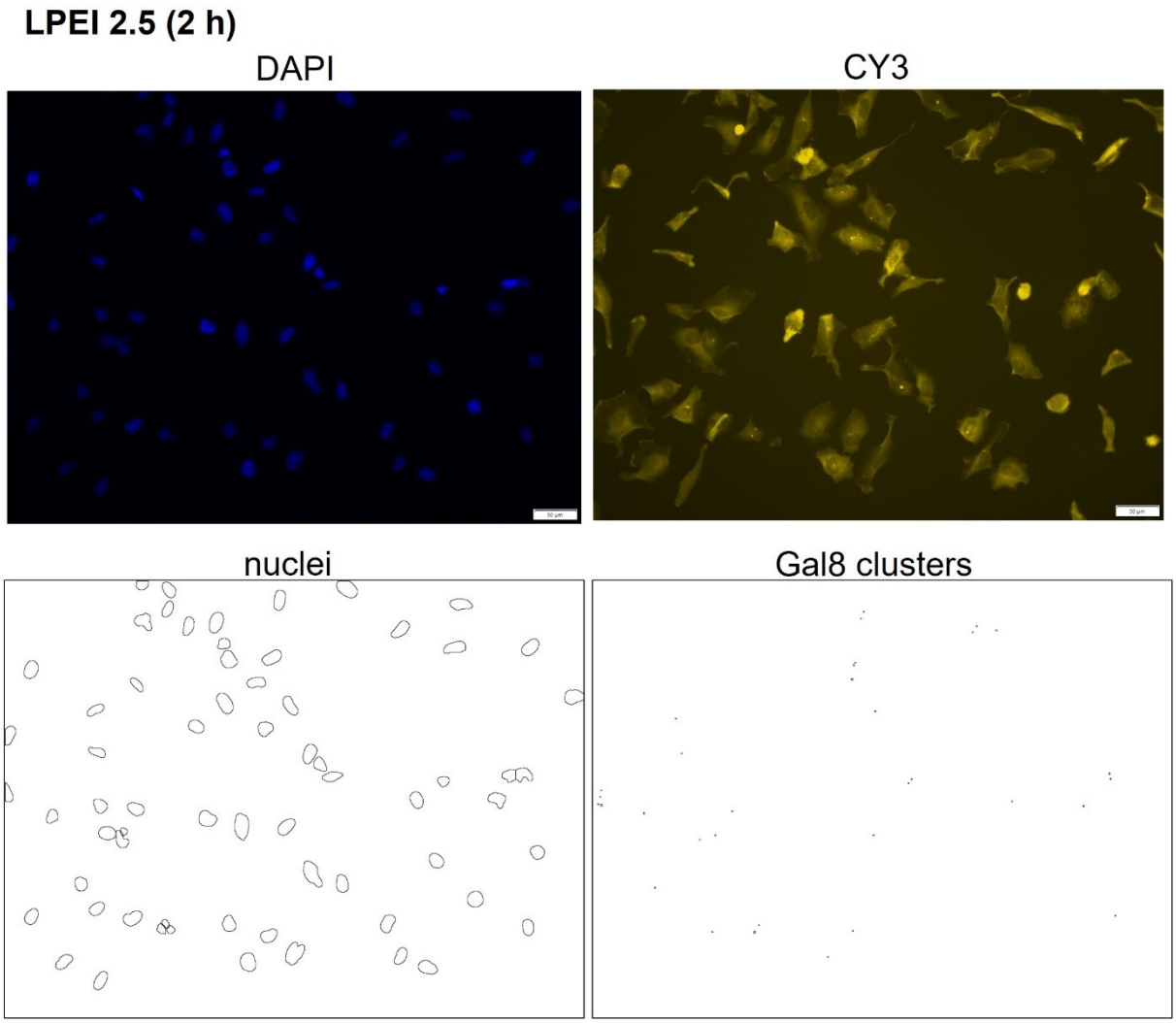

Figure XII: Visualisation and counting of nuclei and Gal8 clusters 2 h after adding AF750-SSO polyplexes with LPEI 2.5; polyplexes formed with c_{SSOs} = 40 µg/ml; 160 pmol AF750-SSOs added per well; magnification: 20 x, DAPI: 400 ms exposure time; CY3: 2 s exposure time

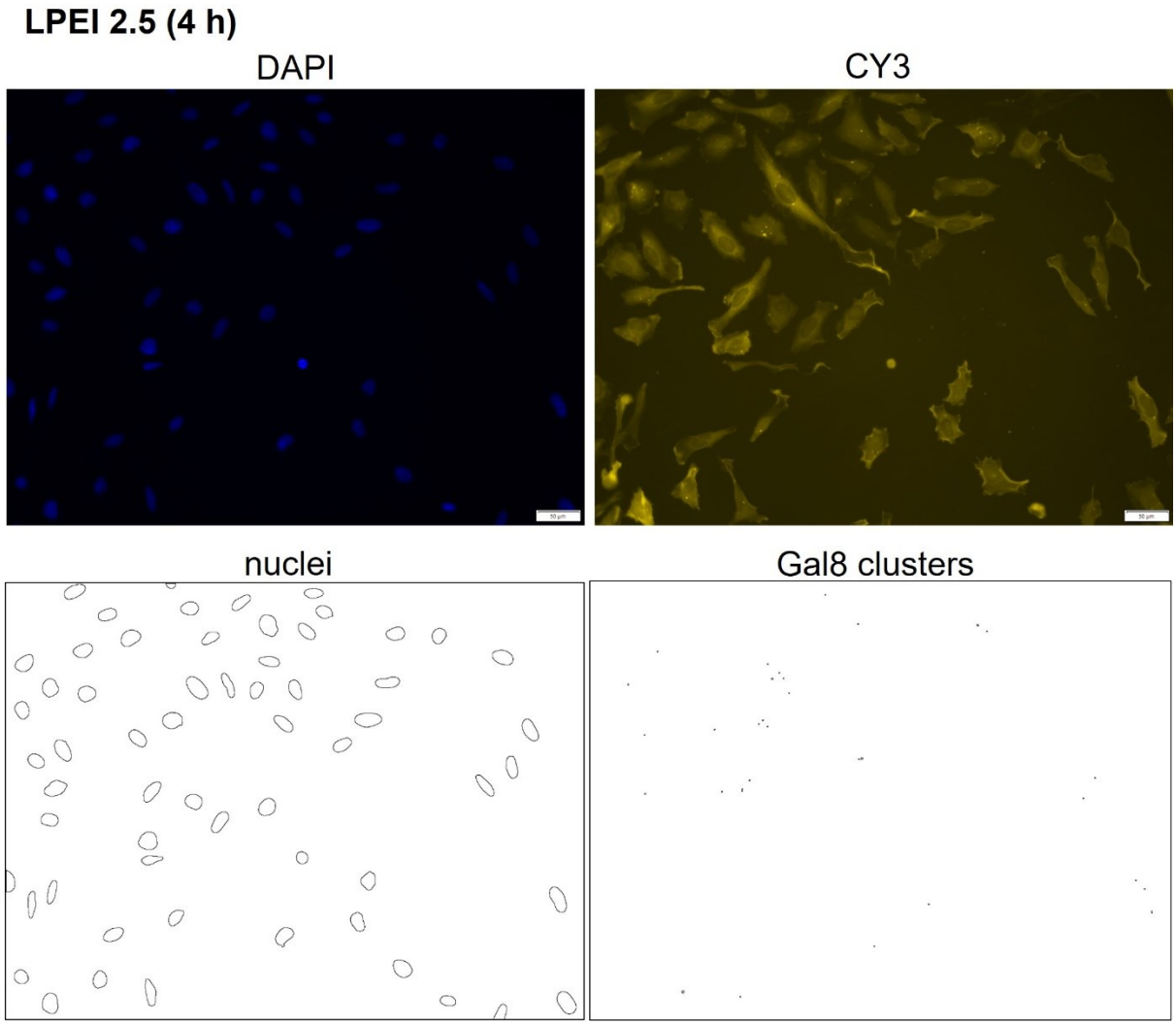

Figure XIII: Visualisation and counting of nuclei and Gal8 clusters 4 h after adding AF750-SSO polyplexes with LPEI 2.5; polyplexes formed with c_{SSOs} = 40 µg/ml; 160 pmol AF750-SSOs added per well; magnification: 20 x, DAPI: 400 ms exposure time; CY3: 2 s exposure time

Abstract

Therapeutische Nukleinsäuren ermöglichen die Behandlung verschiedener Krankheiten, indem sie intrazelluläre Moleküle in Zellen von Patienten manipulieren. Polykationische Polymere, darunter lineares Polyethylenimin (LPEI), können als Trägermoleküle verwendet werden, um exogene Nukleinsäuren effizient an ihren intrazellulären Wirkungsort zu transportieren. In dieser Arbeit wurden 10-kDa-LPEI, 2,5-kDa-LPEI und deren Derivate LPEI 10-PEG-Cys und quervernetztes LPEI als Träger von Boten-RNA und splice-switching Oligonukleotiden (SSOs) bei *in vitro* Transfektionen untersucht. Dabei wurde eine gentechnisch veränderte HeLa-Zelllinie verwendet, die den Nachweis aufgebrochener Endosomen mittels Fluoreszenzmikroskopie ermöglicht, um die Fähigkeit der Polymere zu analysieren, nach ihrer Aufnahme durch Endozytose die Freisetzung von mRNA ins Zytoplasma zu erleichtern. Die Ergebnisse deuten darauf hin, dass 10-kDa-LPEI und 2,5-kDa-LPEI den endosomalen Austritt von mRNA weniger effizient erleichtern als ihre Derivate. Dies legt den Schluss nahe, dass die PEGylierung beziehungsweise die Quervernetzung deren Leistung erhöhen.

In einem weiteren Projekt wurden 2,5-kDa-LPEI und quervernetztes LPEI verwendet, um die Zellen mit Alexa-Fluor-750-markierten SSOs zu transfizieren und so deren Austritt aus den Endosomen und Eintritt in den Zellkern zu visualisieren und semi-quantitativ zu analysieren. Außerdem wurde die Wirkung der Transfektion mit SSOs – die Korrektur von fehlerhaftem Spleißen – an anderen HeLa-Zellen getestet. Diese Zellen sind gentechnisch so verändert, dass sie eine Luziferase produzieren, die aufgrund von fehlerhaftem Spleißen nicht funktionsfähig ist. Den Ergebnissen zufolge ist quervernetztes LPEI effizienter als 2,5-kDa-LPEI bei der Vermittlung des endosomalen Austritts und des Kerneintritts von Alexa-Fluor-750-markierten SSOs sowie bei der Spleißkorrektur.